FLOCCULATION MODELLING OF DIFFERENTIAL SEDIMENTATION BASED ON FUNDAMENTAL PHYSICS OF SETTLING PARTICLES AND FRACTAL THEORY

NOMCEBO PRINCESS SITHEBE

A dissertation submitted in partial fulfilment of the requirement for the degree of

MASTER OF ENGINEERING: WATER UTILISATION ENGINEERING

In the
Faculty of Engineering, Built Environment and Information Technology
Department of Chemical Engineering, University of Pretoria, Pretoria, South Africa

August 2013

DECLARATION

I, NOMCEBO PRINCESS SITHEBE, hereby declare that the work provided in this dissertation is to the best of my knowledge original (except where cited) and that this work has never been submitted for another degree at this or any other educational institution.

_____

Signature of candidate

This …….. day of …… 2013

DEDICATION

This dissertation is dedicated to:

My family and friends

My best friends Bongani, Lihle and Nakiti for making my life so meaningful and enjoyable.

My Mother who ensured I received education even in an underprivileged background.

ACKNOWLEDGEMENTS

My ultimate gratitude goes to my God Jehovah, for His undeserved kindness and mercies, and the gift of life through His son Jesus Christ. With Jehovah, all things are possible.

I would also like to express my deepest gratitude to Prof E. M. N. Chirwa for the supervision of the project. His constant support, inspiration and guidance have been instrumental to the success of the project.

The University of Pretoria grants UP Bursaries to postgraduate students to encourage research, this too, is deeply appreciated.

My sincere appreciation goes to my family for their loving support (financially and emotionally) and constant prayers.

ABSTRACT

Sedimentation is a fundamental operation in wastewater treatment works. A rational design of sedimentation tanks is currently achieved by plotting iso-percentile (iso-percentage) concentration removal profiles from flocculent settling data. A major drawback of the graphical iso-percentage method is that the iso-percentile lines are often manually interpolated and are mere hand drawn estimations. This is because the settling behaviour of sludge particles is highly non-linear. The manual analytical process is therefore very tedious, inaccurate and subjective. Hence, an optimised design of sedimentation tanks is necessary in order to eliminate the errors incurred during data analysis.

In this study, a mechanistic iso-percentile flocculent model (referred to as the velocity flocculation model) is developed to simulate the behaviour of flocculating colloidal particles in turbid water. This model is based on the physical meanings of flocculent settling particles and on fractal theory. It is formulated to produce automated iso-percentile curves which are fundamental in the design of sedimentation tanks.

The iso-percentile model was vertically integrated into a velocity model to produce a model expressing the velocity of particles as a function of removal rate. The velocity model has an obvious advantage over the iso-percentile model in that it is easy to contextualize. It can be reverted back to the iso-percentile trajectory analysis eliminating the need for extensive data interpolation and may in future eliminate the need for settling column analysis altogether. In the current study, the integrated velocity form is used to predict instantaneous flocculent settling velocity of fine suspended particles under near quiescent conditions. This is vital since it is difficult to obtain velocity values in-situ or directly from sedimentation tanks.

Model validity and competency was tested by a direct comparison with existing literature models, such as Ozer's model and Ramatsoma and Chirwa's model. Model comparison was based on the goodness of fit, the least sum of square errors and mathematical consistency with known flocculent settling behaviour. The newly developed iso-percentile model achieved a more accurate simulation of physical experimental data, did not violate any of the mathematical constraints and yielded lower sum of square errors than originally achieved by Ozer and Ramatsoma and Chirwa.

Notably, the proposed velocity model offers a distinctive advantage over conventional interpolated-iso-percentile based models which are prone to numerical errors during interpolation. Its performance (velocity model) was compared against Je and Chang's velocity model. Higher velocity values were observed for the new model than for Je and Chang's model implying that empirically based models would tend to under-predict the velocity values. The model developed in this study brings us one step closer to achieving full automation of the settling tank and clarifier design.

Keywords: flocculation modelling, iso-percentile removals, velocity model, fractal sedimentation, continuum particle dynamics.

TABLE OF CONTENTS

LIST OF FIGURES

LIST OF TABLES

ABBREVIATIONS AND SYMBOL NOMENCLATURE

Abbreviations

PSD Particle size distribution

SSE Sum of square errors

TSS Total suspended solids

Nomenclature

α fitting parameter in San's model (dimensionless)

α_i model fitting parameters in Özer's model (dimensionless) (i = 1, 2, and 3)

α' collision efficiency factor in Smoluchowski's equation (dimensionless)

β fitting parameter in San's model (dimensionless)

$\beta\ (i,j)$ collision frequency function in Smoluchowski's equation (L^3T^{-1})

δ fitting parameter in Maggi's model (dimensionless)

ε porosity (dimensionless)

ε_x, ε_y, ε_z turbulent diffusion coefficients for the x, y and z direction in the water quality model

λ wavelength of radiation in a vacuum (L)

μ water dynamic viscosity in Winterwerp's model ($ML^{-1}T^{-1}$)

ψ fitting parameter in Piro and co-workers' model (LT^{-1})

ρ density (ML^{-3})

ρ_s density of primary particles forming flocs in Winterwerp's model (ML^{-3})

ρ_w density of water (ML^{-3})

θ scattered angle (dimensionless)

ξ fitting parameter in Maggi's model (dimensionless)

A cross sectional area of aggregate (L^2)

a parameter in Je and Chang's velocity model (dimensionless)

a_v approximate velocity relating the particle size distribution and fractal dimension $\left(d_f^{D-1}\right)$ (LT^{-1})

B fitting parameter in Piro and co-workers' model (dimensionless)

b optimisable parameter in the proposed model in this study (dimensionless)

b'' parameter in Je and Chang's velocity model (dimensionless)

C optimisable parameter in the proposed models in this study (dimensionless)

D fractal dimension of flocs (dimensionless)

d depth travelled by particle during settling (L)

d_f, d_{50}, d_{mm} diameter of flocs represented by mass mean diameter d_50 (L)

D_z dispersion coefficient in the vertical direction (L^2T^{-1}).

g specific gravity (dimensionless)

h, H ordinate representing depth (L)

I light intensity (JL^{-2})

k fitting parameter in San's model (dimensionless)

k' maximum settling velocity in the power law model and exponential model

K proportionality constant from Oles equation

l characteristic measure of size (L)

m optimisable parameter in the proposed model in this study (dimensionless)

m' floc mass (M)

n fitting parameter of the power law model and exponential model (dimensionless)

n_i, n_j, n_k number concentrations of particle sizes in Smoluchowski's equation (L^{-3})

$\overline{n}$ refractive index of suspending medium (dimensionless)

N number of particles in aggregate (dimensionless)

$\overline{p}$ perimeter of aggregate (L)

P percentage removed from suspension $(1-X_j/X_o)\times 100$

P'' percentage remaining in suspension $(X_j/X_o)\times 100$

Q wavenumber (L^{-1})

Re Reynolds number in Winterwerp's model (dimensionless)

S system specific constant in Sterling Jr and co-workers' model

r_i semi-empirical optimisable parameters of Ramatsoma and Chirwa's model (i = 1, 2, and 3)

r simplifying parameter in the proposed velocity model in this study (r = 1+C) (dimensionless)

$r'(c,p)$ term representing the rate of change of determinants due to internal transformations.

t time of settling (T)

T ordinate representing time

U_z vertical water velocity (LT^{-1})

V solid volume (L^3)

v settling velocity (LT^{-1})

V_s flocculent settling velocity (LT^{-1}),

V_i volume fraction of flocculated suspension (i = 0, 1, 2, 3, 4, 5, 6, 7) (dimensionless)

w optimisable parameter in the proposed model in this study (dimensionless)

x solids concentration in the power law model and exponential model (ML^{-3})

X_j suspended solids concentration in layer j (ML^{-3})

X_o initial concentration in the column (ML^{-3})

y simplifying parameter in the proposed velocity model in this study (y = b+c) (dimensionless)

z, Z vertical distance (L)

CHAPTER 1

INTRODUCTION

1.1 General Background

Removing fine pollutant particles in wastewater has gained much attention in recent years due to the increasing awareness of the impact of particles on treatability of water. Many of the pollutants adsorb onto the surface of fine-grained suspended particles as products from mines, municipalities and factories and are discharged into the nations' water system. Colloidal particles and flocs can serve as adsorption sites for reluctant organic compounds (Joshi *et al*., 2003). They can also serve as safe havens for viruses and bacteria thereby shielding them from disinfectants (Dawney and Pearce, 2012). A majority of these cohesive sediments cannot settle naturally except through coagulation and flocculation. Therefore understanding the transport and fate of suspended particulate matter will secure the fate of dissolved contaminants and solve the pollution problem.

1.2 Significance

Wastewater treatment systems are widely studied with the aid of mathematical models. However the models developed for the prediction of total suspended solids (TSS) transport or behaviour are either empirical or semi-empirical in nature thus limiting their application. That is the case (empirical) with the majority of the iso-percentile removal models reviewed by Je and Kim (2002). It is believed that flocculation could be better understood or modelled by the fractal behaviour of flocculated particles and particle size distribution (PSD), yet none of the iso-percentile models so far developed have given reference to fractal dimensions of settling particles. Current flocculation models have been based on individual particle collisions, that is, the microscopic phenomena leading to highly complex and impractical models (Thomas *et al*., 1999). In the review by Thomas and coworkers it was concluded that it is better to express flocculation performance in terms of fractals for application to real systems. So far, there is no satisfactory predictive model to relate the physical nature of the flocculation particles to settling behaviour and their removal efficiency.

1.3 Problem Statement

In water and wastewater treatment facilities, the mass transport and behaviour of fine grained cohesive sediments is influenced mainly by flocculation effects and nominal settling

velocities of particles. Therefore it is vital to understand the physical characteristics of fine-grained cohesive sediments during flocculation. The behaviour of flocculating particles and settling trajectories of individual particles is very complex. Constant spatial and temporal variations as well as fluctuating initial conditions in physical sedimentation systems result in difficulty and uncertainty in the predictions of medium-term and long-term behaviour of the settling particles (Xu *et al*., 2008; Mikkelsen *et al*., 2005). Hence understanding batch settling processes of flocs is fundamental for effective thickener/clarifier design and control.

During the design of sedimentation tanks, data from settling columns are interpreted by a graphical technique. Firstly, samples are collected from different column depths at different times and are analysed for total suspended solids concentration. The batch settling data is then utilised to compute iso-percentile removal profiles (or iso-percentage contour lines) as a function of time and depth. From the graphs, one can predict or calculate the removal efficiency, overflow rate and settling velocities of particles. Empirical scaling factors are then used to extrapolate these results for design purposes. This procedure was initiated by Camp (1946) and has been adopted by several authors like Peavy *et al*. (1985), Eckenfelder (1989), Tchobanoglous *et al*. (2003), Metcalf and Eddy (2003).

However, it is common practice in industry to manually construct the iso-percentile curves due to their non-linear nature. That is a major drawback as the practice is tedious, inaccurate and subjective (Pise and Halkude, 2011). Hence, an optimised design of sedimentation tanks is necessary in order to eliminate the errors incurred during data analysis.

There is also the problem of irreproducibility since no two different technicians can construct exactly the same curves. When using currently proposed models to fit the percentage removal data, some fit the data well only at short retention times and others tend to violate the physical meaning of settling data profiles (Je and Kim, 2002). The use of inaccurate settling equations could lead to significant errors of aggregate properties.

1.4 Objectives

The main objective of this project was to derive an automated data analysis package for plotting iso-percentile removal profiles for settling columns. The package is comprised of an interpolation script and a dynamic-mechanistic flocculation model. The script interpolates experimental data and generates suspended solids removal profiles based on column depth

and solids residence time. The flocculation model is to be derived from the physical principles of a settling particle. It would represent the behaviour of particles in quiescent flow, incorporating the particle size distribution and the fractal nature of particles during settling. Incorporating variable fractal dimensions onto the iso-percentile model is vital since it would enable the characterisation of the behaviour of any flocculating system.

The second objective is to derive an integrated form of the rule based iso-percentile flocculation model for the prediction of instantaneous settling velocities. This is crucial since it is difficult to deduce settling velocities *in situ*. Also, when equipped with a robust velocity model, the analysis could then be analytically reverted back to the iso-percentile trajectory analysis without the need for data interpolation from a settling column. This approach would introduce accuracy and reproducibility, and will save time in the sedimentation zone and clarifier designs.

1.5 Outline of Dissertation

The dissertation is structured into four major parts:

Literature review - focuses on differential sedimentation through flocculation principles. It also touches on previous and recent developments of flocculation modeling and settling velocity.

Materials and methods – presents all the material and methods adopted during the study.

Iso-percentile model development – contains all the theory utilized to deduce the flocculation model and presents it in practical terms.

Settling velocity model development – inherits the principles used in deriving the iso-percentile flocculation model and is enhanced with hydrodynamic characteristics of flowing particles.

Summary- highlights the purpose and findings of the study and recommends a way forward for future research.

CHAPTER 2

LITERATURE REVIEW

2.1 Flocculation Mechanisms

Cohesive sediments are found in water treatment systems, rivers and estuaries. These sediments are responsible for the muddy or turbid appearance of water. The sediments consist of fine clay and silt particles. Non cohesive sediments, on the other hand, are composed of large grained particles like sand. Cohesive sediments tend to remain in suspension for long periods of time without settling. Treatment of turbid waters can be achieved by coagulation and flocculation in sedimentation tanks.

Particle destabilization by means of coagulation and subsequent agglomeration through flocculation of colloids and fine grained particles into larger particles is a proven means of removing impurities in water treatment works. Coagulation reduces the negative surface charge of small particles rendering them unstable while flocculation encourages particle agglomeration forming mass fractal aggregates. The size and structure of flocs is key to the efficient operation of sedimentation tanks (Bridgeman *et al*., 2009). Mathematical modelling of flocculation is traditionally based on two discrete steps which are transport and attachment (Thomas *et al*., 1999). The transport leads to collision of particles whilst the attachment is reliant on the nature of particles. The different flocculation mechanisms are perikinetic flocculation, orthokinetic flocculation and differential sedimentation. Other processes involved are shown in Figure 2-1. Particles aggregate to form flocs but there can also be floc breakage, restructuring, and reformation leading to more compact flocs (He *et al*., 2012).

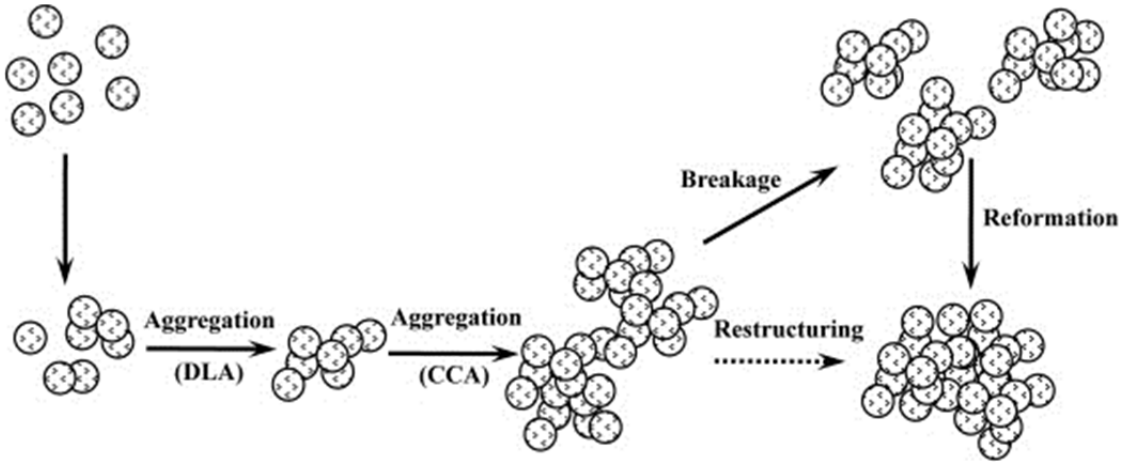

Figure 2-1: Schematic of floc growth adapted from He *et al*. (2012).

2.2 Fractal Theory

2.2.1 Fractal Characterization

Fractal theory was introduced by Mandelbrot in the 1970's leading to the establishment of fractal geometry in describing the complicated structure of aggregated particles (Mandelbrot, 1977; Selomulya *et al.*, 2003; Selomulya *et al.*, 2001; Chakraborti *et al.*, 2003; Chakraborti *et al.*, 2000). In water and wastewater systems natural aggregates are not spherical so fractal geometry is employed to account for the different shapes (Li and Ganczarczyk, 1986). Flocculated aggregates are examples of mass fractal objects. Equation 2-1 shows a relationship between floc mass, *m'*, and its fractal dimension, *D*.

$$m' \approx l^{D} \tag{2-1}$$

where *l* is a characteristic measure of size.

According to Jarvis *et al*. (2005), fractal objects may be defined as objects that:
(1) show statistical self-similarity.
(2) express a power-law relationship between two variables
(3) can be characterised by a non-integer fractal dimension

The fractal dimension (D_e) characterizes how an aggregate property changes with size. So the power law relationships of fractal objects between two variables may include:

$$N \alpha l^{D_3} \qquad A \alpha l^{D_2} \qquad \overline{P} \alpha l^{D_3-3} \qquad \varepsilon \alpha l^{D_3-3} \tag{2- 2}$$

where, *e* = the subscript in fractal dimension *D* denoting two dimension or three dimension

N = number of particles in aggregate

A = cross sectional area of aggregate

$\overline{P}$ = perimeter of aggregate

l = characteristic length

A summary of the power law scaling relationships is given in Table 2-1 below:

Table 2-1: Power law scaling relationships.

Fractal Property	**Fractal Scaling Relationship**
Solid Volume	$V = a_v l^{D_3}$
Mass	$m' = a_m l^{D_3}$
Area	$A = a_A l^{D_2}$
Density	$\rho = a_p l^{D_3 - 3}$

Source: Logan (http://www.engr.psu.edu/ce/enve/logan.html)

Fractal objects show non Euclidean dimensionality with the range ($1 \leq D < 3$) for three dimensional shapes. For a Euclidean object the fractal dimension is 3 for a three dimensional shape, 2 for a two dimensional planar shape and 1 for a linear line (Jarvis *et al*., 2005). If a floc is highly porous the fractal dimension will be closer to one but for more compact flocs the fractal value approaches three. As the floc size increases the porosity also increases but the density decreases. Porous flocs (characterised by low D) tend to allow fluid to flow through them. Mathematical porosity is defined as follows (Sterling Jr *et al*., 2005; Thomas *et al*., 1999):

$$\varepsilon = 1 - SR^{D-3} \tag{2-3}$$

where ε is the floc porosity, S is a system specific constant, R is the floc radius and D is the fractal dimension.

The mechanism of aggregate growth is also determined by the fractal dimension. When particles collide during flocculation, mass is conserved but the volume is not conserved because the density varies. This has an effect on the type of aggregates that are formed. Particle-cluster, which are aggregates formed through the addition of particles into a cluster one at a time, have fractal dimensions (three-dimensional) ranging from 2.5-3 (Logan and Wilkinson, 1990; Schaefer, 1989). Cluster-cluster, aggregates formed through the collision of clusters are classified by lower fractal dimensions, $1.6 \leq D_3 \leq 2.2$ (Witten and Cates, 1986; Logan and Wilkinson, 1990). According to Lee *at al*. (2002) aggregates generated in water and wastewater treatment processes exhibit fractal dimensions ranging from 1.4 to 2.8.

The rate of reaction can also be used to classify aggregates. In diffusion-limited colloidal aggregation (DLCA), the reaction (coagulation) is very rapid, and the rate of aggregate growth is affected or limited by particle transport. The stickiness efficiency of the particles is closer to one. Whilst in the reaction-limited colloidal aggregation (RLCA), the reaction

becomes slower, as the attachment probability approaches zero. With a low stickiness factor, the particles may collide a multiple of times before being part of the cluster (Logan and Wilkinson, 1990).

2.2.2 Microscopic Approach

The fundamental flocculation equation was first derived by Smoluchowski (1917) laying a foundation for most flocculation models. Smoluchowski's temporal variation, Equation 2-4, represents the rate of change in the number concentration of particles of size *k*.

$$\frac{dn_k}{dt} = \frac{1}{2}\sum_{i+j=k}\alpha'\beta(i,j)n_i n_j - n_k\sum_{i=1}^{\infty}\alpha'\beta(i,k)n_i \tag{2-4}$$

where the first term on the right hand side is the aggregation term and the second one is the floc break-up term, $\beta(i,j)$ is the collision frequency function, α' is the collision efficiency factor, i, j and k denote particle size categories, n_i, n_j and n_k are the number concentrations of particle sizes.

According to Thomas *et al*. (1999), Smoluchowski had to make a couple of simplifying assumptions for the model to be practical. The assumptions are: 1) Collisions involve only two particles, 2) No floc breakage occurs, 3) All particles are spherical in shape and remain so after collision, 4) The particles are monodispersed, 5) The collision efficiency factor is unity for all collisions, and 6) Fluid motion undergoes laminar shear. A majority of these assumptions (1-4) are not a true reflection of what happens during flocculation. As a result a lot of modifications have been suggested by many authors like Camp and Stein (1943), Han and Lawler (1991), Han and Lawler (1992).

The traditional kinetic approach to model flocculation relies on the calculation of collision efficiencies and collision frequencies. Particle dynamics are defined through rectilinear models or curvilinear models depending on whether hydrodynamic effects are considered or not. The curvilinear approach assumes that flocs are totally impermeable and that the fluid only flows around the floc rather than through the flocs. It also accounts for hydrodynamic effects on the collision efficiency based on the correction factors that were later presented by Han and Lawer (1992). On the other hand, the rectilinear approach (like Smoluchowski's model) assumes that flocs are totally porous and ignores hydrodynamic effects (Sterling Jr *et*

al., 2005; Thomas *et al*., 1999). None of the assumptions considered for the curvilinear /rectilinear approach are entirely applicable to the flocculation of particles.

Many attempts have been made to improve and even incorporate fractal dimensions to the rectilinear and curvilinear models. Lee *et al*. (2000) derived a flocculation model based on coalesced fractal sphere assumptions. Lee *et al*. (2002) also included fractals and noticed that the rectilinear approach was more consistent with observed data than the curvilinear approach. Sterling Jr *et al*. (2005) relaxed the coalesced fractal sphere assumptions by introducing multiple monomer densities and aggregate fractal dimensions. Additional research was also done by Wiesner (1992), Hill (1992) and Jackson (1995). However these models are too rigorous to be implemented for industrial or wastewater treatment purposes. Nonetheless, it is preferable to model flocculation using macroscopic measures rather than microscopic or empirical measures (Thomas *et al*., 1999).

2.2.3 Macroscopic Approach

The microscopic approach to flocculation is more rigorous yet it only presents bounds in between which real systems act (Sterling Jr *et al*., 2005; Li and Logan, 1997a, b). Empirical models though have a problem of irreproducibility and data extrapolation. So instead of relying on empirical models or the microscopic approach it is best to model flocculation using macroscopic approaches. The fractal dimension is one representation of a macroscopic measure. This approach is preferred because the fractal dimension has great significance in flocculation. It is linked to a number of important flocculation variables and parameters. Its link to particle size, mass and porosity affects: 1) the settling velocity of a floc, 2) floc strength, 3) the amount of water contained within a floc, 4) the rate of collision of a floc and the degree of advection through the floc (Thomas *et al*., 1999).

2.2.3.1 Variable Fractal Dimension

Numerous studies have revealed that floc fractal dimension varies with floc size, contrary to previous believes (Vahedi and Gorczyca, 2012). A majority of authors attest to the fact that during flocculation there is a transition from Euclidean dimension (3) to a fractal dimension (<3) (Maggi, 2007; Maggi and Winterwerp, 2004; Khelifa and Hill, 2006). The authors concluded that the capacity or fractal dimension decreases with increasing floc size. This introduces a different angle, that flocs are in general not self-similar. This is due the diversity of properties such as particle size distribution, organic matter content and mineral content.

Some examples of varying mass fractal dimension, D, relationships include:

$$D = \begin{cases} -0.0047 d_f + 3.0183 & d_f \leq 50\ \mu m \quad R^2 = 0.93 \\ -0.0007 d_f + 2.7529 & d_f > 50\ \mu m \quad R^2 = 0.69 \end{cases} \tag{2-5}$$

where d_f is the particle size (Vahedi and Gorczyca, 2011).

Another example by Maggi (2007) and Maggi *et al*. (2007):

$$D(L) = \delta \ell^{\xi} = \delta \left(d_f / d_o \right)^{\xi} \tag{2-6}$$

where D is the three dimension fractal capacity, δ and ξ are estimated by data fitting, d_o and d_f are the sizes of primary particles and flocs respectively. The parameter, δ, can be interpreted as the capacity dimension of the primary particles, and it amounts to about δ = 3. The parameter, ξ, represents the rate at which D decreases for $d_f > d_o$, and is taken to be ξ = -0.1.

2.2.4 Methods for Determining Fractal Dimensions

2.2.4.1 Image Analysis

A combination of image analysis and microscopy has been utilized by a number of researchers to determine floc fractal dimensions. The image analysis gives a two dimensional fractal dimension through the relationship between floc area and floc characteristic length. To determine the capacity dimension a log-log plot of floc area against size is plotted to obtain a straight line. The slope of the straight line is the fractal dimension of a floc (Chakraborti *et al*., 2000; Chakraborti *et al*., 2003; Cousin and Ganczarczyk, 1998). Another method of determining floc fractal dimension (the box counting method) was reported by Bushell *et al*. (2002). It is necessary though to obtain high quality floc images in order for the commercial image software packages to be able to distinguish the floc from the background.

2.2.4.2 Small Angle light Scattering (SALS) and Volume Fraction Ratio

The fractal dimension of flocs composed of primary particles smaller than the wavelength of scattered light, are determined by the negative slope of a log-log plot of the light intensity (I) scattered by the floc as a function of the wavenumber (Q) as shown in Equation 2-7.

$$I(Q) \alpha Q^{-D_f} \tag{2-7}$$

where $Q = \frac{4\pi\bar{n}\sin\left(\theta/2\right)}{\lambda}$, $\bar{n}$ is the refractive index of the suspending medium, θ is the scattered angle, λ is the wavelength of the radiation in a vacuum.

Small angle light scattering measurements by the Malvern Mastersizer 3000 (Malvern Instruments) are normally utilised to evaluate the floc size distribution. The scattering behaviour of suspended particles is dependent on the ratio of primary particles size, d_o or d_{fo}, to the wavelength of light scattered, λ.

Another method of determining the fractal dimensions, D, using SALS is to utilise Equation 2-8 which gives a relationship between particle volume distribution, particle size distribution and fractal dimensions (Spicer *et al.*,1998; Oles, 1992; Flesch *et al.*,1999; Kusters, 1997).

$$\frac{V_o}{V_i} \alpha\, d_{mm}^{D-3} \qquad \text{or equivalently} \qquad \frac{\phi_p}{\phi_f} \alpha\, d_{mm}^{D-3} \tag{2-8}$$

where $V_o = \phi_P$ volume fraction of initial suspended particles
$V_i = \phi_f$ volume fraction of flocculated suspension
$d_{mm} =$ mass mean diameter = $d_{50} = d_f$ (floc diameter)
$D =$ fractal dimension

Equation 2-8 is linearized by introducing logs:

$$\log\left(\frac{V_o}{V_i}\right) = D - 3\log\left(d_{mm}\right) + \log\left(k'\right) \tag{2-9}$$

where k' is the proportionality constant.

The fractal dimension is then determined from the slope $\left(m = D - 3\right)$.

2.2.5 Physical Characteristics of Flocculating Particles in Differential Sedimentation

Physical conditions considered during the simulation of sedimentation should satisfy the following conditions at any layer j, time t and depth d: (i) The concentration of total suspended solids (TSS) remaining in solution should be a function of time and depth, (ii) The settling velocity should always be positive, (iii) TSS concentration remaining should increase

with depth, (iv) TSS concentration remaining should decrease with time, and (v) variation of TSS concentration remaining should not increase with depth (the curves must not be convex). These conditions are represented by Equation 2-10 to 2-14 (Je and Kim, 2002).

$$X_j = f(t, d) \tag{2-10}$$

$$\frac{\partial d}{\partial t} \geq 0 \tag{2-11}$$

$$\frac{\partial X_j}{\partial d} \geq 0 \tag{2-12}$$

$$\frac{\partial X_j}{\partial t} \leq 0 \tag{2-13}$$

$$\frac{\partial^2 X}{\partial d^2} \leq 0 \tag{2-14}$$

where X_j = suspended solids concentration (TSS) (ML^{-3}), d = depth, the distance travelled by particle (L), t = time of travel (T).

2.2.6 Existing Models for Iso-Percentile Removal Profiles

Modelling of the particle settling processes relies on the understanding of the dynamics of the flocculation system, variability of sediment concentration and composition, floc size, microbiological activity, salinity and temperature (Khelifa and Hill, 2006). Most current models assume a one dimensional flow of particles in space and are therefore modelled by a set of linear differential equations. However, the true nature of settling particles is highly nonlinear and is influenced by fluctuating initial conditions.

Several analytical systems have been suggested for the simulation of iso-percentile concentration removal profiles. Any suggested model may pass or fail on mathematical grounds or inconsistency with physical systems. According to Je and Kim (2002), a model can fit and predict flocculent settling profiles, only if it does not violate the physical meanings of flocculent settling curves as mentioned earlier (section 2.2.5).

Available iso-percentiles removal models from literature include Ozer's model (1994), Sans' model (1989), Berthouex and Stevens (1982), rule based model by Montgomery (1979), a combination of the rule based with regression by Hayes (1992) , the power law model by Piro and coworkers (2011) and Ramatsoma and Chirwa's model (2012). Amongst the four that were reviewed by Je and Kim (2002), only the Berthouex and Stevens' (1982) model violated the criterion of constraint for settling particles and could not fit data at long settling times.

The best simulation results have so far been obtained using four empirical models below, i.e, Ozer's (1994) model, San's (1989) model, Piro and coworkers' (2011) model and lately Ramatsoma and Chirwa's (2012) model. Ozer's (1994) analytical approach was based on the observation of rainfall intensity duration frequency. The nonlinear relationship between the rainfall intensity, duration, and frequency of occurrence is viewed as a multiplicative model. Hence the author utilised this analogy to model the relationship between concentration percentage, $P^{"}$, remaining in suspension with time and column depth as follows:

$$P^{"} = \alpha_1 d^{\alpha_2} t^{\alpha_3} \tag{2-15}$$

$$P^{"} = \alpha_1 d^{\alpha_2} t^{\alpha_3} - 1 \tag{2-16}$$

where $P^{"}$ = percentage remaining $(X_j/X_o)\times 100$, X_o = initial concentration in the column (ML^{-3}), d = depth travelled by particle during settling (L), and t = time of settling (T). The parameters α_1, α_2, α_3 = empirical fit parameters for the iso-percentile lines.

Sans' (1989) expressed the percentage total suspended solids (TSS) remaining in tank, $P^{"}$, as a function of settling time (T) and depth d (L) in a quiescent settling column, Equation 2-17.

$$P^{"} = \frac{t^{\beta}}{\alpha d^{k} + t^{\beta}} \tag{2-17}$$

where α, β and k = optimisable parameters.
San's and Ozer's models have been shown to comply with the assumptions stated by Je and Kim (2002).

Piro *et al*. (2011) developed the simplest settling model presented by a power law function, Equation 2-18, where the removal of particles is expressed as a function of time at a particular distance from the top of a water column.

$$h = \psi\, t^{B} \tag{2-18}$$

where h represents the depth d (L), t (T) is the residence time, ψ and B are empirical parameters. If a derivative of distance is taken against time, the term decays to the velocity term, Equation 2-19.

$$\frac{dh}{dt} = \psi\, Bt^{B-1} \tag{2-19}$$

Based on this power law, the settling of the particles is descrete (Type I settling) if $B = 1$ and is flocculent if $B > 1$ and ψ is the velocity term (LT^{-1}).

Ramatsoma and Chirwa's semi-empirical model was based on the original assumptions by Özer (1994) to arrive at an analogous model (Ramatsoma and Chirwa, 2012):

$$H_i = H_{\max} + r_1 P^2 t^{r_2} - r_3 P^2 t \tag{2-20}$$

where r_1, r_2 and r_3 are semi-empirical optimisable parameters, H_i = height of sampling points, $H_{\max}$ = design height of proposed tank, and P = percentage removal $(1\text{-}X_j/X_o)\times 100$.

On rearranging Equation 2-20 and writing it with the full range of parameters:

$$P = \left(\frac{-d}{r_1 t^{r_2} - r_3 t} \right)^{0.5} \tag{2-21}$$

where, the following parameter constraints apply within the meaningful physical space with real mass concentration: $d = H_{\max} - H_i$, $r_1 < 0$, $r_2 > 0$ and $0 \le r_3 \sim \frac{0.1}{r_2}$.

Equation 2-21 is then utilised to construct iso-percentile removal profiles for the settling process. Ramatsoma and Chirwa ensured that the model adheres to physical meanings of a settling particle.

The cited empirical models could generate iso-percentile curves, but they are limited in their application since they do not depict how the fractal dimensions of flocs vary during flocculation, a key feature during design. As a result the iso-percentile model developed in this study will follow the pattern of the existing models but would be based on a macroscopic approach of flocculent sedimentation, ie, fractal dimension of flocs.

2.2.7 Existing Settling Velocity Models

2.2.7.1 Models without Fractal Consideration

During settling, suspended particles coalesce with smaller solids to form larger flocs. Settling velocities of cohesive sediments are not uniquely related to particle sizes in Stokes' law because the average density of a floc and surface area properties of the particles are time variant and highly irregular. The transport rate depends on floc size, floc density, fractal dimension and gravity (Lee *et al*., 2002).

In earlier studies by Cho *et al*. (1993), the so called "solid flux" concept for settler calculation was introduced. So far, two empirical models have been utilized successfully for solid flux settler design. These include the power law model, Equation 2-22, and the exponential model, Equation 2-23:

$$v = k'x^{-n} \tag{2-22}$$

$$v = k'\exp(-nx) \tag{2-23}$$

where *k'*, *x* and *n* are the maximum settling velocity, solids concentration and model parameter, respectively. The exponential model is reasonable in dilute concentrations but it is more complicated in designing a settler. The power law model on the other hand becomes infinite in a dilute concentration range.

Je and Chang (2004) derived a simple velocity formula, Equation 2-24, based on Ozer's flocculation model and a one dimensional continuity equation. The equation could predict the transport of resuspended sediments introduced by dredging operations. The same analogy was flowed in this paper, but with a more reliable flocculent-fractal model.

$$V_s = \frac{-ad}{(b'' + 1)\cdot t} \tag{2-24}$$

where *d*, *t*, *a* and *b"* are the settling column depth, time and parameters respectively.

2.2.7.2 Models with Fractal Consideration

Previous work with biological aggregates assumed that flocs settle at velocities close to Stokes' law even if they are fractal in nature (structure) (Li *et al*., 2003; Li and Yuan, 2002). Yet, the diverse distributions of aggregates have an impact on the vertical fluxes of

sediments, resulting in macroflocs settling faster than microflocs. Flocs are highly porous therefore the fluid can penetrate freely, increasing the settling speed.

A lot of attempts have been made to modify stokes' law to incorporate fractal dimensions (Tang and Raper, 2002). Matsumoto and Mori (1975) studied the sedimentation of bentonite coagulated with alum. The exponents in the settling velocity equation were assumed to be equal to those of an impermeable sphere, making the equation inaccurate for flocs. No shape factor was included so the flocs were assumed to be spherical. Tambo and Watanabe (1979) included the sphericity in the velocity model only it was assumed to be a constant value of 0.8 which cannot apply to varying floc sizes. Gmachowski (1996) took into account the fractal dimension of the aggregates. The only disadvantage is that the model still assumes that the overall shape of fractal aggregates is spherical.

The most applied model was derived by Winterwerp (1998) from the balance between the gravitational and drag forces. It was formulated for the velocity of single mud flocs in still water:

$$v_{st} = \frac{\alpha}{18\beta}\frac{(\rho_s - \rho_w)g}{\mu} d_p^{3-D} \frac{d_f^{D-1}}{1 + 0.15\,\mathrm{Re}^{0.687}} \tag{2-25}$$

where $\alpha = \beta = 1$ for spherical particles, D is the fractal dimension, μ is the water dynamic viscosity, d_p is the size of primary particles, d_f is the floc size, g is the specific gravity, ρ_w is the density of water, ρ_s is the density of primary particles forming the flocs, and Re is the Reynolds number.

Equation 2-25 assumes that the mass fractal dimension of primary particles within an aggregate is equal to the mass fractal dimension of the aggregate. This is inaccurate as fractal aggregates have different fractal dimensions from primary particles (Vahedi and Gorczyca, 2012; Maggi, 2007; Maggi *et al*., 2007).

Owing to the wide variety of flocculent settling equations, Johnson *et al*. (1996) developed several scaling relationships to relate particle size, fractal dimension and settling velocity:

$$v_s \alpha\, d^{D-1} \tag{2-26}$$

$$v_s \alpha\, d^{D-D_2+1} \tag{2-27}$$

$$v_s \alpha d^{\frac{D-D_2+b}{2-b}} \tag{2-28}$$

where D is the fractal dimension, D_2 is the two dimensional fractal dimension, the value of b is different for different flow regions.

Even with all these modifications, there is still room for improvement: So in this dissertation a different approach is taken. The practical fractal scaling of Winterwerp (1998) (Equation 2-26) is integrated into an iso-percentile model. This scaling will be automatically transferred to a velocity model that will be derived from the proposed iso-percentile model in combination with hydrodynamics.

2.3 Transport Models Employed in Flocculation

Water quality models seek to describe the partial and temporal changes of constituents involved. A model of choice normally depends on the objectives of the analysis. The basic governing water quality model, Equation 2-29, is generally applied in rivers and has also been adopted for flocculation (Cox, 2003; Rauch *et al*., 1998).

$$\frac{\partial c}{\partial t} = -u\frac{\partial c}{\partial x} - v\frac{\partial c}{\partial y} - w\frac{\partial c}{\partial z} + \frac{\partial}{\partial x}\left(\varepsilon_x \frac{\partial c}{\partial x}\right) + \frac{\partial}{\partial y}\left(\varepsilon_y \frac{\partial c}{\partial y}\right) + \frac{\partial}{\partial z}\left(\varepsilon_z \frac{\partial c}{\partial z}\right) + r'(c,p) \tag{2-29}$$

where c is a multi-dimensional mass concentration for each of the determinants, t is the time, x, y and z are the spatial coordinates, u, v and w are the corresponding velocity components, ε_x, ε_y, ε_z are the turbulent diffusion coefficients for the x, y and z direction, r' is a term representing the rate of change of determinants due to internal transformations.

A couple of authors utilised the basic transport model for a settling column to investigate the interplay of flocculation processes with vertical transport, where rate term (interaction term due to coagulation) is substituted by the classical Smoluchowski's equation or a modification of it. The velocity term is normally substituted by Stokes law or modified Stokes (Xu *et al*., 2008; Sterling Jr *et al*., 2005; Lee *et al*., 2000). However the basic governing solute transport equation (Equation 2-29) can be simplified further for fine grained sediments in quiescent flow. Je and Chang (2004) as well as Je *et al*. (2007) proposed a non-reactive transport equation combined with a flocculation model to deduce a settling velocity model. The same analogy will be followed in this dissertation.

CHAPTER 3

MATERIALS AND METHODS

3.1 Planning

Jar tests are to be conducted to select the coagulant concentrations that would be effective for synthetic sewage and soil particles. The initial total suspended solids concentration (represented by turbidity) would be measured after mixing the dirty water with the coagulant. The coagulant concentration should be different for each experiment. Samples are to be taken in 20 minutes intervals up to 80 min or 120 min for slow settling solids. For each interval two samples should be taken, one sample for particle size distribution analysis/ fractal dimensions, and the other sample for suspended solids analysis (turbidity analysis). Three measurements will be taken per sample and the average of the three will be used for calculations.

3.2 Experimental Procedure

Figure 3-1 shows a simple batch column that was used in the collection of physical data. A 100 L mixing tank was used together with a stirrer to mix synthetic sewage with an aluminium sulphate coagulant ($Al_2(SO_4)_3$ (Experiments No.1-5). In a similar manner, a turbid soil solution was also mixed with different alum concentrations (Experiments No. 6-10).The different coagulant concentrations utilised are shown in Table 3-1 and Table 3-2. A 5 L beaker was used to transfer the dilute suspension from the mixing tank to the column (200 cm × 19 cm diameter). Sampling bottles (100 ml) were used to withdraw samples from the seven column ports (counting from the top) at 20 minutes intervals. The samples were then analysed for turbidity by a HACH Turbidity Meter (Model 2100N, Hatch Company, Loveland, CO). The particle size distribution was determined by a Mastersizer 3000 (Malvern Instruments), specifications are shown in Table 3-3. The entire operation was done at room temperature (25ºC ± 2) and a pH of minimum solubility of alum (6-7).

3.3 Simulation of Dirty Water

In the simulation of dirty turbid water, 80 L of water was poured into the mixing tank and approximately 700 g of dry soil was added to make the water dirty. The coagulant was then added and the stirrer was switched on for 3 min at 180 rpm. The colloidal suspension was

then carefully transferred into the test column. Immediately after filling the column, a minute was allowed for the solution to stabilize before starting the timer for data collection.

The same procedure was followed in synthesizing sewage. Tap water (80 L) was mixed with 96 g milk powder, 40 g starch powder, 12.8 g peptone, 8.8 g meat extract, 2.4 g urea, 2.24 g anhydrous dipotassium hydrogen ortho-phosphate, 0.56 g sodium chloride, 0.32 g calcichloride dehydrate and 0.16 g magnesium sulphate heptahydrate. The procedure to synthesize the sewage was taken from the 'OECD Guideline for the testing of chemicals' published in 2001. A slight modification was done to the OECD synthetic sewage, milk and starch was added to increase the turbidity.

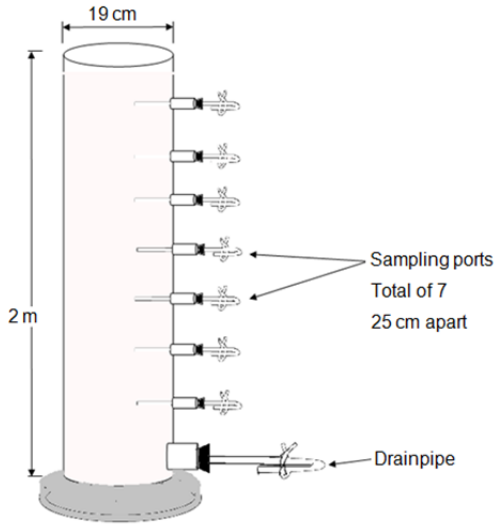

Figure 3-1: Batch Settling Column

Table 3-1: Batch settling column experiments performed for synthetic sewage.

Experiment No.	Coagulant concentration mg/L	Initial turbidity concentration NTU
1	150	389.47
2	200	371.13
3	250	335.00
4	300	425.00
5	350	465.73

Table 3-2: Batch settling column experiments performed for soil particles.

Experiment No.	Coagulant concentration mg/L	Initial turbidity concentration NTU
6	10	227.46
7	20	232.25
8	30	245.02
9	40	216.93
10	50	224.34

Table 3-3: Specifications used in the Mastersizer laser diffraction instrument.

Mastersizer Specifications	
Operator Name	Mastersizer 3000
Sop name	HydroLV.msop
Particle name	Soil or synthetic sewage
Dispersant name	water
Dispersant refractive index	1.330
Particle refractive index (synthetic sewage)	1.35
Particle refractive index (soil)	1.37
Particle absorption index	0.100
Laser Obscuration (%)	Lower limit (2%), higher limit (10%)
Scattering model	Mie
Stirrer speed	Lowest-500 rpm

3.4 Numerical Analysis and Optimisation

Iso-percentile lines were generated by fitting the model, Equation 4-7, to interpolated values of the chosen percentiles from experimental data collected from the settling column. Data interpolation and curve fitting was done using the programming platform, Octave (GNU Octave Version 3.4.2, Free Software Foundation, Boston, MA). The interpolation script can be found in Appendix B. Individual iso-percentile removal profiles were calculated from the geometrical relationship between the TSS percentage removed and column height at any particular time according to the model chosen. Percentage removed concentrations (instead of the mass fraction remaining) were calculated from settling data, Equation 3-1 (Peavy *et al.*, 1985):

$$P_{ij} = 1 - \left(\frac{X_{ij}}{X_o} \right) \tag{3-1}$$

where P_{ij} is the mass percent removed at the ith depth at the jth time interval, X_{ij} is the concentration per port from the column, X_o is the initial suspension concentration.

3.5 Error Analysis in Iso-percentile Profiles

The errors were calculated using the sum of square technique. During simulation, the values from the modelling equation are taken as predicted values. A two way interpolation of experimental data was conducted and the values obtained from interpolation were taken as real values. The sum of square error (SSE) is calculated as the square of the differences of real values and the predicted values:

$$SSE = \sum_i \left(\mathrm{Re}\, al\_values - \mathrm{Pr}\, edicted\_values\right)^2 \qquad (3\text{-}2)$$

\

CHAPTER 4

TOTAL SUSPENDED SOLIDS CONCENTRATION (TSS) ISO-PERCENTILE MODEL DERIVATION

4.1 Achievements by Existing Models

Several authors have developed empirical models to analyse flocculent settling data. The aim was to efficiently draw iso-percentile profiles and deduce the removal efficiency during sedimentation. The models were approved based on adherence to the physical principles of settling particles. Even though a majority of the models can trace iso-removal data, their ability is limited. Some are effective in short retention times and fail at long settling times. Others violate the physical principles of settling particles. None of the iso-percentile models take into consideration the fractal behaviour of particles which is considered key in modelling flocculation. This study aims to introduce the fractal concept in modelling iso-percentile data.

4.2 Model Derivation

Most models used to plot total suspended solids concentration (TSS) sedimentation profiles are empirical in nature. Hence there is a need for a mechanistic way to relate the physical behaviour of particles during settling to observed removal efficiency in clarifiers.

In this study, a flocculation model is developed with due consideration to particle size distribution, fractal dimensions of flocs and iso-percentile flocculation behaviour. The model is in line with the physical characteristics of flocculent settling particles mentioned in section 2.2.5. A model developed earlier by Piro and coworkers (described in chapter 2) saved as a basis for the proposed model. Piro and coworkers concluded that iso-percentile concentration removal data can be represented by a simple power law, Equation 2-18. Piro's model is rewritten here as:

$$h = \psi\, t^{B}$$

where h is the depth (L), t (T) is the residence time, ψ and B are two empirical parameters.

If a derivative of distance is taken against time, in Equation 2-18, the term decays to a velocity term, Equation 2-19:

$$\frac{dh}{dt} = \psi \; Bt^{B-1}$$

This power law best describes discrete particle sedimentation (Type I) when $B = 1$. At higher values of B ($B > 1$) the sedimentation behaviour is flocculent and ψ has the units of velocity (LT^{-1}).

To further attest to this theory, two commonly used empirical literature models (Ozer and San) which are frequently utilised to draw TSS concentration iso-percentile profiles, are expressed as functions of depth as did Piro and coworkers.

Solving for depth d in Sans' model (Equation 2-17) yields the following equation:

$$d = t^{\frac{\beta}{k}}\left(\frac{1-P}{\alpha P}\right)^{\frac{1}{k}} \tag{4-1}$$

where $P^{"}$ = percentage remaining $(X_j/X_o)\times 100$, X_o = initial concentration in the column (ML^{-3}), d = depth travelled by particle during settling (L), and t = time of settling (T). The parameters k, β, α = empirical fit parameters for the iso-percentile lines.

Solving Ozer's model (Equation 2-15) for depth d yields an analogous expression:

$$d = \left(\frac{P}{\alpha_1}\right)^{\frac{1}{\alpha_2}} t^{\frac{-\alpha_3}{\alpha_2}} \tag{4-2}$$

where $P^{"}$ = percentage remaining $(X_j/X_o)\times 100$, X_o = initial concentration in the column (ML^{-3}), d = depth travelled by particle during settling (L), and t = time of settling (T). The parameters α_1, α_2, α_3 = empirical fit parameters for the iso-percentile lines.

Based on mathematical observation of both equations (Ozer and Sans), it can be concluded that flocculent sedimentation adheres to a power law. In order to start evaluating the fundamental settling mechanisms in this study, we simplify the power law to its basic structure which represents the simplified version of Equation 4-1 and 4-2 as follows:

$$d = \; jP^c t^b \tag{4-3}$$

where j represents an approximate velocity as in Piro and coworkers, b and c are simplified constants (parameters that can be optimised). In Equation 4-3, changing one constant does

not affect the other constants, i.e., the suggested coefficients are independent of from each other.

In order to incorporate fractal behaviour in Equation 4-3, fractal dimensions were derived from the volume distribution and particle size distribution of individual flocs using Equation 2-9:

$$\log\left(\frac{V_o}{V_i}\right) = D - 3\log(d_{mm}) + \log(k)$$

$V_o =$ volume fraction of initial suspended particles.

$V_i =$ volume fraction of flocculated suspension at a particular position in the column

$d_{mm} =$ mass mean diameter = $d_{50} = d_f$ (floc diameter)

$D =$ fractal dimension

The relation between the fractal dimension (D), particle/floc diameter (d_f) and an approximate settling velocity determined by Winterwerp (1998) (Equation 2-26) was then adopted. Equation 2-26 is rewritten here as:

$$v \approx d_f^{D-1}$$

Since this is not the actual velocity of flocs, the 'v' term is replaced by term 'a_v'.

$$a_V \approx d_f^{D-1} \tag{4-4}$$

The approximate velocity term, 'a_v', was then plotted against the column height (H) to deduce how it varies down the column during settling. An exponential behaviour was observed in all the coagulants concentrations. Representative graphs are in Figure 4-1.

$$a_V(H) = d_f^{D-1} = m\,e^{-wH} \tag{4-5}$$

where m and w are fit parameters from the plot of 'a_v' versus H.

The relationship between the approximate particle velocity and a specific column height is determined from Equation 4-5 as shown below:

$$H = -\frac{1}{w}\ln\left(\frac{a_V}{m}\right) \tag{4-6}$$

Substituting Equation 4-6 into Equation 4-3, by replacing the approximate term '*j*', yields the iso-percentile flocculation equation in terms of depth (*d*) as a function of fractal dimensions (*D*), PSD (d_f), concentration removed (*P*), residence time (*t*) and model fit parameters, *m, w*, *c* and *b*:

$$d = -\frac{1}{w}\ln\left(\frac{a_V}{m}\right)P^c t^b \tag{4-7}$$

where *d* is the column depth, $a_v = d_f^{D-1}$, *P* is the concentration removed = $(1-X_j/X_o)\times 100$, X_o is the initial TSS concentration, X_j is the TSS sample concentration per column port, *t* is the residence time and *m*, *w*, *c* and *b* are model parameters for iso-percentile fit, with *m* and *w* greater than zero. The parameters *c* and *b* are the power law constants that can be optimized.

Expressing the proposed iso-percentile model (Equation 4-7) in terms of the concentration removed *P* (for use in chapter 5):

$$P = \left(\frac{-wd}{\ln\left(\frac{a_V}{m}\right)t^b}\right)^{\frac{1}{C}} \tag{4-8}$$

The proposed model (Equation 4-7), is compared to Ozer's model and Ramatsoma and Chirwa's model. It is further transformed to a velocity model in chapter 5 to improve the analysis of settling particles. The iso-percentile profiles give an indication of the removal efficiency. The velocity on the other hand gives a practical feel of how fast the particles are settling.

The velocity of particles is also a key feature in the design or sizing of sedimentation tanks. It determines the fate of particles, ie, which particles will be removed or remain in suspension, something that is not clear cut in iso-percentile profiles. It is possible to deduce the velocity from the iso-percentile profiles. The slope at any point in the iso-percentile line is the instantaneous velocity of the fraction of particles represented by that line (Peavy *et al*., 1985). Rather than drawing slopes at every point of the iso-percentile curves to calculate the instantaneous velocity, it is reasonable to derive an equation that will predict the velocity. This is vital since it is difficult to deduce settling velocities *in situ*.

4.3 Model Assumptions

The relationship between particle diameter and fractal dimension, given by parameter 'a_v' (approximate velocity), was plotted to deduce how it varies during settling (down the column) (Figure 4-1). An exponential decay was observed for each coagulant concentration implying a quick shift from the Euclidean to fractal dimension. This trend of a_v as a function of height ($a_v(H)$), lead to simplifying assumptions of the iso-percentile model.

In order to simplify the iso-percentile model, the behaviour of the function a_v *(H)* was analysed. It was observed that the function takes two forms, the transient state and equilibrium state. The transient state was dominant on the first three column ports whereas the equilibrium state was evident at the last four column ports. At the transient state the values of function a_v *(H)* are highly variant. As a result the values of a_v *(H)* for one alum concentration could not be related to other values of a_v *(H)* at different alum concentrations. Hence values of a_v *(H)* considered to be of major significance in the model (representative a_v *(H)* values) are based on the equilibrium state region.

The equilibrium state part of the function (Equation 4-5) was equated or associated with the limit of the function. In other words, as the function a_v *(H)* approaches its limit value, it lies within the interval of a_v *(H*$_4$*)* and a_v *(H*$_7$*)* (the numbers 4 and 7 refer to the fourth and seventh port form the top of the column) (Figure 4-1). An average of these values was calculated for each alum concentration to represent the approximate velocity 'a_v' utilized in the iso-percentile model, Equation 4-7 (those values are displayed in the sum of square error tables along with other model parameters in a subsequent discussion). The limit value of a_v *(H)* for fractal aggregates is one, such that any value of a_v below one indicates that the majority of the aggregates are disjointed masses, Equation 4-9. The values of a_v are presented in Table 4-3 and 4-4 along with average floc diameters.

$$\lim_{H\to 0.25} a_V(H) \equiv \lim_{D\to 1} d_f^{D-1} = 1 \qquad (4\text{-}9)$$

where H = 0.25 m is the lowest column height (the seventh port down the column) equivalent to the depth d of 1.75 m from the top of the column. D is the fractal dimension and d_f is the mass mean diameter (d_{50}) of the flocs.

Spicer and Prasins (1996) showed that aggregates reach an equilibrium state structure and floc size distribution. In their discussion they reasoned that a stable particle size distribution is maintained by floc breakage, which also minimises further aggregate growth. This implies that the flocs may increase until a constant diameter is reached with constant velocity and remain either as flocs or break due to high porosity and fragility. This fact also further supports the assumption of utilising equilibrium state values of a_v *(H)* in this study.

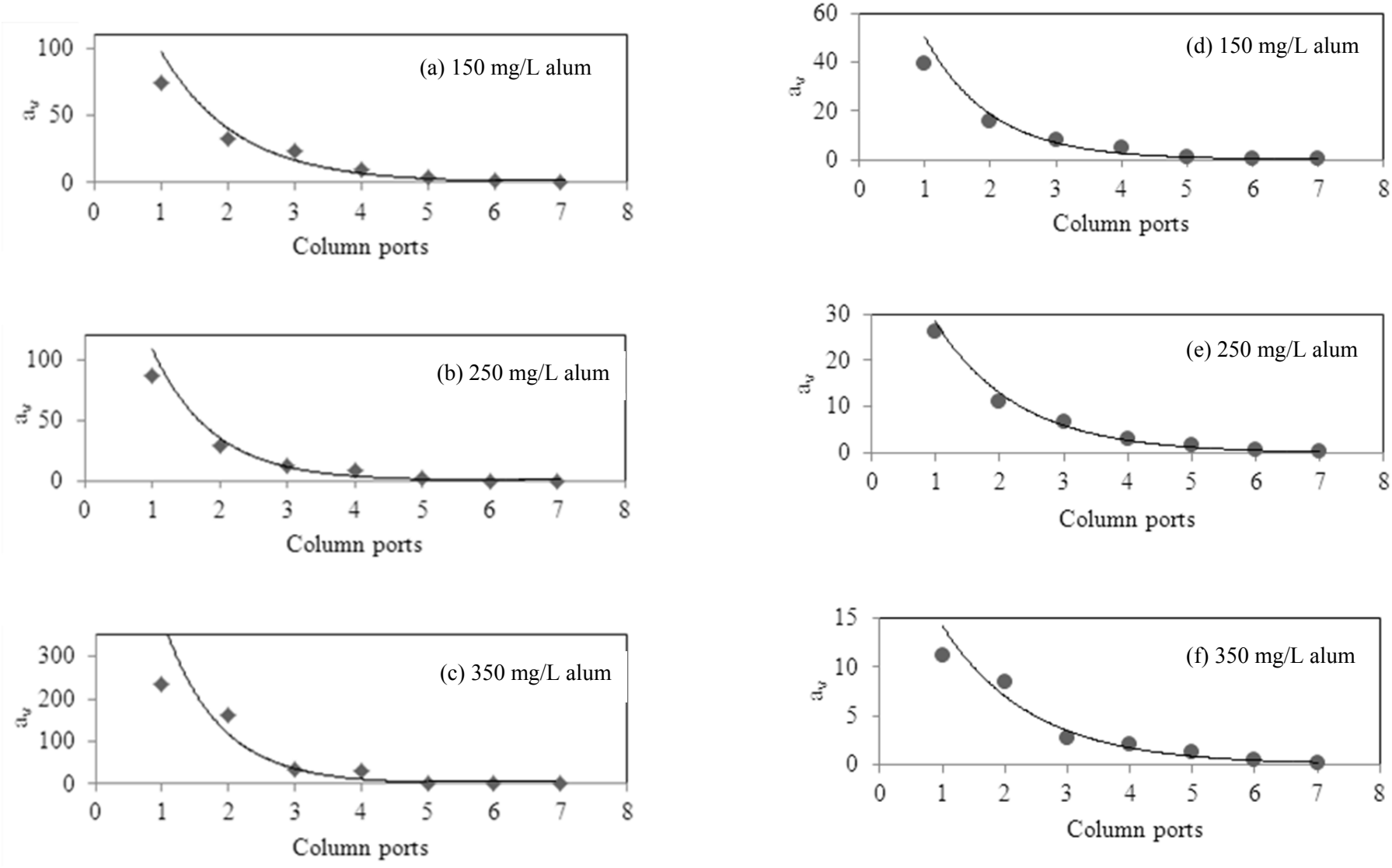

Figure 4-1: The exponential behaviour of $a_V = d_f^{D-1}$ down the column for synthetic sewage (a, b, c) and soil particles (d, e, f).

4.4 Determination of Fractal Behaviour of Particles

The evolution of the normalised floc size distribution is shown for the minimum (150 mg/L), middle (250 mg/L) and maximum (350 mg/L) coagulant concentration with synthetic sewage (Figure 4-2). In the soil particles (Figure 4-3), the lowest alum concentration considered is 20 mg/L instead of 10 mg/L because the 10 mg/L alum was too low to produce presentable results in all the iso-percentile models. The middle concentration is 30 mg/L and the highest is 50 mg/L alum. Similar trends of the particle size distribution (PSD) for the other coagulant concentrations are shown in Appendix A (Figure A-1).

The volume distribution was plotted against particle size for specific heights only for the sole purpose of extracting the normal distribution information for fractal dimensions. The PSD or volume distribution curves shown are for the samples taken from the seven ports down the column for the first 20 min of flocculation. There was a range of sizes where the majority of the particles belonged. For the synthetic sewage the majority of the flocs were between 5µm and 60 µm. The soil flocs were between 5 µm and 80 µm after 20 min (Figure 4-2 and 4-3).

From the PSD it is evident that flocculation increases the diameter of particles. At the initial stages of flocculation, where the alum concentration is dominant, the primary particles collide rapidly and grow. As a result the PSD evolves rapidly from monodispersity broadening into larger floc diameters. Figure 4-2 and 4-3 also show that the PSD also evolves per coagulant concentration. This is evident by the increase of the peak height indicating the initial volume distribution for each concentration in both sewage and soil particles. This is in good agreement with literature findings like that of Spicer *et al*. (1998).

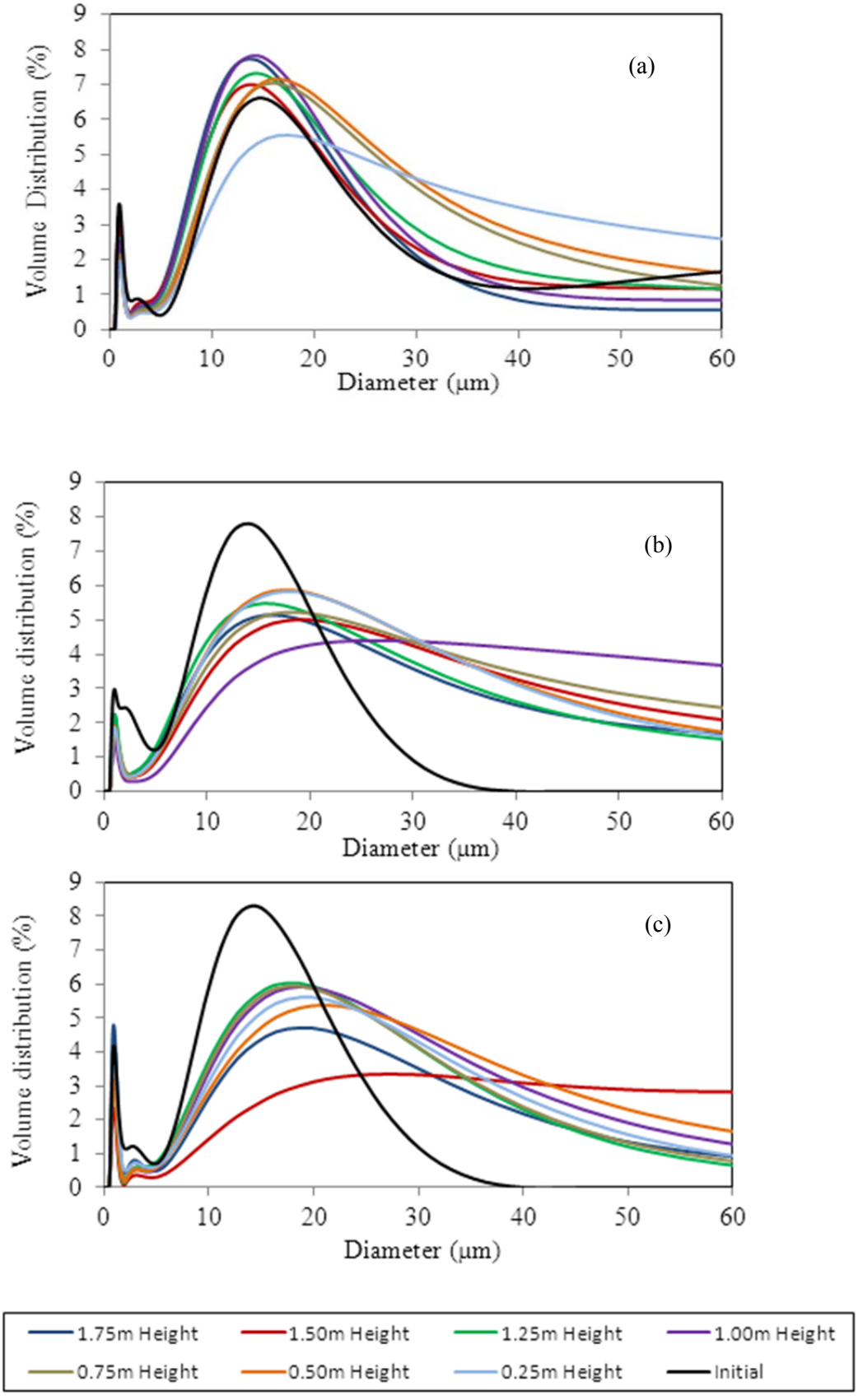

Figure 4-2: PSD for synthetic sewage with: a) 150 mg/L alum b) 250 mg/L alum c) 350 mg/L alum.

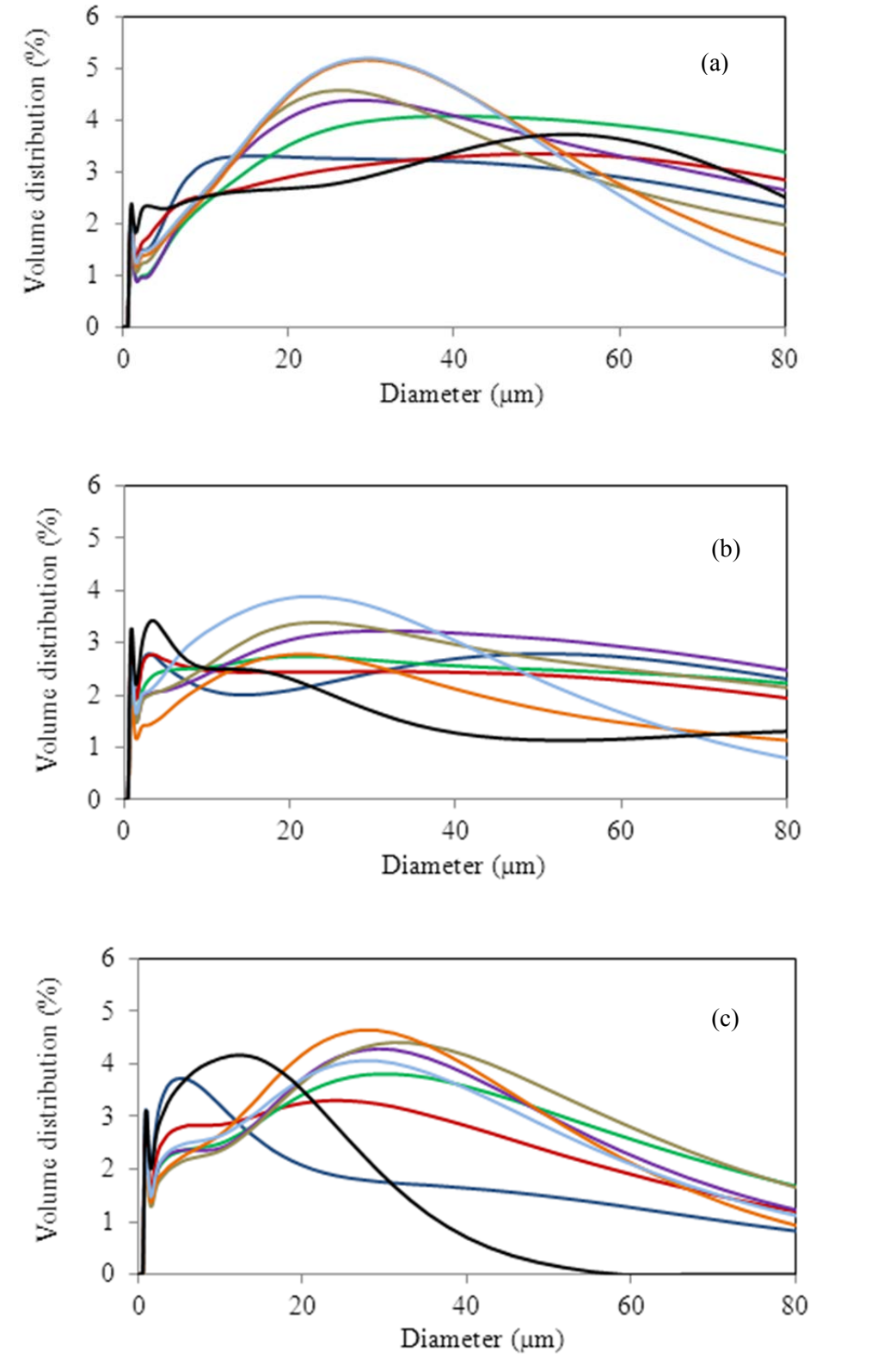

Figure 4-3: PSD for soil particles with: a) 20 mg/L alum b) 30 mg/L alum c) 50 mg/L alum.

Fractal dimensions were then deduced from the PSD using Equation 2-9 as shown in Figure 4-4.The straight lines produced are in line with literature results where the equation was taken (Spicer *et al*., 1998; Oles, 1992; Flesch *et al*., 1999; Kusters, 1997). The variation in size of the volume distribution profiles, as noticed in Figure 4-2 and 4-3, lead to the different axis scaling observed in Figure 4-4. The different slopes are proof that the fractal dimension varied during settling (down the column). The fractal dimensions are determined from the slopes $(m = D - 3)$ of the graphs in Figure 4-4 and are documented in Table 4-1.

In Table 4-1 and 4-2, it can be noted that fractal dimensions decreased with increasing floc sizes, since flocs size increases during aggregation and settling. The fractal capacity (dimension) is different for all time frames and column ports. This could be due to the existence of different pore sizes within the flocs, which are caused by different packing of primary particles and hydrodynamic flow patterns within and around the flocs. Previously it was assumed that the fractal dimension remained constant over the floc population. However in this study we show that porous flocs are characterised by low fractal or capacity dimensions (<3) as observed in Table 4-1 and 4-2. This implies that the porosity increased as the density of flocs decreased leading to different flow or settling patterns. This finding is also in line with recent literature modifications on fractal scaling by other authors such as Maggi, (2007); Maggi *et al*. (2007); Vahedi and Gorczyca, (2012).

According to Wu *et al*. (2002), fractal dimensions range between 1 and 3 ($1 \leq D < 3$), yet in Table 4-1 and 4-2 it is observed that some of the values are below 1, especially towards the end of the column. This may be due to floc breakup or restructuring which occurs during flocculation. This implies that flocs with fractal dimensions less than one exist as multiple disjointed masses rather than a contiguous unit mass (Maggi, 2007). Moreover the accumulation of flocs with time at the bottom of the column may alter the true floc dimension at the lowest ports. Non-fractal dimensions in this study are also evident due to the nature of the flocs formed. Alum flocs have been reported to be highly fragile and vulnerable to breakage by Zhai and Liu (2009).

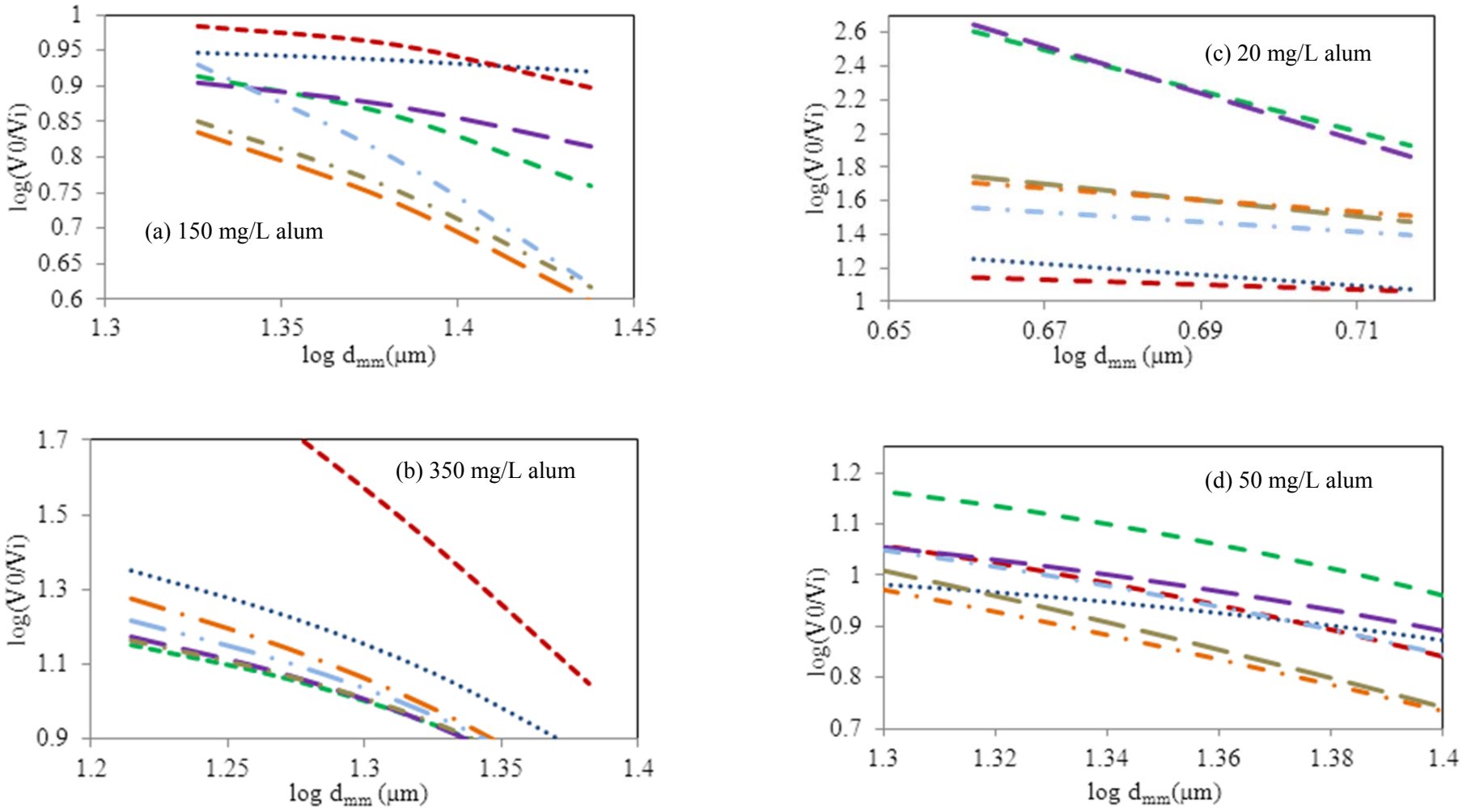

Figure 4-4: Determination of fractal dimensions from the slope of volume fraction for sewage flocs (a, b) and soil flocs (c, d).

Table 4-1: Fractal dimensions for synthetic sewage with: a) 150 mg/L alum b) 250 mg/L alum c) 350 mg/L alum.

a)

	fractal dimension *D* (dimensionless) (150 mg/L)				
Depth (m)	20 min	40 min	60 min	80 min	average D
0.25	2.71	2.69	2.76	2.68	2.71
0.50	2.53	2.19	2.16	2.51	2.35
0.75	2.18	2.34	2.06	2.19	2.19
1.00	1.88	1.73	1.92	1.83	1.84
1.25	0.98	1.48	1.85	1.52	1.46
1.50	0.43	0.81	1.53	1.73	1.13
1.75	0.23	0.31	0.84	0.98	0.59

b)

	fractal dimension *D* (dimensionless) (250 mg/L)				
Depth (m)	20 min	40 min	60 min	80 min	average *D*
0.25	2.69	2.54	2.53	2.78	2.63
0.50	2.32	2.21	2.14	2.16	2.21
0.75	1.94	1.87	2.54	1.16	1.88
1.00	2.11	1.63	1.90	1.22	1.72
1.25	1.85	0.85	1.06	0.91	1.17
1.50	0.30	0.46	0.27	0.67	0.43
1.75	0.80	0.16	0.22	0.39	0.39

c)

	fractal dimension *D* (dimensionless) (350 mg/L)				
Depth (m)	20 min	40 min	60 min	80 min	Average D
0.25	2.93	2.99	2.80	3.00	2.93
0.50	2.75	2.65	2.61	2.58	2.65
0.75	2.55	0.94	2.45	2.30	2.06
1.00	2.72	1.89	1.41	1.97	2.00
1.25	1.39	1.35	0.56	1.88	1.30
1.50	1.36	0.70	0.10	0.92	0.77
1.75	1.31	0.68	0.26	0.69	0.74

Table 4-2: Fractal dimensions for soil particles with: a) 20 mg/L alum b) 30 mg/L alum c) 50 mg/L alum.

a)

	fractal dimension *D* (dimensionless) (20 mg/L)				
Depth (m)	20 min	40 min	60 min	80 min	average D
0.25	1.85	2.75	2.91	2.75	2.56
0.50	1.37	2.50	2.33	2.42	2.15
0.75	0.88	1.40	2.58	2.22	1.77
1.00	0.99	1.20	2.18	2.01	1.60
1.25	0.51	0.13	2.16	0.98	0.95
1.50	0.51	0.31	1.05	0.55	0.60
1.75	0.10	0.16	0.35	0.42	0.26

b)

	fractal dimension *D* (dimensionless) (30 mg/L)				
Depth (m)	20 min	40 min	60 min	80 min	average D
0.25	1.96	2.52	2.40	2.77	2.41
0.50	1.12	1.99	2.78	2.21	2.02
0.75	1.37	1.55	2.05	2.07	1.76
1.00	1.31	1.45	1.84	1.10	1.43
1.25	1.22	0.73	1.78	0.91	1.16
1.50	0.84	0.66	0.72	0.88	0.77
1.75	0.61	0.08	0.50	0.75	0.48

c)

	fractal dimension *D* (dimensionless) (50 mg/L)				
Depth (m)	20 min	40 min	60 min	80 min	average D
0.25	2.70	2.43	2.51	2.30	2.48
0.50	2.14	2.04	2.03	2.11	2.08
0.75	1.58	1.24	1.19	1.86	1.47
1.00	1.47	1.36	1.13	1.25	1.30
1.25	1.04	1.17	1.09	1.08	1.10
1.50	0.74	0.94	0.57	0.55	0.70
1.75	0.22	0.17	0.23	0.48	0.27

The dominant flocculation mechanisms include both particle-cluster ($2.5 \leq D \leq 3$) and cluster-cluster ($1.6 \leq D \leq 2.2$) since both fractal ranges are evident in the fractal results. Visual observation of the variant fractal dimension down the column also suggests that diffusion-limited colloidal aggregation was dominant at the top of the column whereas the reaction-limited colloidal aggregation was dominant at the bottom. Similar mechanisms are observed for both the synthetic sewage, Table 4-1, and the soil samples, Table 4-2.

The validity of the fractal behaviour in this study was also tested using the power law fractal model by Maggi, (2007); Maggi *et al*. (2007). The graphs of fractal dimension D versus the dimensionless size $\ell = d_f/do$, (where do is the size of primary particles and d_f is the floc size) were plotted, Figure 4-5. The linear relationship observed in Figure 4-5 proves that the fractal behaviour in this study also follows a power law. This concept extends the understanding of the behaviour of the flocculent particles at the microscopic structural level, which could enhance the accuracy of predicting the behaviour of flocculent settling.

The mass median diameters of the flocs (d_{50}), representing the floc diameter (d_f), are tabulated in Table 4-3 and 4-4, along with calculations for parameter 'a_v' and the dimensionless ratio $\ell = d_f/do$. The mean diameters are seen to be increasing down the column, as anticipated. Floc growth is caused by frequent inter-particle collisions due to orthokinetic flocculation (while mixing the coagulant with dirty water), perikinetic flocculation (particle movement due to Brownian motion) and differential sedimentation (settling of particles). Contrary to some literature reports, there was no significant increase in diameter with increase in residence time. This could be because there are no multiple additions of the coagulant in this study. The model developed focused on differential sedimentation.

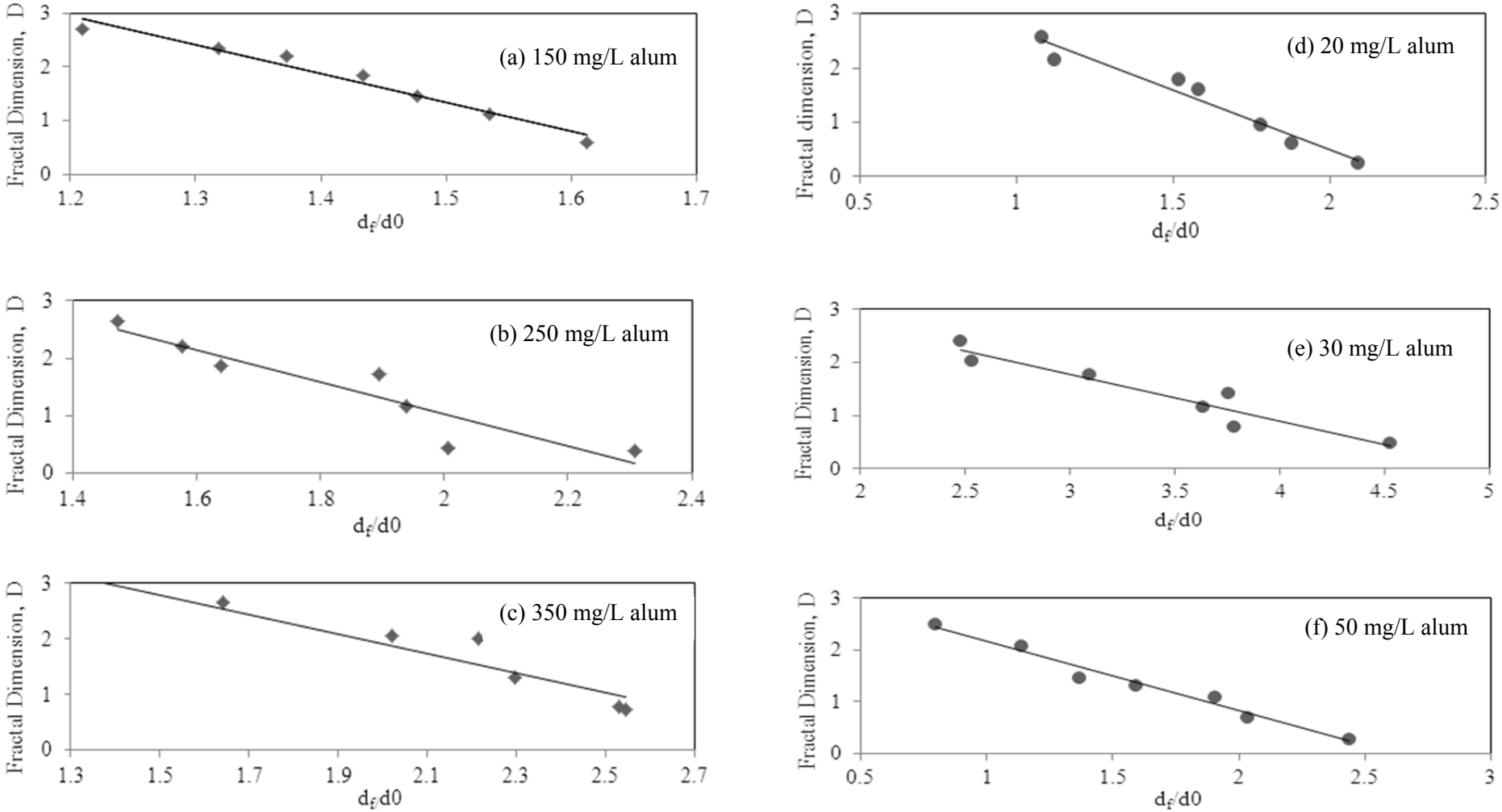

Figure 4-5: Power law relationship of fractal dimensions with dimensionless size $\ell = d_f/do$ for synthetic sewage flocs (a, b, c) and soil flocs (d, e, f).

Table 4-3: The variation of , $a_V = d_f^{D-1}$, d_f, and d_f/do down the column for synthetic sewage with a) 150 mg/L alum b) 250 mg/L alum c) 350 mg/L alum.

a)

	d_f = d_50 µm (150 mg/L)						
Depth (m)	20 min	40 min	60 min	80 min	average d_f	d_f/d0	$a_v = d_f$^D-1
0.25	12.15	11.67	13.67	12.04	12.38	1.21	74.00
0.50	13.42	12.16	15.97	12.44	13.50	1.32	33.24
0.75	13.01	13.43	15.67	14.08	14.05	1.37	23.36
1.00	14.67	14.76	15.83	13.44	14.68	1.43	9.55
1.25	14.57	15.09	14.98	15.82	15.12	1.48	3.45
1.50	16.67	13.93	15.17	17.07	15.71	1.54	1.41
1.75	18.43	14.66	17.33	15.60	16.51	1.61	0.32
d0	10.23						

b)

	d_f = d_50 µm (250 mg/L)						
Depth (m)	20 min	40 min	60 min	80 min	Average d_f	d_f/d0	$a_v = d_f$^D-1
0.25	14.80	14.17	18.03	14.40	15.35	1.47	86.54
0.50	15.10	13.27	22.80	14.60	16.44	1.58	29.37
0.75	19.73	16.23	16.50	15.90	17.09	1.64	12.03
1.00	12.60	28.33	21.60	16.50	19.76	1.89	8.45
1.25	21.83	19.93	20.40	18.73	20.22	1.94	1.65
1.50	20.27	21.67	21.53	20.27	20.93	2.01	0.17
1.75	22.13	24.20	25.80	24.16	24.07	2.31	0.14
d0	10.43						

c)

	d_f = d_50 µm (350 mg/L)						
Depth (m)	20 min	40 min	60 min	80 min	average d_f	d_f/d0	$a_v = d_f$^D-1
0.25	16.30	18.33	17.00	16.43	17.02	1.27	236.69
0.50	20.33	21.17	21.47	24.83	21.95	1.64	161.74
0.75	26.40	27.93	27.13	26.60	27.02	2.02	32.83
1.00	28.67	29.20	28.30	32.37	29.63	2.22	29.31
1.25	33.37	26.93	27.60	34.90	30.70	2.30	2.75
1.50	33.70	35.47	30.63	35.50	33.83	2.53	0.45
1.75	33.37	30.03	36.43	36.33	34.04	2.55	0.39

Table 4-4: The variation of $a_V = d_f^{D-1}$, d_f, and d_f/do down the column for soil particles with a) 20 mg/L alum b) 30 mg/L alum c) 50 mg/L alum.

a)

	d_f = d_50 µm (20 mg/L)						
Depth (m)	20 min	40 min	60 min	80 min	average d_f	d_f/d0	$a_v = d_f$^D-1
0.25	15.17	8.04	8.96	10.00	10.54	1.08	39.69
0.50	16.80	10.42	10.17	6.42	10.95	1.12	15.84
0.75	25.07	10.87	12.50	10.87	14.83	1.52	8.00
1.00	22.70	11.85	15.33	11.85	15.43	1.58	5.11
1.25	19.47	16.20	17.47	16.20	17.34	1.78	0.86
1.50	18.97	17.80	18.67	17.80	18.31	1.88	0.32
1.75	17.70	21.93	19.93	21.93	20.37	2.09	0.11
d0	9.74						

b)

	d_f = d_50 µm (30 mg/L)						
Depth (m)	20 min	40 min	60 min	80 min	average d_f	d_f/d0	$a_v = d_f$^D-1
0.25	3.87	9.16	13.13	14.33	10.12	2.48	26.12
0.50	5.11	8.70	10.75	16.84	10.35	2.53	10.95
0.75	6.35	12.13	13.81	18.21	12.63	3.09	6.85
1.00	10.94	15.27	14.63	20.53	15.34	3.76	3.20
1.25	8.64	14.67	15.07	21.01	14.85	3.64	1.53
1.50	10.40	13.00	16.02	22.33	15.44	3.78	0.54
1.75	14.07	17.20	17.79	24.88	18.49	4.53	0.22
d0	4.08						

c)

	d_f = d_50 µm (50 mg/L)						
Depth (m)	20 min	40 min	60 min	80 min	average d_f	d_f/d0	$a_v = d_f$^D-1
0.25	9.87	1.38	4.97	4.05	5.07	0.80	11.14
0.50	9.59	5.30	7.60	6.54	7.26	1.14	8.51
0.75	13.50	7.89	6.34	7.13	8.72	1.37	2.75
1.00	13.57	8.33	8.44	10.24	10.14	1.59	2.01
1.25	16.67	11.59	5.46	14.86	12.14	1.91	1.27
1.50	14.40	10.87	12.28	14.30	12.96	2.04	0.46
1.75	15.53	12.83	18.49	15.31	15.54	2.44	0.14
d0	6.36						

4.5 Evaluation of Model against Settling Data

Suspended solids concentration data was collected from settling columns in experimental runs of 80 min (or 120 min for those taking longer to settle) in a 2.0 m column. Representative results of suspended solids concentration data from settling column tests and their corresponding percentage removal data are shown in Appendix A, Table A-1 and Table A-2 for synthetic sewage particles and Table A-3 and A-4 for soil particles. The results collected were characteristic of most data from similar water samples (where, TSS concentration increases during settling due to floc formation). Examples are found in a range of technical texts including MetCalf and Eddy (2003), Reynolds and Richards (1996), Sawyer *et al*. (2003) and others. The conventional methods of analysing these data is by calculating percentage removals (usually by spreadsheet), plotting interpolation points, followed by plotting smoothed iso-percentile lines using a model. These results are further analysed in chapter 5.

4.5.1 Interpolation and Simulation

Before the simulation of model iso-percentile lines, a computational algorithm was used to generate raw percentage removal data points by interpolating data from a settling column. Normally, this exercise is done by hand in industry. The automated interpolation (of experimental data) was conducted across the grid in the zero and ninety degree directions from a given data point (interpolation script is shown in Appendix B). The accuracy of the interpolated data set is critical to the accuracy of the final percentiles since these provide the fixed scaffold points for parameter optimisation and therefore determine the degree of the overall model accuracy. For this reason, the improvement of the interpolation procedure is regarded in this study as the key to achieving parameters of highest possible accuracy for the physical design of separation systems such as clarifiers.

The model presented in Equation 4-7 was used to provide the smooth lines to approximate the trajectory of constant percentile removal profiles. The model was tested against data collected in the laboratory. The proposed model's performance (fitting of datasets) was compared to literature models such as Ozer's model and Ramatsoma and Chirwa's model, since the foregoing models were shown to be consistent with the physical basis of flocculent sedimentation. Ozer's model is also considered simple and mostly applicable in industry (Je and Chang, 2004). However Ramatsoma and Chirwa (2012) provided a better performing model in data collected under laboratory conditions. Ramatsoma and Chirwa's model

produced a lower sum of squared errors when compared to Ozer's model.

Typically, iso-percentile plots do not fit all areas of the data equally well. In practice, the accuracy of the interpolation is only seen after simulation of the whole data set and is evaluated holistically. This process can be improved by including two or more data points from the surrounding iso-percentile line then establish a point and use statistical means to improve accuracy.

In this study, the comparison of results for iso-percentile synthetic sewage profiles is based on the lowest coagulant concentration tested in the study (150 mg/L alum), the middle coagulant concentration (250 mg/L alum) and the highest coagulant concentration tested (350 mg/L alum). The same procedure was followed in comparing results in the test using suspended soil particles. The lowest coagulant concentration considered is 20 mg/L alum, then a middle coagulant concentration of 30 mg/L and the highest concentration of 50 mg/L alum in the soil particle test. The rest of the results are shown in Appendix A (Figures A-5 to A-8).

Overall visual inspection of the iso-percentile computations using the proposed mechanistic model achieves a reasonably accurate representation of the percentile removals. The proposed model was proficient in fitting the experimental data and therefore resulted in low sum of square errors. Even at long retention times, it still could trace the interpolated data accurately. Representative data is presented in Figures 4-6 (a), 4-7 (a) and 4-8 (a) for synthetic sewage flocs.

The model developed in this study (referred to as the velocity flocculation model), displayed a better fit when compared with Ozer and Ramatsoma and Chirwa's models (Figure 4-6) at an alum concentration of 150 mg/L. Ozer's model in Figure 4-6 (b) overestimated the interpolated data at 60%, 70% and 80% removal profiles. Ramatsoma and Chirwa's model in Figure 4-6 (c) underestimated the interpolated profiles such that a 70% model line fits a 60% interpolation line and the 80% model line fits the 70% interpolation line. This is attributed to low coagulant concentrations which are evident when 50% of the solids have been removed. Hence the semi-empirical models fail to predict the behaviour of less intense flocculation or of highly dilute solutions with removal percentiles above 60% in the 150 mg/L alum solution. This suggests that the empirical models could only function in a narrow iso-removal range.

At 250 mg/L alum concentration, a proper fit is still observed for the proposed velocity flocculation model. The other models (Ozer and Ramatsoma and Chirwa) could also trace the interpolated profiles for the 250 mg/L alum dose (Figure 4-7). Ramatsoma and Chirwa's model only overestimates the 60% and 90% interpolation profiles, but the overall fit is satisfactory (Figure 4-7 (c)). Ozer's model overestimates the 70%, 80% and 90% interpolation lines. This is evident at long retention times (after 70 min), where the difference between the real profile and the model profile increases, and the 80% model line runs through the 90% interpolation profile (Figure 4-7 (b)). The data also suggests that Ozer's model is most suitable at short retention times.

At 350 mg/L alum concentration, the proposed velocity flocculation model still shows an ideal fit (Figure 4-8 (a)). Ozer's model underestimates the 70% interpolation line and overestimated the 90% interpolation line. However, the overall fit is reasonable (Figure 4-8 (b)). Ramatsoma and Chirwa's model fits well but overestimates the 90% interpolation profile (Figure 4-8 (c)). The inconsistency of semi-empirical models (Ozer's model and Ramatsoma and Chirwa's model) suggests that these models may not be used with confidence to predict long term changes in flocculation. This is probably because they lack fractal characterisation which is profound in flocculation behaviour.

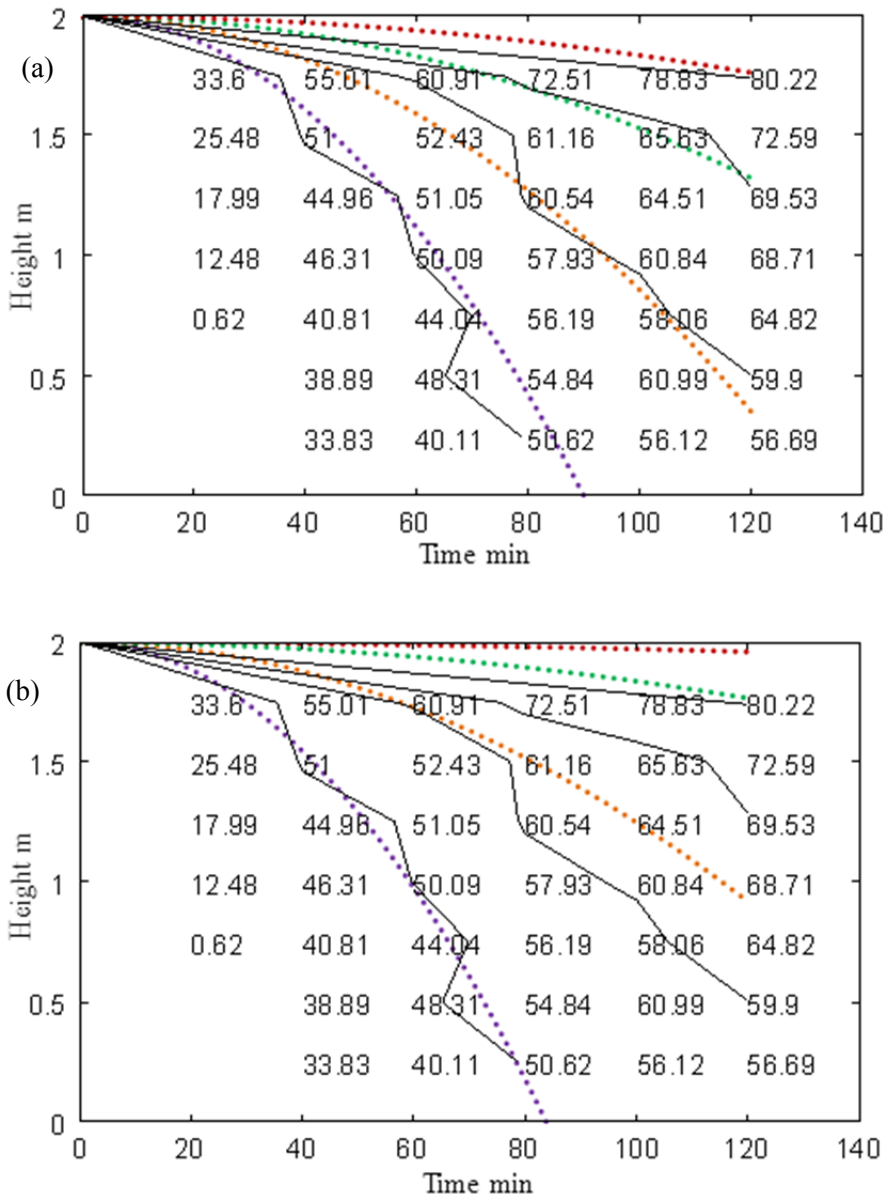

Figure 4-6: Interpolation results and iso-percentile removal profiles for 150 mg/L alum and synthetic sewage simulated by: (a) the proposed model, (b) Ozer's model and (c) Ramatsoma and Chirwa's model.

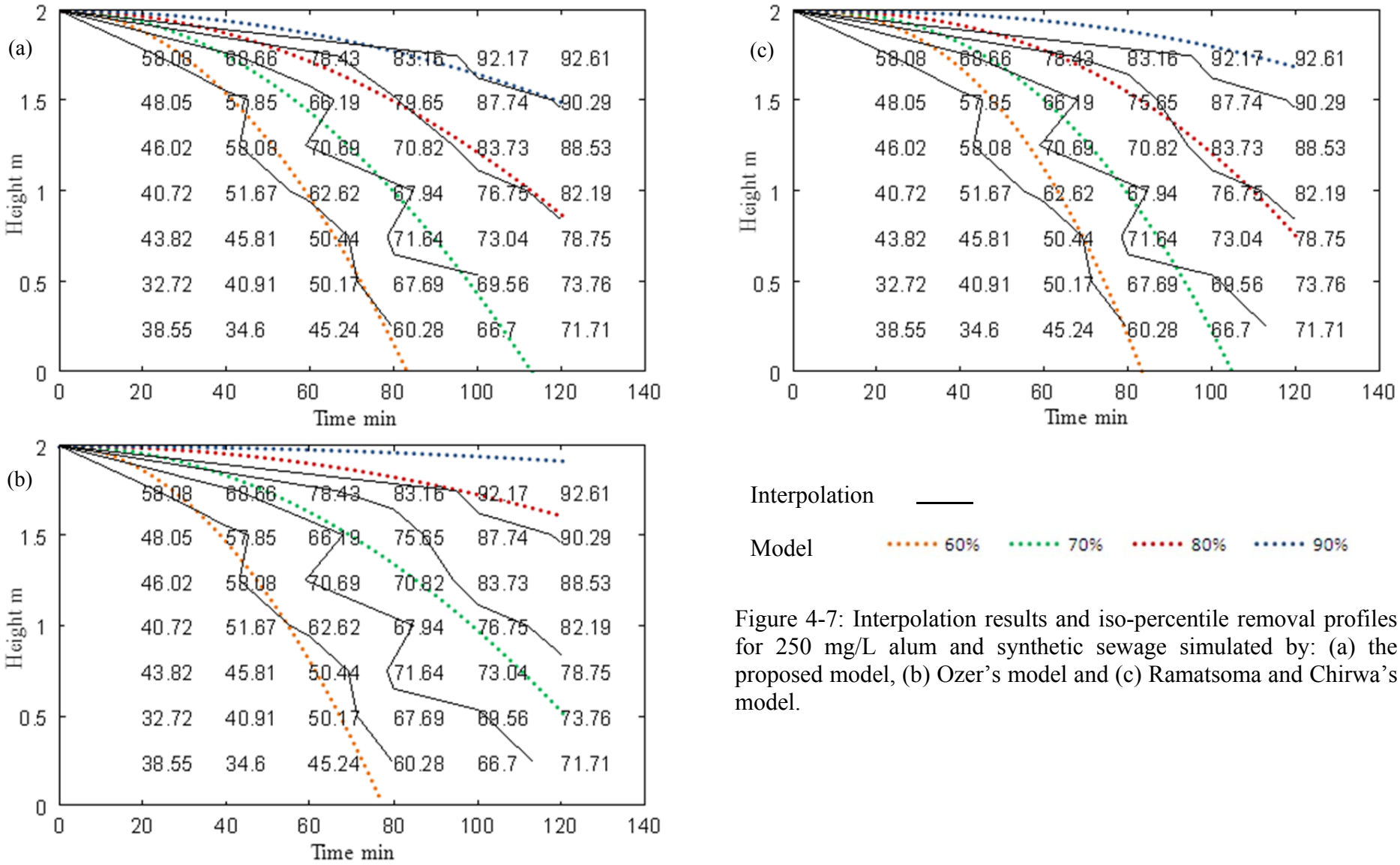

Figure 4-7: Interpolation results and iso-percentile removal profiles for 250 mg/L alum and synthetic sewage simulated by: (a) the proposed model, (b) Ozer's model and (c) Ramatsoma and Chirwa's model.

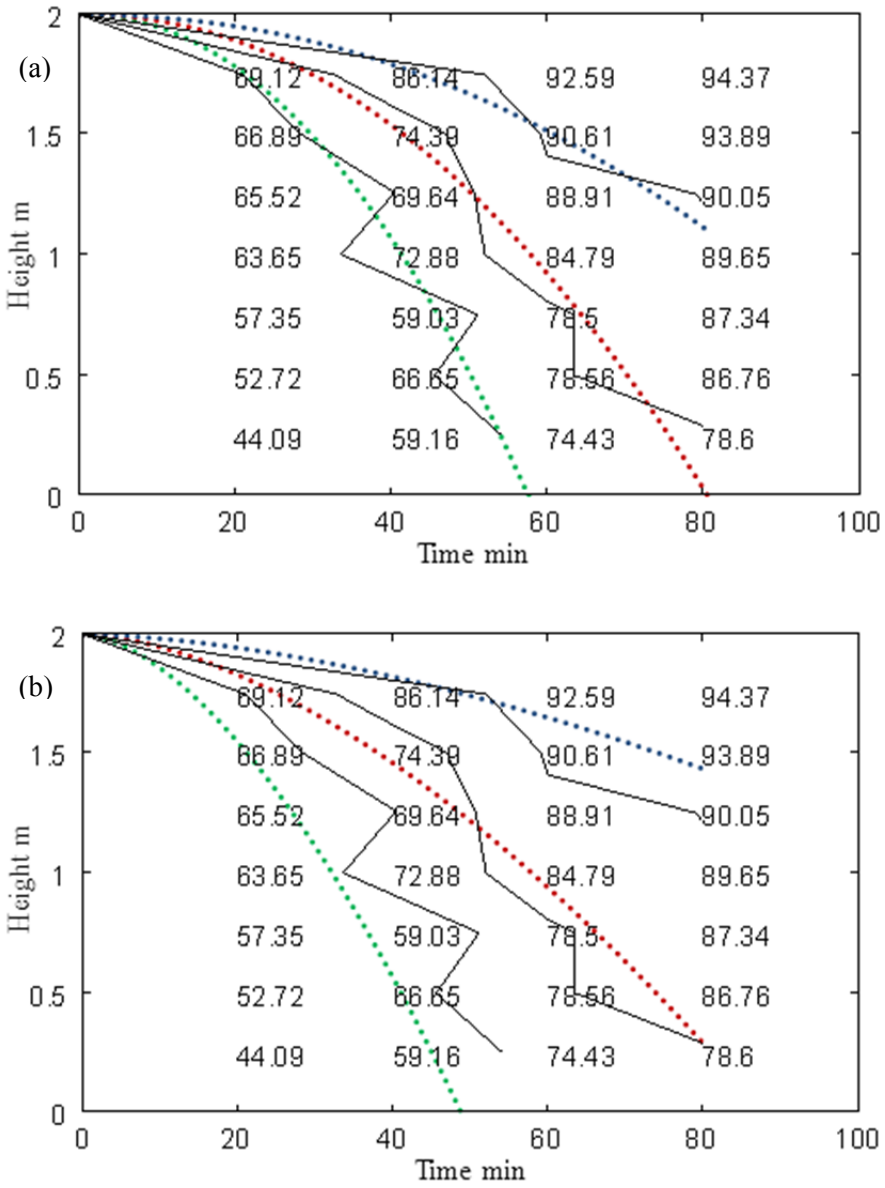

Figure 4-8: Interpolation results and iso-percentile removal profiles for 350 mg/L alum and synthetic sewage simulated by: (a) the proposed model, (b) Ozer's model and (c) Ramatsoma and Chirwa's model.

For the soil particles the proposed velocity flocculation model successfully tracked the interpolated data points especially for the 50 mg/L alum concentration. Slight discrepancies were noticed for the 30 mg/L and 20 mg/L alum concentrations. This shows that even at lower coagulant concentrations the model successfully predicted the flocculent sedimentation behaviour better than previously proposed models.

At 20 mg/L alum the velocity flocculation model overestimates the 70% and 80% interpolation profiles between 30 min and 60 min, Figure 4-9 (a). Ozer' model could barely fit the 80% and 90% interpolation profiles with the model overestimating the all the removal profiles. The 90% interpolation line was fitted by the 80% model profile. Ramatsoma and Chirwa's model could hardly fit the interpolation profiles, underestimating both the 70% and 80% interpolation profiles. This could be due to insufficient flocculation that occurs at low alum concentrations. Since the models are designed to trace flocculated particles, slow forming flocs or particles that did not flocculate are mis-represented by the models. At such low alum concentrations the coagulant would take time to initiate the flocculation process thus longer retention times are necessary in order for the models to quantitatively estimate interpolation profiles.

The velocity flocculation model underestimated all the removal profiles for the 30 mg/L alum dose, Figure 4-10 (a). The 70% removal profile only displays a reasonable fit after 40 minutes. The 80% and 90% model lines intersect the interpolation lines after 60 minutes. A longer residence time was necessary for the flocculation to take effect. The low coagulant dose could have caused slow forming, fragile aggregates which are more prone to breakage and restructuring. In the transition phase (breakage and restructuring) a majority of particles are not solid flocs but disjointed masses. Since the proposed velocity flocculation model was designed based on fractal dimensions, it inevitably fails when particles display non fractal nature.

Ozer's model also had difficulty tracing the iso-percentile profiles for the 30 mg/L alum dose, Figure 4-10 (b). It completely lost track of the 70% interpolation profile approximating a lower settling profile. The other profiles (80% and 90%) only fit after 60 minutes. The same scenario is observed for Ramatsoma and Chirwa's model although the model fits better than Ozer's model, Figure 4-10 (c). This is also attributed to low coagulant concentrations and thus less intense flocculation. Since the semi-empirical models are not designed based on

fractal dimensions, uncertainties in their predictions are expected.

The velocity flocculation model and Ramatsoma and Chirwa's model effectively traced the real data for the 50 mg/L alum concentration. Only Ramatsoma and Chirwa's model did not fit properly the 90% removal profile. Ozer's model overestimated the 80% and 90% interpolation profiles and underestimated the 70% interpolation lines at longer retention times (after 30 min), Figure 4-11. In this study the semi-empirical models could characterise flocculation best at short retention times, where the coagulant concentration is dominant.

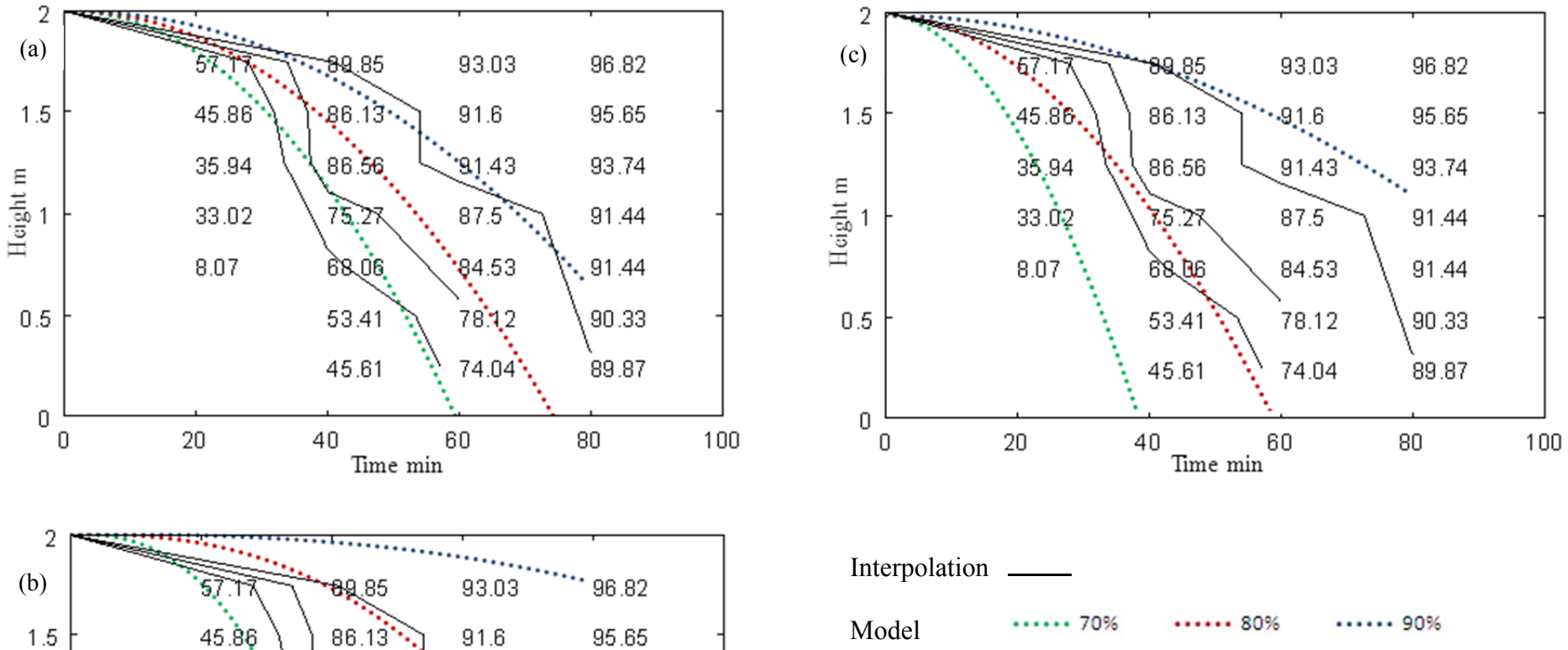

Figure 4-9: Interpolation results and iso-percentile removal profiles for 20 mg/L alum and soil particles simulated by: (a) the proposed model, (b) Ozer's model and (c) Ramatsoma and Chirwa's model.

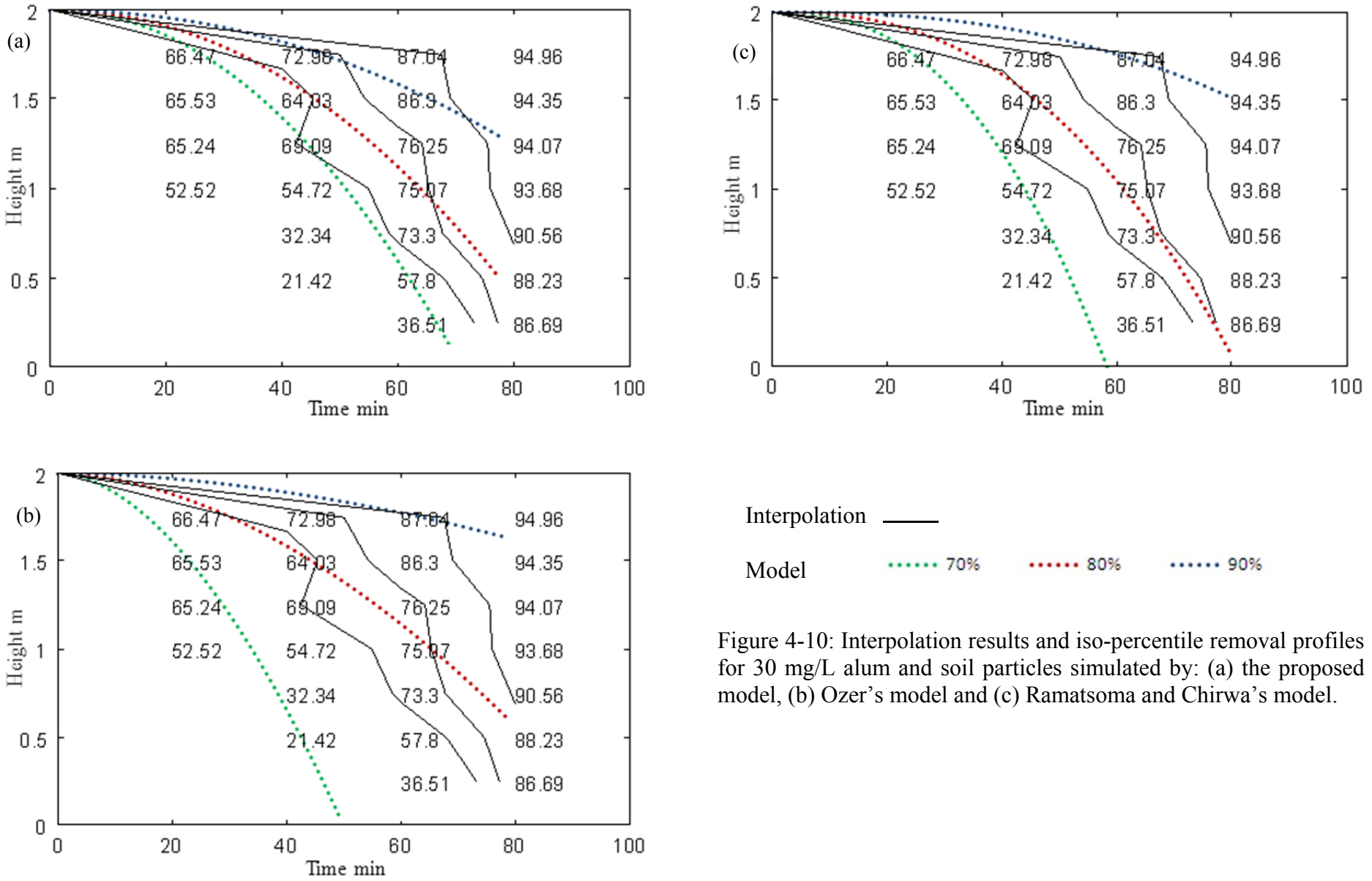

Figure 4-10: Interpolation results and iso-percentile removal profiles for 30 mg/L alum and soil particles simulated by: (a) the proposed model, (b) Ozer's model and (c) Ramatsoma and Chirwa's model.

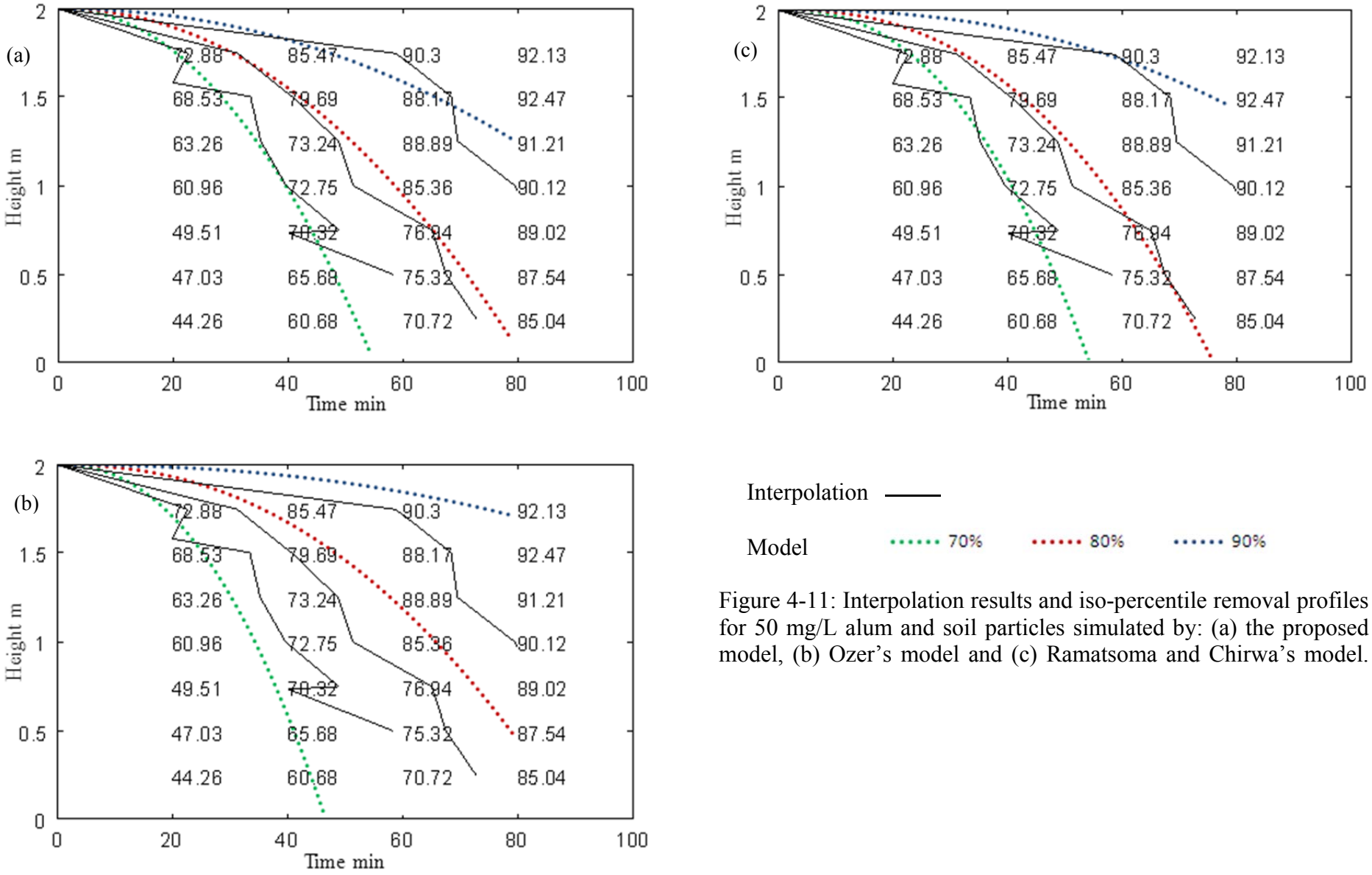

Figure 4-11: Interpolation results and iso-percentile removal profiles for 50 mg/L alum and soil particles simulated by: (a) the proposed model, (b) Ozer's model and (c) Ramatsoma and Chirwa's model.

4.5.2 Summary of Iso-percentage Profiles Characterisation

At short retention times, there's intense flocculation, and all the models fit the data reasonably well. But the empirical models fail at longer retention times because there are less solids in the column, less aggregation, floc break up, re-structuring and re-flocculation. It seems that since the models are not developed from the fractal dimension of flocs per column port, they either overestimate or underestimate the interpolated data.

4.5.3 Error Analysis

In order to check the accuracy or performance of the model, the interpolated values were used as the real values and compared with the predicted model values. Then the difference between the observed (interpolated data) and predicted model data was used to compute the sum of square errors (SSE). The accuracy of the velocity flocculation model is shown in Table 4-5 and Table 4-6 for sewage and soil particles respectively, where the fitness is determined by the statistical data presented by the sum of squared errors. The new model had lower SSE values compared to Ozer's model and Ramatsoma and Chirwa's model. For instance the velocity flocculation model had lower SSE than Ozer's model for both sewage and soil particles except at 40 mg/L alum. The velocity flocculation model also displayed lower SSE than Ramatsoma and Chirwa's model except at 200 mg/L alum and 10 mg/L alum. This indicates a better overall performance for the velocity flocculation model.

Table 4-5: Comparison of SSE for synthetic sewage profiles using the three models.

	Sum of square errors (synthetic sewage profiles)		
Alum concentration	Proposed model	Ozer's model	Ramatsoma and Chirwa's model
150 mg/L	0.44328	1.4503	9.4385
200 mg/L	0.89712	5.9467	0.81047
250 mg/L	0.45282	4.8406	1.5551
300 mg/L	0.61128	1.9838	1.5250
350 mg/L	0.67835	3.0360	1.0893

Table 4-6: Comparison of SSE for soil profiles using the three models.

Sum of square errors (soil profiles)			
Alum concentration	Proposed model	Ozer's model	Ramatsoma and Chirwa's model
10 mg/L	4.6159	7.7932	0.93395
20 mg/L	0.80323	6.5754	2.4646
30 mg/L	1. 3067	2.8305	2.2170
40 mg/L	1.45770	0.51384	2.1141
50 mg/L	1.17460	2.3786	1.6509

The outstanding performance of the velocity flocculation model is in good agreement with the findings of authors like Cox (2003). In an earlier study, Cox observed a better performance of mechanistic models (rule-based) over empirical models under certain data ranges. The lack of fit of empirical models was later attributed to a limited range of operation as they failed to approximate data around the outer boundaries of the calibrated areas. Empirical models can never be used with confidence to predict long term changes.

4.5.4 Model Parameters

The model worked best using the parameters in Table 4-7 and Table 4-8 for the synthetic sewage and soil particles respectively. The values of the approximate velocity, $a_{v,}$ were calculated by averaging the equilibrium state values of the a_v *(H)* function presented in section 4.3 for model assumptions. The other parameters (*b*, *c*, *m* and *w*) were estimated by the Gauss-Newton algorithm. Initial values of *w* and *m* were taken from the plots of a_v against *H*, Figure 4-1, which was deduced from Equation 4-5. Initial values of *a* and *b* were randomly chosen. Since the fractal dimensions and PSD values are unique per concentration, a_v values will be different for each concentration. The controlling parameter was a_v which depends on the PSD and the fractal dimensions. Model parameters for Ozer's model and Ramatsoma and Chirwa's model are in Appendix A (Table A-8).

Table 4-7: Proposed model performance using synthetic sewage experimental data.

Parameters and Sum of square errors (synthetic sewage)						
Proposed model	a_v	b	c	m	w	SSE
150 mg/L	3.68	2.02	5.80	525.71	6000	0.44328
200 mg/L	1.98	2.00	5.20	396.00	6000	0.89712
250 mg/L	2.60	2.00	5.20	54.170	6000	0.45282
300 mg/L	1.44	2.00	5.50	16.941	6000	0.61128
350 mg/L	8.225	2.10	6.00	822.50	6000	0.67835

Table 4-8: Proposed model performance using soil particles experimental data.

	Parameters and Sum of square errors (soil particles)					
Proposed model	a_v	b	c	m	w	SSE
10 mg/L	1.05	2.10	7.2	35.13	5000	4.6159
20 mg/L	1.60	2.10	4.0	26.67	5000	0.80323
30 mg/L	1.37	2.10	4.0	9.79	5000	1.3067
40 mg/L	1.33	2.12	7.0	40.25	5000	1.4577
50 mg/L	1.33	2.10	7.0	132.6	5000	1.1746

4.5.5 Model Performance

The observed order of performance in fitting experimental data was the proposed velocity flocculation model > Ramatsoma and Chirwa's model > Ozer's model. Theoretically, a rule-based (mechanistic) model is envisaged to be suitable for highly variant conditions whereas most empirical models operate well within a narrow range of conditions. This expectation was confirmed in this study by the better performance of the mechanistic velocity flocculation model in the dilute to high concentration ranges.

4.5.6 Model Validity

The fitting capability of the velocity flocculation model was investigated using data from the laboratory and comparison against literature flocculation models. The comparison criteria used was mathematical consistency, goodness of fit and sum of square errors, an approach also followed by Je and Kim (2002). Mathematical constraints were investigated based on the physical meaning of flocculent setting particles. Model failure to satisfy the constraints would render it inadequate for flocculent data analysis. Thorough inspection of the velocity flocculation model against the physical meaning of flocculent particles revealed no violation the constraints listed in section 2.2.5. The goodness of fit involved visual inspection of how well the predicted model data fits the interpolated data. The sum of square error was calculated based on model fit. The velocity flocculation model displayed reasonable fits and hence lower sum of square errors rendering it fit for predicting flocculent settling data.

4.6 Conclusion

Since the velocity flocculation model adheres to the physical characteristics of flocculating particles mentioned in section 2.2.5 (that is, it does not violate any rule), it produced lower sum of square errors and could successfully trace interpolated settling data, it can be suitably used in industry. The model was derived from the macroscopic fractal approach, a major

parameter in modeling flocculation. This fractal parameter links it to a number of important flocculation variables (mentioned in the literature section 2.2.3), so it (the proposed model) can be manipulated or improved depending on the dominant mechanism in a different environment.

CHAPTER 5

VELOCITY MODEL DERIVATION

5.1 Velocity Model Derivation

If it is assumed that the velocity is simply the differential form of Equation 4-7, then Equation 5-1 will be obtained:

$$\frac{dd}{dt} = -\frac{-b}{w}\ln\left(\frac{a_V}{m}\right)P^C t^{b-1} \tag{5-1}$$

However, the velocity of flocs is greatly influenced by hydrodynamics. The fractal velocity model developed in this research is different from previous velocity models in that it is based on recently proposed fractal theories, like that of varying fractal dimensions as particles settle. Also the velocity is not deduced from Stokes law or a modification of it, but comes from the manipulation of the transport equation and a flocculation model derived in chapter 4 of this study.

A general sediment transport equation in a quiescent settling column is described by a one dimensional continuity equation, Equation 5-2, which is a simplified version of Equation (2-29) (Je and Chang, 2004).

$$\frac{\partial C}{\partial t} = \frac{\partial\left(D_z \partial C\right)}{\partial Z^2} - \frac{\partial\left(U_z C\right)}{\partial Z} + \frac{\partial\left(V_s C\right)}{\partial Z} \tag{5-2}$$

where t = settling time (h), Z = settling column depth (m) ≡ d (in chapter 4), U_Z = vertical water velocity (m/h), V_S = flocculent settling velocity (m/h), D_Z = dispersion coefficient in the vertical direction (m^2/h).

In a batch column with quiescent flow, the continuity equation can be further simplified by applying the following assumptions:

- There is no vertical flow passing through the settling column.
- There is no vertical dispersion within the settling column.
- Since there is no bottom re-suspension, additional source terms do not apply.

Using the above assumptions Equation 5-2 is simplified to Equation 5-3:

$$\frac{\partial C}{\partial t} = \frac{\partial (V_s C)}{\partial Z} \tag{5-3}$$

Equation 5-3 is then integrated with respect to depth, z, to give Equation 5-4:

$$V_s C = -\int \frac{\partial C}{\partial t} dz \tag{5-4}$$

On substituting the proposed flocculation model (Equation 4-8) into Equation 5-4:

$$V_s \left(\frac{-wd}{\ln\left(\frac{a_V}{m}\right) t^b} \right)^{\frac{1}{C}} = -\int \frac{\partial}{\partial t} \left(\frac{-wd}{\ln\left(\frac{a_V}{m}\right) t^b} \right)^{\frac{1}{C}} dz \tag{5-5}$$

where $z = d$ is the column depth and P from Equation 4-8 is equivalent to C, ie, $P \equiv C$.

On solving Equation 5-5, following the method by Je and Chang (2004), the actual velocity model is given by:

$$V_s = \frac{b}{r} \left(\frac{-\ln\left(\frac{a_V}{m}\right) t^y}{w d^r} \right)^{\frac{-1}{C}} \tag{5-6}$$

where $a_v = d_f^{D-1}$, with d_f being the floc diameter and D the fractal dimension of the flocs, d the column depth, t (T) is the residence time, $r = 1+c$ and $y = b+c$, c, w, b and m are model fit parameters (as defined in chapter 4).

5.2 Results and Discussion

Floc growth is a dominant factor that influences the settling velocity of flocs. Therefore to conclusively describe the velocity of flocs in the settling column, the total suspended solids (TSS) concentration was analysed. It is observed in Table 5-1 and Appendix A (Table A-1 and A-3) that the addition of the coagulant (within 20 min) resulted in the decrease of TSS concentration on the top part of the column and an increase of TSS concentration in the bottom part of the column. The reduction in TSS in the top part of the column is an indication of high floc velocity due to frequent inter-particle collisions within the column caused by Brownian motion of particles and differential sedimentation. The same scenario applies for 40 min, 60 min up to 80 min.

However significant floc growth was observed mainly in the top parts of the column. The bottom ports were characterised by either constant TSS concentrations or slightly varying TSS concentrations. When that happens, flocs are believed to have reached steady state size (Wu *et al*., 2002). This is evident in Table 5-1 at a concentration of 150 mg/L alum (20 min; 0.75 m, 0.5 m, 0.25 m). Another noticeable tread is a general increase till a certain port height, then an occasional decline in TSS concentration. That is proof that during flocculation there are many processes involved, like aggregation, floc break up or fragmentation and restructuring. Examples of sporadic decline in TSS concentration (in Table 5-1) are seen at these ports: 150 mg/L ([40 min; 1 m], [60 min; 0.5 m], [100 min; 0.5 m]). This makes the deduction of the fractal dimension per port a much more reasonable method of characterising flocs in a settling column.

Table 5-1: Suspended solids concentration data from settling column test at X_o = 389.4667 NTU (coagulant dose = 150 mg/L $Al_2(SO_4)_3$).

Concentration (NTU) at different times, X_o = 389.4667 NTU						
Height m	20 min	40 min	60 min	80 min	100 min	120 min
1.75	258.61	175.22	152.24	107.06	82.45	77.04
1.50	290.35	190.84	185.27	151.27	133.86	106.75
1.25	319.40	214.36	190.64	153.68	138.22	118.67
1.00	340.86	92.26	194.38	163.85	152.52	121.86
0.75	387.05	230.53	217.95	170.12	163.34	136.77
0.50	389.47	238.00	201.32	175.88	151.93	156.18
0.25	389.47	257.71	233.25	192.32	170.90	168.68

Another angle of floc characterisation is to calculate the difference between the TSS concentration at the lowest height (0.25 m) and the one at the highest height (1.75 m) for all the time frames. As observed in Table 5-2 for soil particles and Table 5-3 for synthetic sewage, there is a general decrease in the amount of flocs (concentration) removed with time. This is due to a high aggregation rate at the initial stage of flocculation forming larger heavier flocs that settle faster. A large amount of solids were removed within the first 40 minutes. The only exception in soil particles is at: (30 mg/L alum, 20 min) and (40 mg/L alum, 20 min), which could be due to insufficient flocculation for low alum concentrations at the initial stage.

For the synthetic sewage the decrease in overall removal concentration was not continuous. The decrease is observed between 20 min and 60 min for 150 mg/L alum, then between 40 min and 80 min for 200 mg/L alum, 250 mg/L alum and 300 mg/L alum. However at 150 mg/L alum (80 min, 100 min and 120 min) for synthetic sewage (Table 5-3), a slight increase in TSS concentration is observed which could be due to re-flocculation that occurs after floc break-up and re-structuring. Cluster fragmentation may have been caused by the drag around and thorough the clusters during sedimentation.

Table 5-2: TSS concentration differences for soil particles.

	TSS concentration differences for soil particles			
Alum_soil	20 min	40 min	60 min	80 min
10 mg/L	105.43	36.78	23.14	16.13
20 mg/L	114.04	86.49	30.17	16.38
30 mg/L	34.18	178.74	69.91	39.86
40 mg/L	37.48	137.83	48.60	36.75
50 mg/L	64.21	55.61	43.93	16.02

Table 5-3: TSS concentration differences for synthetic sewage.

	TSS concentration differences for synthetic sewage					
Alum_sewage	20 min	40 min	60 min	80 min	100 min	120 min
150 mg/L	130.86	82.49	81.01	85.26	88.45	91.64
200 mg/L	89.05	123.77	102.69	94.68	----	----
250 mg/L	76.85	134.03	130.60	88.85	100.23	82.24
300 mg/L	87.04	112.67	112.20	63.54	81.00	69.24
350 mg/L	79.31	125.66	84.58	125.66	----	----

From the above reasoning, it is evident that as the floc formation increases the velocity also increases. However if one considers the instantaneous velocity, it can be noticed that the velocity at 20 min and a depth of 1.75 m is higher than the one at the same depth but at a later time, 60 min, for all the coagulant concentrations (Figure 5-1 (a), (b), (c)) and (Figure 5-2 (a), (b), (c)). With time the velocity of the aggregates slows down to a lower value as the majority of larger aggregates quickly settled within the first 40 min. By that time the column looks less turbid. Also the effect of the coagulant dose becomes less pronounced hence a low settling velocity is inevitable with time. This trend (decline in velocity with time) is observed in both sewage and soil particles.

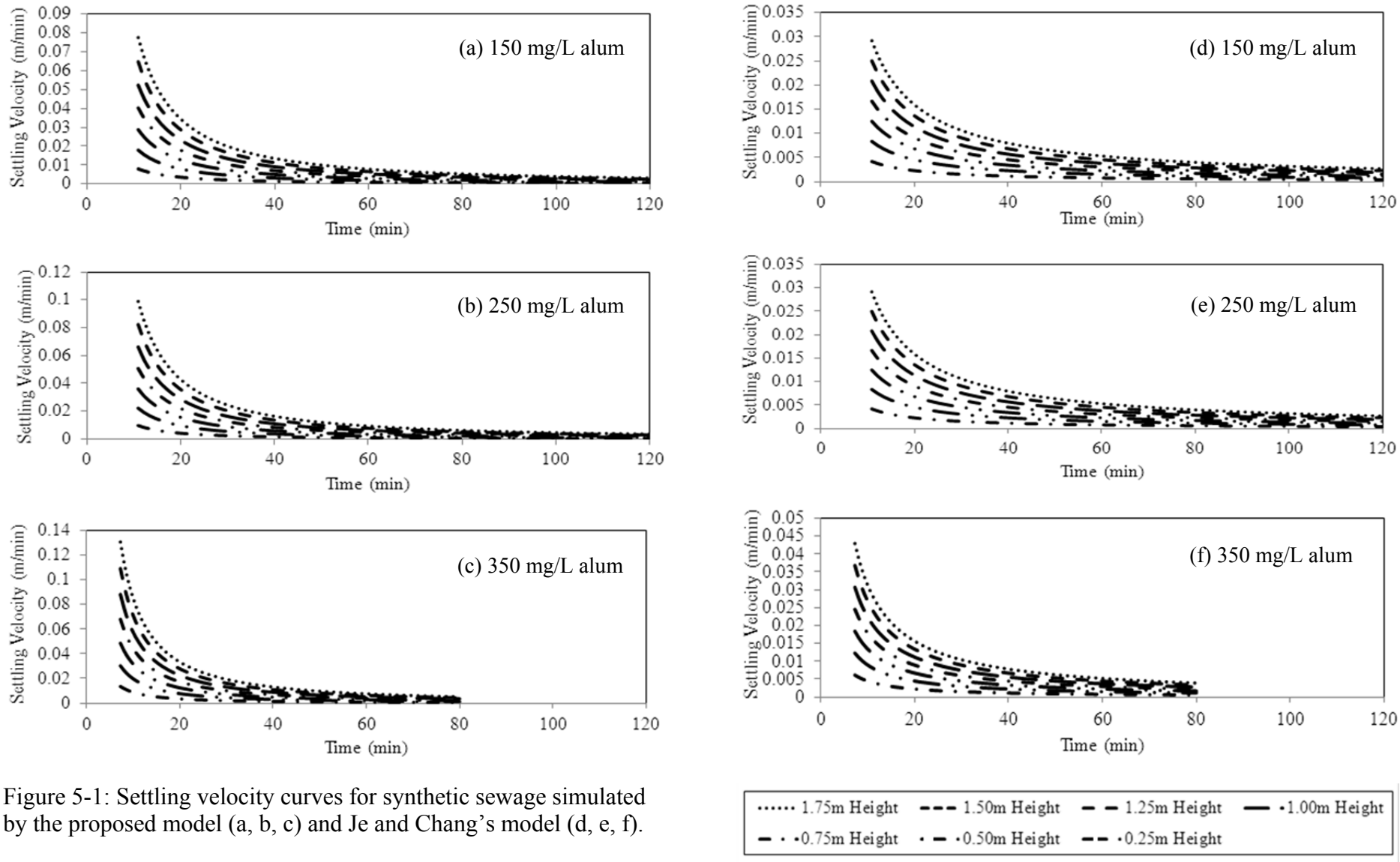

Figure 5-1: Settling velocity curves for synthetic sewage simulated by the proposed model (a, b, c) and Je and Chang's model (d, e, f).

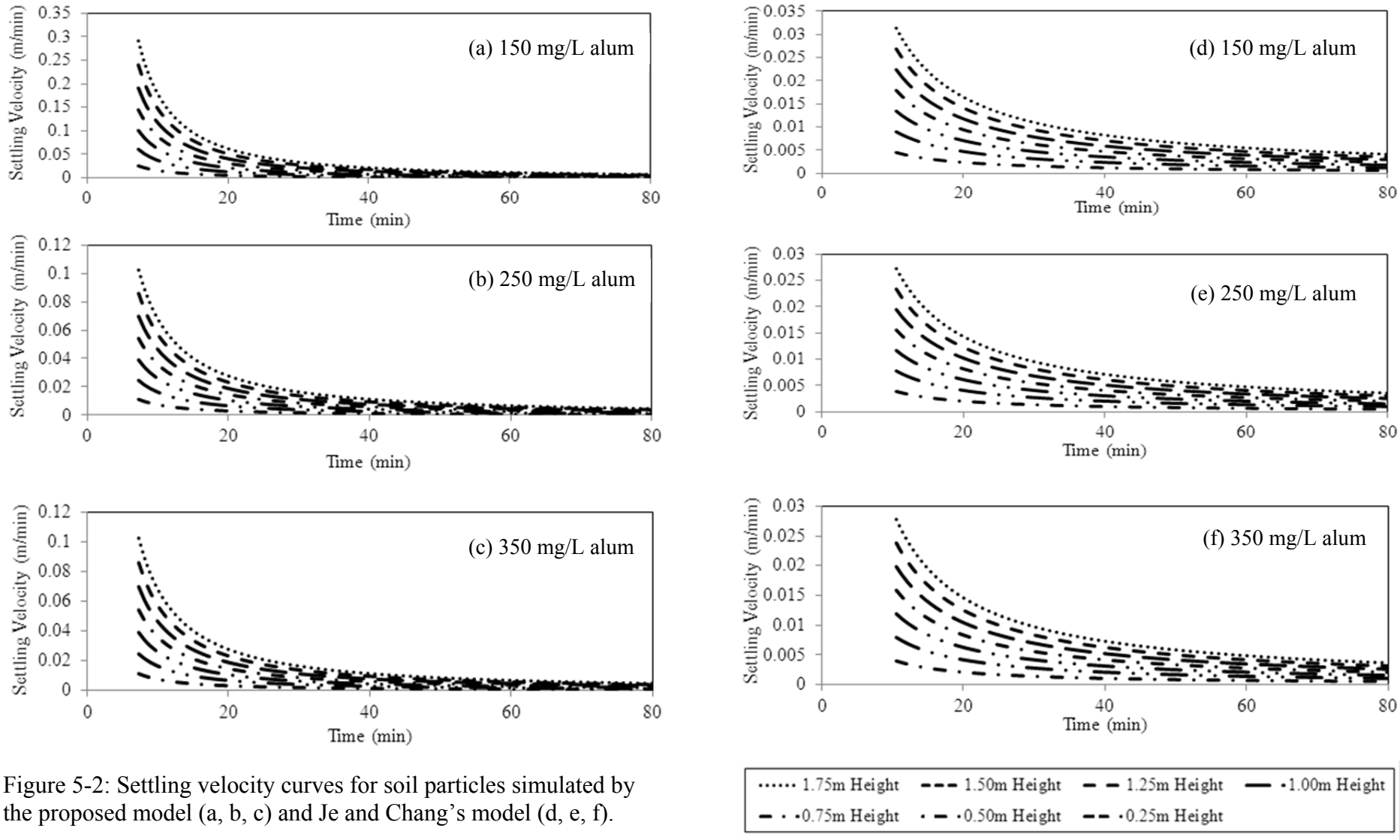

Figure 5-2: Settling velocity curves for soil particles simulated by the proposed model (a, b, c) and Je and Chang's model (d, e, f).

The performance of the new velocity model has been compared to a literature velocity model, Je and Chang's model, at selected alum concentrations (low, middle and high concentrations) and time frames, Table 5-4 and 5-5. Je and Chang's velocity model was chosen because it was deduced from an iso-percentile flocculation model (Ozer's model) and a continuity equation, the same way as the velocity model in this study.

When compared to Je and Chang's model, the proposed velocity model displayed higher velocities as shown in Table 5-4 and 5-5. This is also evident in the higher velocity scaling of the velocity profiles for the new model and the lower velocity scaling for Je and Chang's model, Figure 5-1 and 5-2). Therefore Je and Chang's velocity model underestimates the settling velocities of flocs for the soil particles and sewage particles. The high velocities in the proposed model could be attributed to the extra consideration of particle characterisation like PSD and fractal dimensions, which could enhance the model to estimate more accurate velocities. However the settling trend of the proposed model is similar to that of Je and Chang implying that the proposed velocity model predictions are in line with existing models, Figure 5-1 and 5-2.

Table 5-4: Performance evaluation of velocity models for sewage samples, at a lower, middle and higher coagulation concentration and a column port height of 1.25 m.

		Velocities at different times and concentrations (m/min)	
alum concentration	Time	Proposed model	Je and Chang's model
150 mg/L	20 min	0.022197	0.011029
	60 min	0.005183	0.003750
250 mg/L	20 min	0.027454	0.011029
	60 min	0.006164	0.003750
350 mg/L	20 min	0.022236	0.011049
	60 min	0.005046	0.003683

Table 5-5: Performance evaluation of velocity models for soil samples, at a lower, middle and higher coagulation concentration and a column port height of 1.25 m.

		Velocities at different times and concentrations (m/min)	
alum concentration	Time	Proposed model	Je and Chang's model
10 mg/L	20 min	0.018651	0.011675
	60 min	0.004513	0.003892
30 mg/L	20 min	0.040272	0.010688
	60 min	0.007540	0.003562
50 mg/L	20 min	0.018473	0.010313
	60 min	0.004429	0.003437

5.3 Conclusion

It can be concluded that as the floc size increases due to increases in collision frequency by Brownian motion and differential settling, the floc velocity also increases. However the high velocity would decrease with settling time to a lower value as the column becomes clearer (less turbid). In addition, the highly varying velocities prove that porous fractal aggregates with low fractal dimensions (less than 3) behave very differently from impermeable spherical particles. The proposed velocity model successfully tracked the velocity of the settling flocs both in high middle and low concentrations hence it can be utilised determine the instantaneous velocity of flocs.

CHAPTER 6

SUMMARY AND FUTURE RESEARCH /RECOMMENDATIONS

6.1 Summary

Pollution of water bodies by sediment contamination is a subject of paramount concern globally. Environmental remediation has been possible through the removal of particles from a suspension by coagulation, flocculation and sedimentation in water and wastewater treatment systems. Due to the wide application of flocculation/sedimentation in waterworks, the efficiency of the separation systems like clarifiers has to be improved. Therefore batch column studies were conducted in this study to model the flocculation process during differential sedimentation using an iso-percentile flocculation model and a velocity model. These models are based on PSD and fractal dimensions of flocs.

The iso-percentile flocculation model derived (referred to as the velocity flocculation model) could successfully trace or estimate the real interpolated iso-percentile data deeming it sufficient for use in industry. It produced low sum of square errors when compared to literature iso-percentile flocculation models (Ozer and Ramatsoma and Chirwa's model).

The velocity model was then derived from a combination of the proposed iso-percentile velocity flocculation model and a one dimensional transport equation. The proposed velocity model could predict the instantaneous velocity of the flocs as they settled down the column. The velocity of flocs increased with floc size and decreased with flocculation time. Flocs with large diameters caused by inter-particle collisions settled faster at the initial stages of flocculation (within the first 40 minutes in this study) but as time elapsed, the velocity slowed down to a lower value. Reduction in velocity with time is to be anticipated since a majority of the total suspended solids (large flocs) settle fast at the initial stages of flocculation leaving a less turbid column with slow settling flocs.

6.2 Recommendations

6.2.1 Iso-percentile Model and Interpolation script

-The automation of data analysis through interpolation can be improved to perform a three-way and a four-way data interpolation to minimize the errors incurred through interpolation by hand and improve the design accuracy.

-Fractal dimensions can also be investigated using an image analysis. Microscopy and photography gives a feel of the shape characteristics of the floc and type of floc under investigation. Further investigations can also clarify the scenario of fractal dimensions less than one.

-Different mechanisms during flocculation may lead to different arrangements or packing of internal particles in flocs. Hence part of the floc population may be characterized by the same size but have different shapes that cannot be defined by a single fractal dimension. Multiple fractal dimensions within a floc are a subject of further investigation.
-The function a_v *(H)* that relates the particle size distribution and the fractal dimensions was only considered at the equilibrium state in this study. Therefore a full investigation of the transient state is necessary to achieve a conclusive iso-percentile flocculation model.

6.2.2 Velocity Model

-Clearly the degree of advection was evident in our experiments where the fractal dimension was less than 2. Therefore future models will be improved by incorporating the degree of advection and diffusive effects under turbulent flow. This means that more terms from the transport equation have to be included (or evaluated) in deducing the velocity model but still maintaining the simplicity/ practicability of the model in wastewater treatment plants as well as industry.

-Highly porous flocs (flocs with low fractal dimensions) have several pathways and markedly influence the fluid flow within flocs. Fluid flow within flocs needs further investigation as it affects the velocity of flocs.

REFERENCES

Berthouex, P. M., and Stevens, D. K. (1982). Computer analysis of settling data. *ASCE Journal of Environmental Engineering*, 108(5), 1065-1069.

Bridgeman, J., Jefferson, B., and Parson, S.A. (2009). Computational fluid dynamics modeling of flocculation in water treatment: A review. *Engineering Applications of Computational Fluid Mechanics*, 3(2), 220-241.

Bushell, G. C., Yan, Y. D., Woodfield, D., Raper, J., and Amal, R. (2002). On techniques for the measurement of the mass fractal dimension of aggregates. *Advances in colloid and Interface Science*, 95, 1-50.

Camp, T. R., and Stein, P.C. (1943). Velocity gradients and internal work in fluid motion. *Journal of the Boston Society of Civil Engineers*, 30, 219-237.

Camp, T. R. (1946). Sedimentation and the design of settling tanks. *Transactions of the American Society of Civil Engineers* (*ASCE*), 111, 895-936.

Chakraborti, R. J., Atkinson, J. F., and Van Benschoten, J. E. (2000). Characterisation of alum floc by image analysis. *Environmental Science and Technology*, 34, 3969-3976.

Chakraborti, R. K., Gardner, K. H., Atkinson, J. F., and Van Benschoten, J. E. (2003). Changes in fractal dimension during aggregation. *Water Research*. 37(4), 873-883.

Cho, S. H., Colin, F., Sardin, M., and Prost, C. (1993). Settling velocity model of activated sludge. *Water Research*, 27(7), 1237-1242.

Cousin, C. P., and Ganczarczyk, J. (1998). Effects of salinity on physical characteristics of activated sludge flocs. *Water Quality Research Journal of Canada*, 33(4), 565-587.

Cox, B. A. (2003). A review of currently available in-stream water-quality models and their applicability for simulating dissolved oxygen in lowland rivers. *The Science of the Total Environment*, 314-316, 335-377.

Dawney, B., and Pearce, J. M. (2012). Optimizing the solar water disinfection (SODIS) method by decreasing turbidity with NaCl. *Water, Sanitation and Hygiene for Development*, 2(2) 87-94.

Eckenfelder, W. W. (1989). *Industrial water pollution control,* 2nd ed., McGraw-Hill, New York, U.S.A.

Flesch, J. C., Spicer, P.T., and Pratsinis, S. E. (1999). Laminar and Turbulent Shear-Induced Flocculation of Fractal Aggregates. *American Institute of Chemical Engineers*, 45(5), 1114-1124.

Gmachowwski, L. (1996). Hydrodynamics of aggregated media. *Journal of Colloid and Interface Science*. 178, 80-86.

Han, M. Y., and Lawler, D. F. (1991). Interactions of two settling spheres: settling rates and collision efficiencies. *Hydraulic Engineering ASCE*,117, 1269-1289.

Han, M. Y., and Lawler, D. F. (1992). The (relative) insignificance of G in flocculation. *American Water Works Association*, 84, 79-91.

Hayes, G. F. (1992). Documentation of the SETTLE Module for ADDAMS: Design of Confined Disposal Facilities for Solids Retention and Initial Storage, USAE Waterways Experiment Station, MS.

He, W., Nan, J., Li, H., and Li, S. (2012). Characteristic analysis on temporal evolution of floc size and structure in low-shear flow. *Water Research*, 46, 509-520.

Hill, P.S. (1992). Reconciling aggregation theory with observed vertical fluxes following phytoplankton blooms. *Geophysical Research*, 97(C2), 2295-2308.

Jackson, G. A. (1995). Comparing observed changes in particle size spectra with those predicted using coagulation theory. *Deep Sea Research*, 42, 159-184.

Jarvis, P., Jefferson, B., and Parsons, S. A. (2005). Measuring floc structural characteristics. *Environmental Science and Biotechnology*, 4(1-2), 1-18.

Je, C., and Kim, K. (2002). Evaluation of mathematical models for analyzing flocculent settling data. *Environmental Progress*. 21(4) 255-264.

Je, C., and Chang, S. (2004). Simple approach to estimate flocculent settling velocity in a dilute suspension. *Environmental Geology*, 45, 1002-1009.

Je, C., Hayes, D. F., and Kim, K. S. (2007). Simulation of resuspended sediments resulting from dredging operations by a numerical flocculent transport model. *Chemosphere*, 70(2), 187-195.

Johnson, C. P., Li, X., and Logan, B. E. (1996). Settling velocities of fractal aggregates. Environ. Sci. Technol, 30(6),1911-1919.

Joshi, M., Bansal, R., and Purwar, R. (2003). Colour removal from textile effluents. *Indian Journal of Fibre and Textile Research*, 29, 239-259.

Khelifa, A., and Hill, P. S. (2006). Models for effective density and settling velocity of flocs. *Hydraulic Research*, 44(3), 390-401.

Kusters, K. A., Wijers, J. G., and Thoenes, D. (1997). Aggregation kinetics of small particles in agitated vessels. *Chemical Engineering Science*, 52, 107.

Lee, D. G., Bonner, J. S., Garton, L. S., Ernest, A. N. S., and Autenrieth, R. L. (2000). Modeling coagulation kinetics incorporating fractal theories: A fractal rectilinear approach. *Water Research*, 34(7), 1987-2000.

Lee, D. G., Bonner, J. S., Garton, L. S., Ernest, A. N. S., and Autenrieth, R. L. (2002). Modeling coagulation kinetics incorporating fractal theories: Comparison with observed data. *Water Research*, 36, 1056-1066.

Li, D. H., and Ganczarczyk, J. J. (1986). Physical Characteristics of activated sludge flocs. *CRC Critical Reviews in Environmental Control*, 17(1), 53-87.

Li, X., Yuan, Y., and Wang, H. (2003). Hydrodynamics of biological aggregates of different sludge ages: an insight into the mass transport mechanisms of bioaggregates. *Environmental Science and Technology*, 37(2), 292-299.

Li, X., Yuan, Y. (2002). Settling velocities and permeabilities of microbial aggregates. *Water Research*, 36(12), 3110-3120.

Li, X., and Logan, B. E. (1997, a). Collision Frequencies of Fractal Aggregates with Small Particles by Differential Sedimentation. Environ. Sci. Technol, 31(4), 1229-1236.

Li, X., and Logan, B. E. (1997, b). Collision Frequencies between Fractal Aggregates and Small Particles in a Turbulently Sheared Fluid. Environ. Sci. Technol., 31(4), 1237-1242.

Logan, B. E., and Wilkinson, D. B. (1990). Fractal Geometry of Marine Snow and Other Biological Aggregates. *Limnology and Oceanography*, 35(1), 130-136.

Logan B. E. Fractal Coagulation Kinetics. *Department of Civil & Environmental Engineering. The Pennsylvania State University*. Retrieved from: http://www.engr.psu.edu/ce/enve/logan.html

Maggi, F. (2007). Variable fractal dimension: A major control for floc structure and flocculation kinematics of suspended cohesive sediment. *Journal of Geophysical Research*, 112, C07012, doi:10.1029/2006JC003951.

Maggi, F., Mietta, F., and Winterwerp, J. C. (2007). Effect of variable fractal dimension on the floc size distribution of suspended cohesive sediment. *Journal of Hydrology*, 343, 43-55.

Maggi, F., and Winterwerp, J. C. (2004). Method for computing the three-dimensional capacity dimension from two-dimensional projections of fractal aggregates. *Physical Review E (Statistical, Nonlinear, and Soft Matter Physics), 69*(011405), 011405-1-011405-8.

Mandelbrot, B. B. (1977). Fractals: form, chance and dimension. San Francisco California. W. H. Freeman.

Matsumoto, K., and Mori, Y. (1975). Settling velocity of floc-new measurement method of floc density. *Journal of Chemical Engineering of Japan*, 8(2), 143-147.

Metcalf, and Eddy, (2003). *Wastewater Engineering*. Fourth Edition. Tchobanoglous,G., Burton, F., and Stensel, H. D. (Eds.) Metcalf & Eddy, Inc., McGraw-Hill, New York.

Mikkelsen, O. A., Hill, P. S., Milligan, T.G., and Chant, R. J. (2005). In situ particle size distributions and volume concentrations from a LISST-100 laser particle sizer and a digital floc camera. *Continental Shelf Research*, 25, 1959-1978.

Montgomery, R. (1979). *Development of a methodology for designing fine-grained dredged material sedimentation basins*. Doctoral Thesis, Vanderbilt University, Nashville, TN.

OECD - Twelfth Addendum (2001) Guideline for testing of chemicals.

Oles, V. (1992). Shear –induced aggregation and breakup of polystyrene latex particles. *Journal of Colloid and Interface Science*, 154(2) 351-358.

Ozer, A. (1994). Simple equations to express settling column data. *ASCE Journal of Environmental Engineering*, 120. 677-682.

Peavy, H. S., Rowe, D. R., and Tchobanoglous, G. (1985). *Environmental Engineering*, McGraw-Hill, New York, U.S.A.

Piro, P., Carbone, M., Penna, N., and Marsalek, J. (2011). Characterization of the settling process for wastewater from a combined sewer system. *Water Research*, 45, 6615-6624.

Pise, C. P., and Halkude, S. A. (2011). A modified column data analysis. *International Journal of Engineering Science and Technology*, 3(4), 3177-3183.

Ramatsoma, M. S., and Chirwa, E. M. N. (2012). Computational simulation of flocculent sedimentation based on experimental results. *Water Science and Technology*, 65(6), 1007-1013.

Rauch, W., Henze, M., Koncsos, L., Reichert, P., Shanahan, P., Somlyody, L., and Vanrolleghem, P. (1998). River water quality modeling: I. state of the art. *IAWQ Biennial International Conference*, 1-8.

Reynolds, T., and Richards, P. A. (1996). *Unit Operations and Process in Environmental Engineering*, 2nd ed., International Thomson Publishing, New York, U.S.A.

San, H. A. (1989). Analytical approach for evaluation of settling column data. *ASCE Journal of Environmental Engineering*, 115(2), 455-461.

Sawyer, C.N., Mccarthy, P.L., and Parkin, G. F. (2003). *Chemistry for Environmental Engineering*, Fifth Edition, McGraw-Hill, New York.

Selomulya, C., Amal, R., Bushell, G., and Waite, T. D. (2001). Evidence of Shear Rate Dependence on Restructuring and Breakup of Latex Aggregates. *Colloid and Interface Science*, 236(1), 67-77.

Selomulya, C., Bushell, G., Amal, R., and Waite, T. D. (2003). Understanding the role of restructuring in flocculation: The application of a population balance model. *Chemical Engineering Science*, 58(2), 327-338.

Schaefer, D.W. (1989). Polymers, fractals and ceramic materials. *Science*, 243, 1023-1027.

Smoluchowski, M. (1917). Versuch einer Mathematischen Theorie der Kaogulationskinetik Kolloider Losungen. *Z Phys. Chem*, 92, 129-168.

Spicer, P. T., Pratsinis, S. E., Raper, J., Amal, R., Bushell, G., and Meesters, G. (1998). Effect of shear schedule on particle size, density, and structure during flocculation in stirred tanks. *Powder Technology*, 97, 26-34.

Spicer, P. T., and Prasinis, S.E. (1996). Shear induced flocculation: the evolution of floc structure and the shape of the size distribution at steady state. *Water Research*, 30(5), 1049-56.

Sterling Jr, M. C., Bonner, J. S., Ernest, A. N. S., Page, C. A., and Autenrieth, R. L. (2005). Application of fractal flocculation and vertical transport model to aquatic sol-sediment systems. *Water Research*, 39, 1818-1830.

Tambo, N., Watanabe, Y. (1979). Physical characteristics of flocs-I. The flocs density function and aluminum floc. *Water Research*, 13, 409-419.

Tang, P., and Raper, J. A. (2002). Modelling the settling behaviour of fractal aggregates-a review. *Powder Technology*, 123, 114-125.

Tchobanoglous ,G., Burton, F.L., and Stensel, H.D.(2003). Meltcalf & Eddy, Inc.'s *Wastewater Engineering: Treatment, Disposal, and Reuse*, 4th Edition. McGraw-Hill, Inc., New York.

Thomas, D. N., Judd, S. J., and Fawcett, N. (1999). Flocculation modelling: A review. *Water Research*, 33(7), 1579-1592.

Vahedi, A., and Gorczyca, B. (2012). Predicting the settling velocity of flocs formed in water treatment using multiple fractal dimensions. *Water Research*, 46, 4188-4194.

Vahedi, A., and Gorczyca, B. (2011). Application of fractal dimensions to study the structure of flocs formed in lime softening process. *Water Research*, 45(2), 545-556.

Wiesner, M. R. (1992). Kinetics of aggregate formation in rapid mix. *Water Research*, 26(3), 379-387.

Winterwerp, J. C. (1998). A simple model for turbulence induced flocculation of cohesive sediment. *Journal of Hydraulic Research*, 36(3), 309-326.

Witten, T. A., and Cates, M. E. (1986). Tenuous structures from disorderly growth processes. *Science*, 232, 1607-1612.

Wu, R.M., Lee, D.J., Waite, T.D., and Guan, J. (2002). Multilevel Structure of Sludge Flocs. *Journal of Colloid and Interfacial Science*, 252, 383-392.

Xu, F., Wang, D. P., and Riemer, N. (2008). Modeling flocculation processes of fine-grained particles using a size-resolved method: Comparison with published laboratory experiments. *Continental Shelf Research*, 28, 2668-2677.

Zhai, X. D., and Liu, J. F. (2009). Characterization of particle size distribution (PSD) evolution during flocculation by image acquisition and analysis system. *International Conference on Environmental Science and Information Application Technology*, 362-366.

APPENDIX A

ADDITIONAL RESULTS

Table A-1: Suspended solids concentration data from settling column test for synthetic sewage particles with alum at: (a) 150 mg/L, (b) 250 mg/L and 350 mg/L

a)

Concentration (NTU) at Different times, X_o = 389.4667 NTU						
Height m	20 min	40 min	60 min	80 min	100 min	120 min
1.75	258.61	175.22	152.24	107.06	82.45	77.04
1.50	290.35	190.84	185.27	151.27	133.86	106.75
1.25	319.40	214.36	190.64	153.68	138.22	118.67
1.00	340.86	92.26	194.38	163.85	152.52	121.86
0.75	387.05	230.53	217.95	170.12	163.34	136.77
0.50	389.47	238.00	201.32	175.88	151.93	156.18
0.25	389.47	257.71	233.25	192.32	170.90	168.68

b)

Concentration (NTU) at Different times, X_o = 335 NTU						
Height m	20 min	40 min	60 min	80 min	100 min	120 min
1.75	140.43	104.99	72.26	56.41	26.23	24.76
1.50	174.03	141.20	113.26	81.57	41.07	32.53
1.25	180.83	157.18	98.19	97.75	54.50	38.42
1.00	198.59	161.91	145.32	107.40	77.89	59.66
0.75	188.20	181.54	166.03	95.01	90.32	71.19
0.50	225.39	197.95	166.93	108.57	101.97	87.90
0.25	205.86	219.09	183.45	132.06	111.56	94.77

c)

Concentration (NTU) at Different times, X_o = 465.73 NTU				
Height m	20 min	40 min	60 min	80 min
1.75	181.08	64.55	34.51	26.22
1.50	154.20	119.27	43.73	28.46
1.25	160.58	141.40	51.65	46.34
1.00	169.29	126.31	70.84	48.20
0.75	198.64	190.67	100.13	58.96
0.50	220.20	155.32	99.85	61.66
0.25	260.39	190.21	119.09	98.74

Table A-2: Percentage removal data from settling column test for synthetic sewage particles with alum at: a) 150 mg/L, b) 250 mg/L and c) 350 mg/L.

a)

Removal Percentage at Different Times, X_o = 389.4667 NTU						
Height m	20 min	40 min	60 min	80 min	100 min	120 min
1.75	33.60	55.01	60.91	72.51	78.83	80.22
1.50	25.45	51.00	52.43	61.16	65.63	72.59
1.25	17.99	44.96	51.05	60.54	64.51	69.53
1.00	12.48	76.31	50.09	57.93	60.84	68.71
0.75	0.62	40.81	44.04	56.32	58.06	64.88
0.50	0.00	38.89	48.31	54.84	60.99	59.90
0.25	0.00	33.83	40.11	50.62	56.12	56.69

b)

Removal Percentage at Different Times, X_o = 335 NTU						
Height m	20 min	40 min	60 min	80 min	100 min	120 min
1.75	58.09	68.66	78.43	83.16	92.17	92.61
1.50	48.05	57.85	66.19	75.65	87.74	90.29
1.25	46.02	53.08	70.69	70.82	83.73	88.53
1.00	40.72	51.67	56.62	67.94	76.75	82.19
0.75	43.82	45.81	50.44	71.64	73.04	78.75
0.50	32.72	40.91	50.17	67.59	69.56	73.76
0.25	38.55	34.60	45.24	60.58	66.70	71.71

c)

Removal Percentage at Different Times, X_o = 465.73 NTU				
Height m	20 min	40 min	60 min	80 min
1.75	69.12	86.14	92.59	94.37
1.50	66.89	74.39	90.61	93.89
1.25	65.52	69.64	88.91	90.05
1.00	63.65	72.88	84.79	89.65
0.75	57.35	59.06	78.50	87.34
0.50	52.72	66.65	78.56	86.76
0.25	44.09	59.16	74.43	78.80

Table A-3: Suspended solids concentration data from settling column test for soil particles with alum at: (a) 20 mg/L, (b) 30 mg/L and 50 mg/L

a)

Concentration (NTU) at Different times, X_o = 232.25				
Height m	20 min	40 min	60 min	80 min
1.75	85.33	38.39	22.53	18.84
1.50	103.03	45.92	23.18	20.41
1.25	117.29	47.17	23.41	22.95
1.00	146.25	62.15	28.20	25.76
0.75	170.84	57.60	28.54	28.20
0.50	172.10	68.86	44.03	34.74
0.25	232.25	232.25	232.25	232.25

b)

Concentration (NTU) at Different Times, X_o = 245.02 NTU				
Height m	20 min	40 min	60 min	80 min
1.7	82.16	66.28	31.75	12.35
1.50	84.46	88.13	33.57	13.84
1.25	85.17	75.74	58.19	14.53
1.00	116.34	110.95	61.08	15.49
0.75	245.02	165.78	65.42	23.13
0.50	245.02	192.54	103.40	28.84
0.25	245.02	245.02	155.56	32.61

c)

Concentration (NTU) at Different times, X_o = 224.34 NTU				
Height m	20 min	40 min	60 min	80 min
1.75m	82.42	37.08	21.76	18.19
1.50m	99.52	44.35	22.39	19.72
1.25m	113.29	45.56	22.61	22.16
1.00m	141.27	60.03	27.23	24.88
0.75m	165.02	55.64	27.57	27.23
0.50m	166.24	66.52	42.53	33.56
0.25m	224.34	224.34	224.34	224.34

Table A-4: Percentage removal data from settling column test for soil particles with alum at: a) 20 mg/L, b) 30 mg/L and c) 50 mg/L

a)

	Removal Percentage at Different Times, X_o = 232.25 NTU			
Height m	20 min	40 min	60 min	80 min
1.75	57.17	82.85	93.03	96.92
1.50	46.86	86.13	91.60	95.65
1.25	35.94	86.56	91.43	93.74
1.00	33.03	75.27	87.50	91.44
0.75	8.07	68.06	85.53	91.44
0.50	0.00	53.41	86.12	90.33
0.25	0.00	45.61	80.04	89.87

b)

	Removal Percentage at Different Times, X_o = 245.02 NTU			
Height m	20 min	40 min	60 min	80 min
1.75	66.47	72.95	87.04	94.96
1.50	65.53	64.03	86.30	94.35
1.25	65.24	69.09	76.25	94.07
1.00	52.52	54.72	75.07	93.68
0.75	0.00	32.34	73.30	90.56
0.50	0.00	21.42	57.80	88.23
0.25	0.00	0.00	36.51	86.69

c)

	Removal Percentage at Different Times, X_o = 224.34 NTU			
Height m	20 min	40 min	60 min	80 min
1.75	72.88	85.47	90.30	92.18
1.50	68.53	79.69	88.17	92.47
1.25	63.26	73.24	88.89	91.21
1.00	60.96	72.75	85.36	90.12
0.75	49.51	90.32	76.94	89.02
0.50	47.03	65.68	75.32	87.54
0.25	44.26	60.68	70.72	85.04

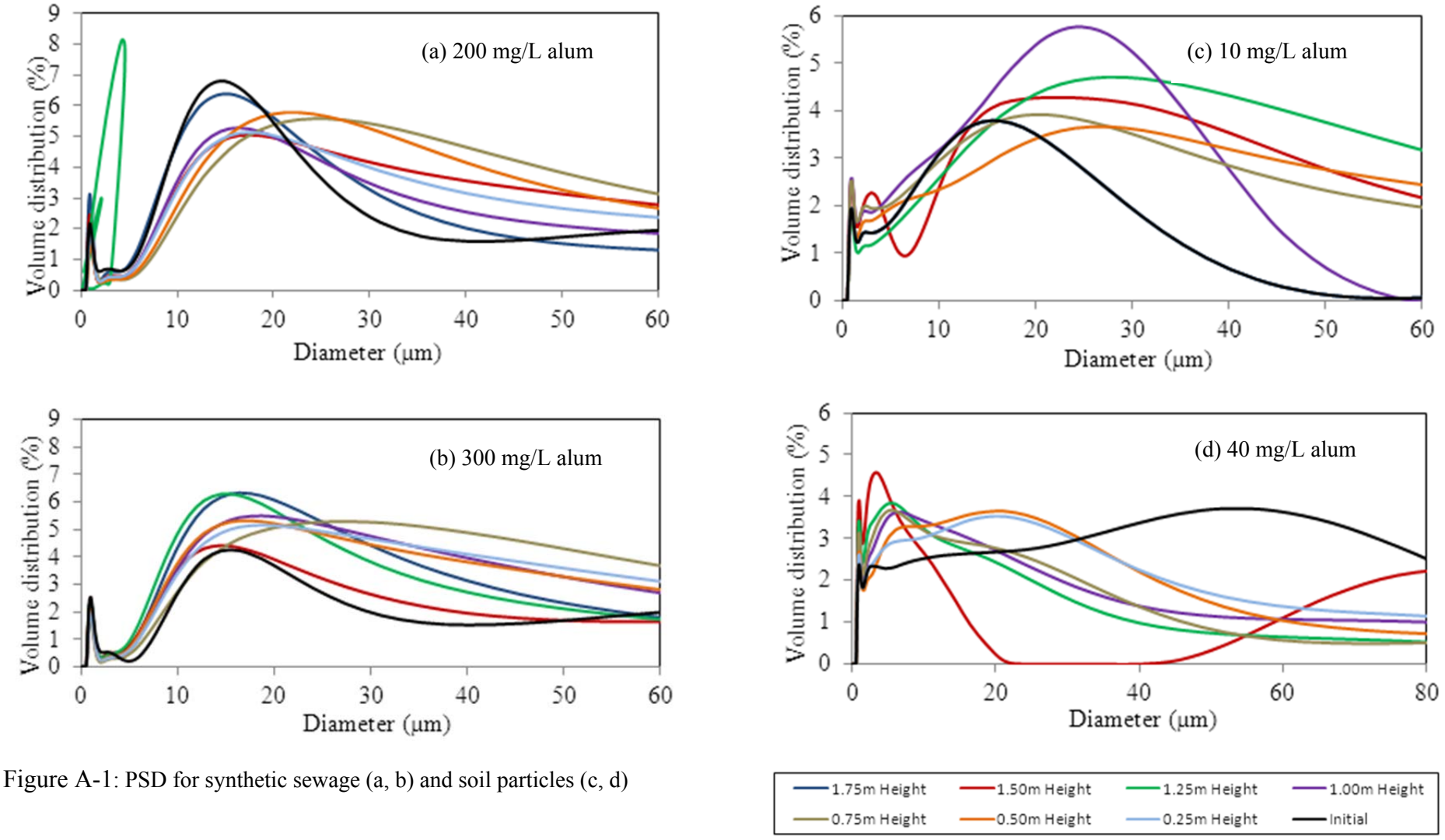

Figure A-1: PSD for synthetic sewage (a, b) and soil particles (c, d)

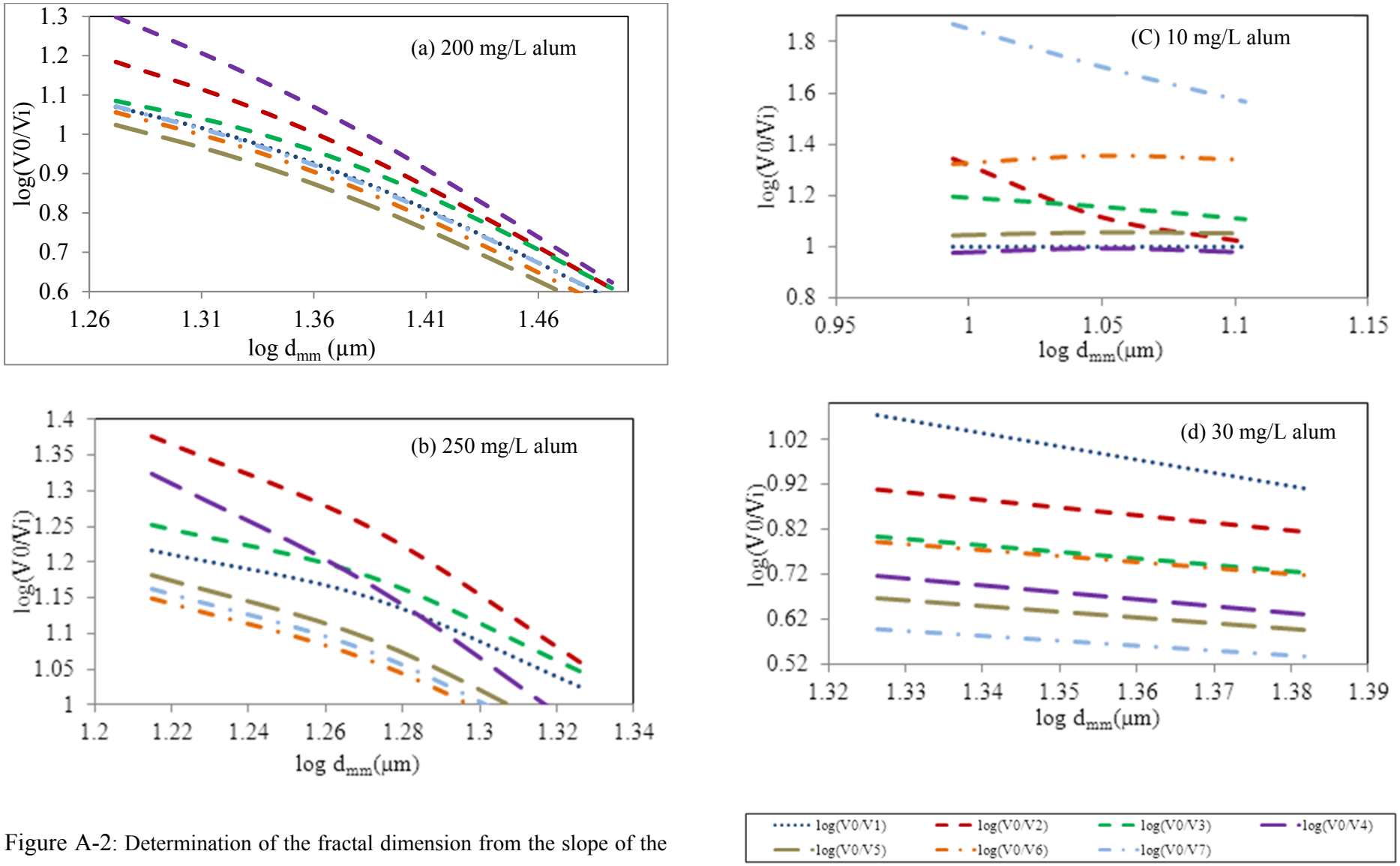

Figure A-2: Determination of the fractal dimension from the slope of the volume fraction for sewage flocs (a, b) soil flocs (c, d).

Table A-5: Fractal dimensions for synthetic sewage with: a) 200 mg/L alum b) 250 mg/L alum, and for soil particles with c) 10 mg/L d) 40 mg/L

a)

	fractal dimension *D* (dimensionless) (200 mg/L)				
Depth (m)	20 min	40 min	60 min	80 min	average D
0.25	2.66	2.77	2.02	2.84	2.57
0.50	1.54	2.38	2.39	2.24	2.14
0.75	1.44	1.83	2.07	1.92	1.82
1.00	1.05	1.81	1.42	1.71	1.50
1.25	1.02	1.78	1.06	1.03	1.22
1.50	0.95	0.97	0.96	0.93	0.95
1.75	0.69	0.77	0.81	0.81	0.77

b)

	fractal dimension *D* (dimensionless) (300 mg/L)				
Depth (m)	20 min	40 min	60 min	80 min	average D
0.25	1.76	1.93	1.68	1.94	1.83
0.50	1.54	1.75	1.51	1.78	1.65
0.75	1.43	1.70	1.47	1.53	1.53
1.00	1.43	1.45	1.34	1.46	1.42
1.25	0.88	1.01	1.01	1.21	1.03
1.50	1.07	0.62	1.19	0.99	0.97
1.75	1.00	0.48	0.32	1.05	0.71

c)

	fractal dimension *D* (dimensionless) (10 mg/L)				
Depth (m)	20 min	40 min	60 min	80 min	average D
0.25	2.03	2.08	1.33	2.40	1.96
0.50	2.18	1.10	1.17	1.73	1.54
0.75	1.48	1.03	1.33	1.30	1.29
1.00	0.96	1.92	1.03	0.98	1.22
1.25	1.61	0.60	0.89	0.75	0.96
1.50	0.21	0.84	0.45	0.51	0.50
1.75	0.08	0.02	0.22	0.44	0.19

d)

	fractal dimension *D* (dimensionless) (40 mg/L)				
Depth (m)	20 min	40 min	60 min	80 min	average D
0.25	2.28	2.52	2.33	2.52	2.41
0.50	2.10	2.18	2.19	2.13	2.15
0.75	2.07	2.04	2.05	1.71	1.97
1.00	1.87	1.91	1.77	1.49	1.76
1.25	1.14	1.17	1. 08	1.07	1.13
1.50	0.95	0.67	0.62	0.57	0.70
1.75	0.56	0.56	0.48	0.43	0.51

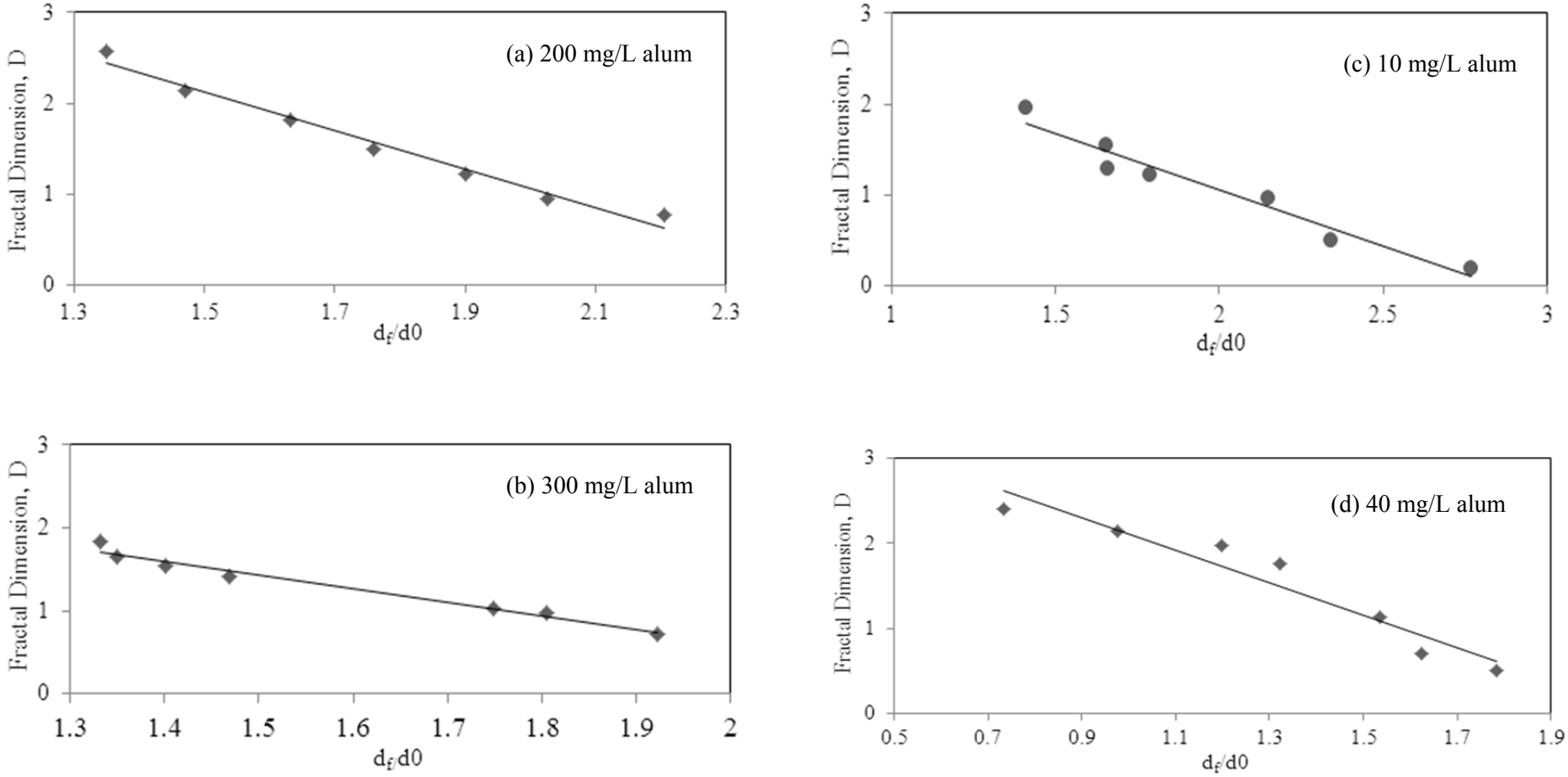

Figure A-3: Power law relationship of fractal dimensions with dimensionless size $\ell = d_f/do$ for synthetic sewage flocs (a, b) and soil flocs (c, d).

Table A-6: The variation of $a_V = d_f^{D-1}$, d_f, and d_f/do down the column for synthetic sewage with a) 200 mg/L alum b) 300 mg/L alum.

a)

	d_f = d_50 µm (200 mg/L)						
Depth (m)	20 min	40 min	60 min	80 min	average d_f	d_f/d0	$a_v = d_f$^D-1
0.25	14.97	16.93	15.93	17.50	16.33	1.35	80.71
0.50	21.20	17.03	16.00	16.97	17.80	1.47	26.35
0.75	22.77	19.97	17.03	19.20	19.74	1.63	11.44
1.00	23.43	20.10	19.27	22.40	21.30	1.76	4.56
1.25	24.97	22.70	21.07	23.30	23.01	1.90	2.02
1.50	26.97	24.50	22.43	24.15	24.51	2.03	0.86
1.75	27.97	26.53	24.07	28.23	26.70	2.21	0.47
d0	12.1						

	d_f = d_50 µm (300 mg/L)						
Depth (m)	20 min	40 min	60 min	80 min	average d_f	d_f/d0	$a_v = d_f$^D-1
0.25	17.63	17.73	14.10	16.60	16.52	1.33	10.16
0.50	21.87	15.80	15.67	13.60	16.73	1.35	6.15
0.75	16.17	20.03	16.33	16.97	17.38	1.40	4.57
1.00	21.70	19.90	18.90	12.33	18.21	1.47	3.39
1.25	26.70	21.57	20.53	17.90	21.68	1.75	1.08
1.50	20.63	28.83	19.67	20.37	22.38	1.80	0.90
1.75	22.57	26.20	24.33	22.23	23.83	1.92	0.40
d0	12.40						

Table A-7: The variation of $a_V = d_f^{D-1}$, d_f, and d_f/do down the column for soil particles with a) 10 mg/L alum b) 40 mg/L alum

a)

	d_f = d_50 µm (10 mg/L)						
Depth (m)	20 min	40 min	60 min	80 min	average d_f	d_f/d0	$a_v = d_f$^D-1
0.25	13.07	13.88	13.22	14.83	13.75	1.41	12.37
0.50	16.47	14.14	17.67	16.14	16.10	1.65	4.53
0.75	13.93	15.17	18.33	17.17	16.15	1.66	2.21
1.00	15.08	16.73	19.13	18.73	17.42	1.79	1.88
1.25	20.70	21.80	21.16	20.13	20.95	2.15	0.90
1.50	26.00	21.17	22.83	21.17	22.79	2.34	0.21
1.75	33.90	25.83	24.24	23.83	26.95	2.77	0.07
d0	9.74						

b)

	d_f = d_50 µm (40 mg/L)						
Depth (m)	20 min	40 min	60 min	80 min	average d_f	d_f/d0	$a_v = d_f$^D-1
0.25	8.33	9.67	9.13	9.33	9.12	0.73	22.68
0.50	10.67	10.68	9.18	10.68	10.30	0.98	14.62
0.75	14.67	13.67	13.85	14.82	14.25	1.20	13.07
1.00	17.33	15.23	15.46	17.52	16.39	1.32	8.37
1.25	19.80	16.97	17.57	20.00	18.59	1.54	1.45
1.50	20.67	18.47	18.17	21.33	19.66	1.62	0.41
1.75	22.33	20.17	20.33	23.49	21.58	1.78	0.22
d0							

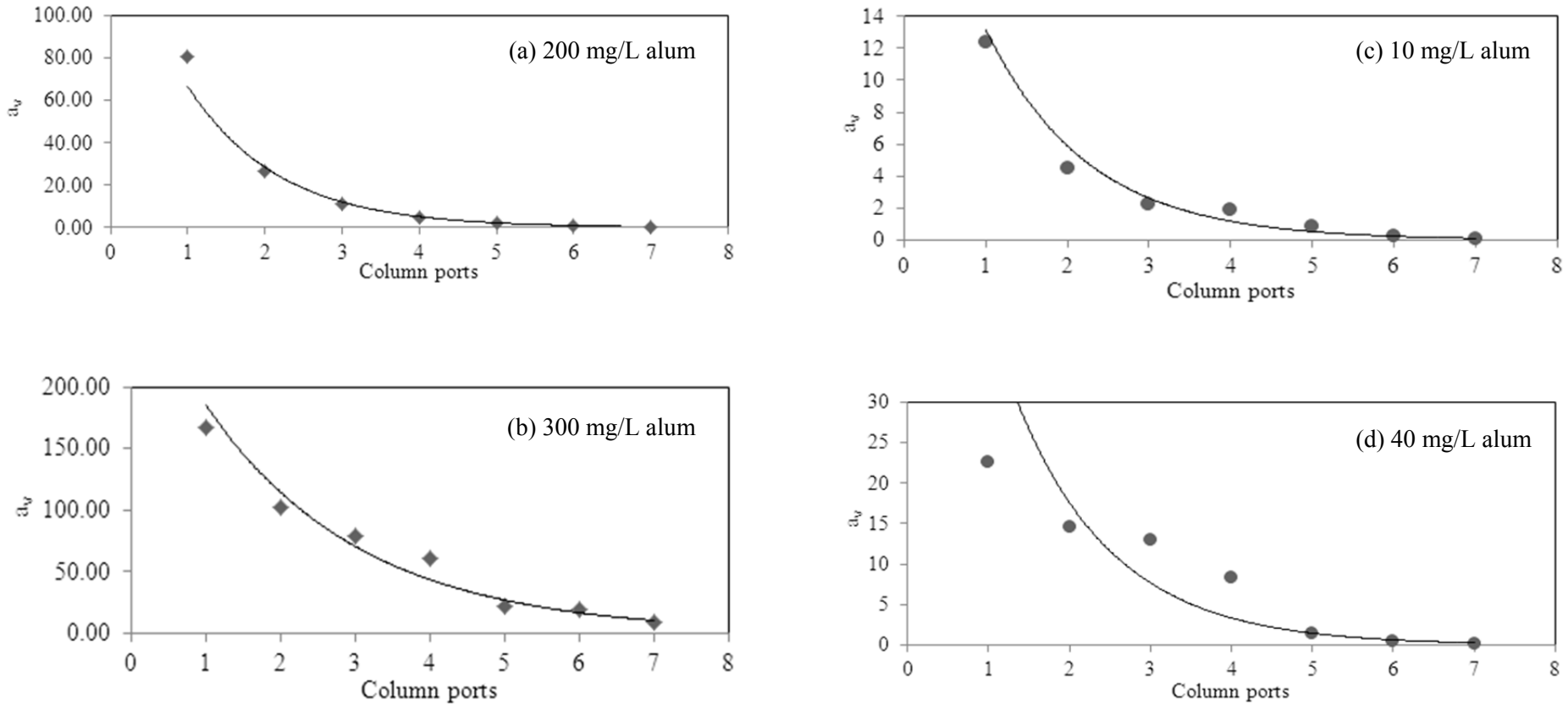

Figure A-4: The exponential behaviour of $a_V = d^{D-1}$ down the column for synthetic sewage (a,b) and soil particles (c,d)

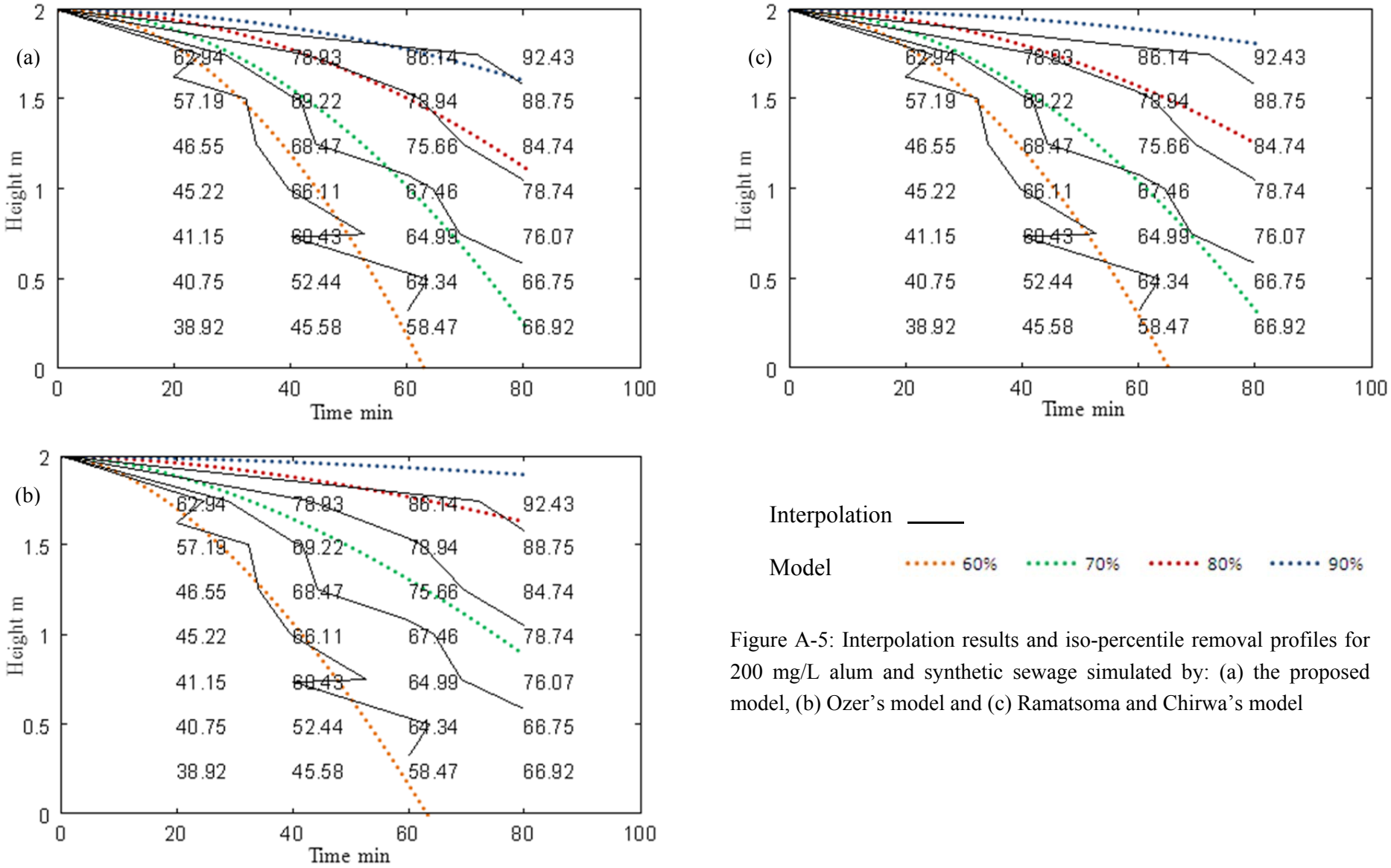

Figure A-5: Interpolation results and iso-percentile removal profiles for 200 mg/L alum and synthetic sewage simulated by: (a) the proposed model, (b) Ozer's model and (c) Ramatsoma and Chirwa's model

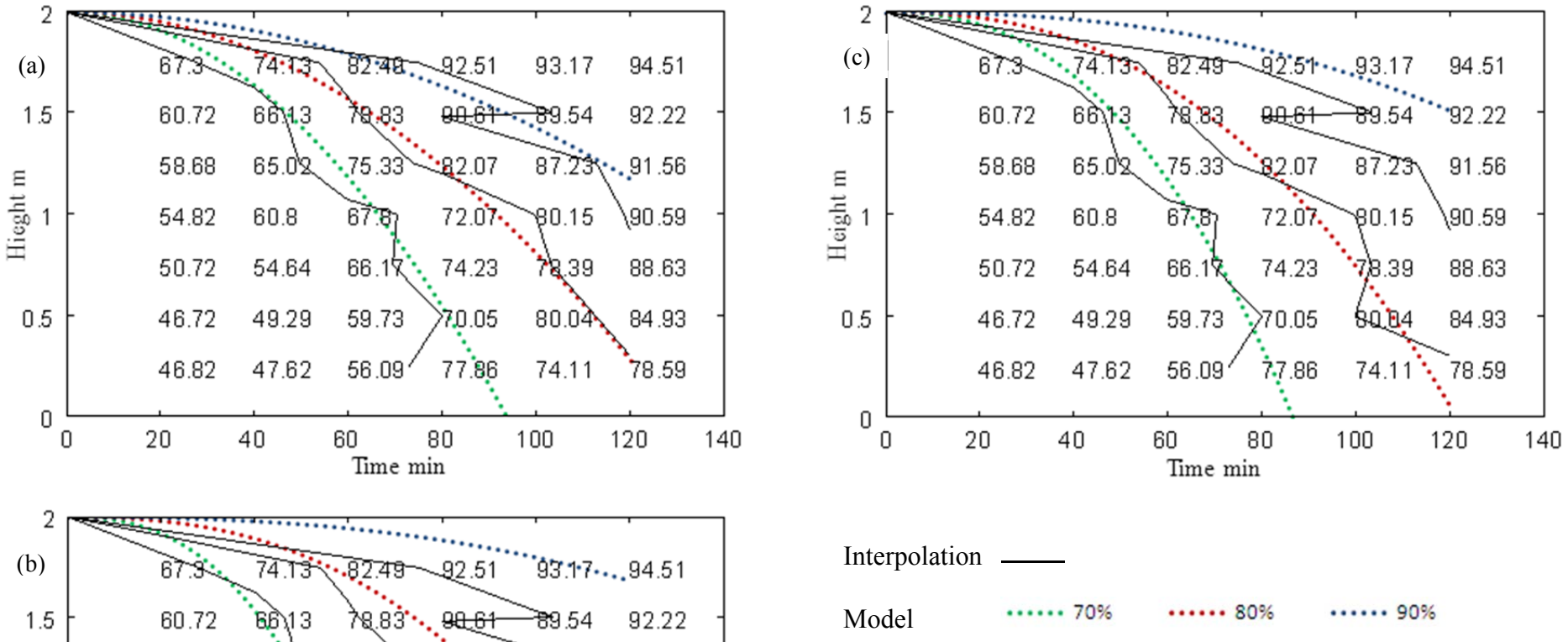

Figure A-6: Interpolation results and iso-percentile removal profiles for 300 mg/L alum and synthetic sewage simulated by: (a) the proposed model, (b) Ozer's model and (c) Ramatsoma and Chirwa's model

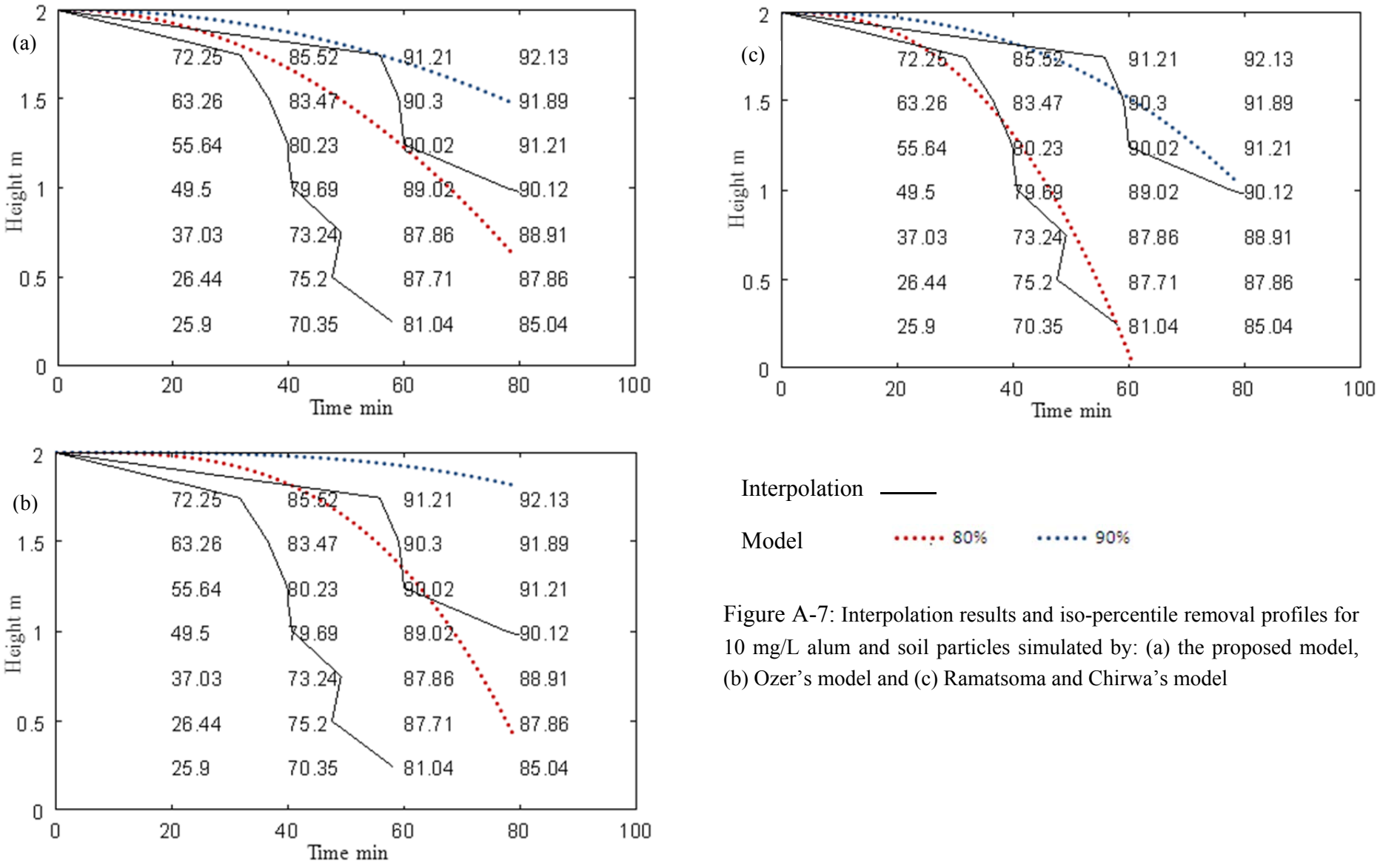

Figure A-7: Interpolation results and iso-percentile removal profiles for 10 mg/L alum and soil particles simulated by: (a) the proposed model, (b) Ozer's model and (c) Ramatsoma and Chirwa's model

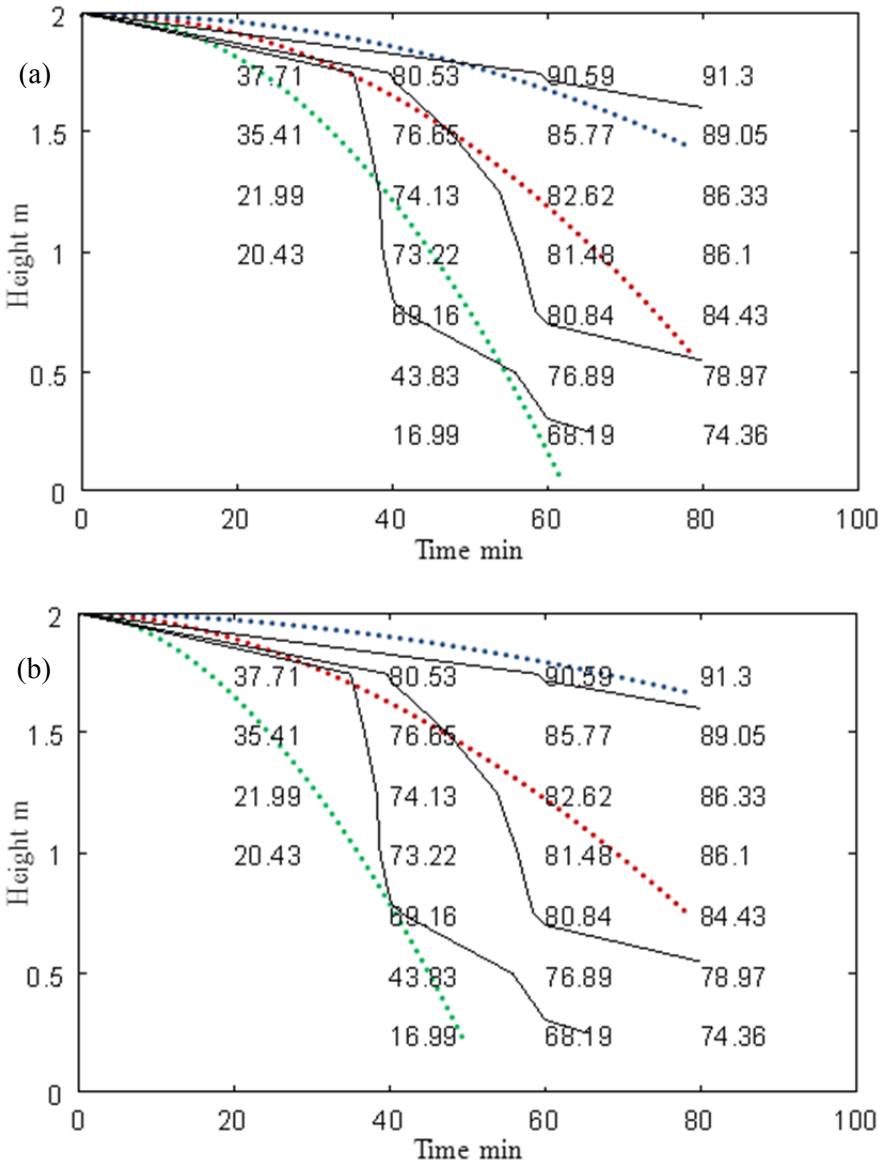

Figure A-8: Interpolation results and iso-percentile removal profiles for 40 mg/L alum and soil particles simulated by: (a) the proposed model, (b) Ozer's model and (c) Ramatsoma and Chirwa's model

Table A-8: Model parameters for Ozer's model and Ramatsoma and Chirwa's model for synthetic sewage (a, b) and soil particles (c, d).

a)

Parameters and sum of square errors				
Ozers model	a1	a2	a3	SSE
150 mg/l	1.81	0.10	-0.2	1.4503
200 mg/l	1.90	0.12	-0.2	5.9467
250 mg/l	2.00	0.10	-0.2	4.8406
300 mg/l	2.00	0.08	-0.2	1.9838
350 mg/l	1.80	0.12	-0.2	3.0360

b)

Parameters and sum of square errors				
Ramatsoma & Chirwa's model	r1	r2	r3	SSE
150 mg/l	0.0002	2.40	0	9.4385
200 mg/l	0.0038	1.94	0	0.81047
250 mg/l	0.0002	2.50	0	1.5551
300 mg/l	0.0005	2.40	0	1.5250
350 mg/l	0.0022	2.30	0	1.0893

c)

Parameters and sum of square errors				
Ozer's model	a1	a2	a3	SSE
10 mg/l	1.86	0.06	-0.20	7.7932
20 mg/l	1.70	0.07	-0.18	6.5754
30 mg/l	1.70	0.10	-0.18	2.8305
40 mg/l	1.70	0.10	-0.18	0.51384
50 mg/l	1.70	0.08	-0.18	2.3786

c)

Parameters and sum of square errors				
Ramatsoma & Chirwa's model	r1	r2	r3	SSE
10 mg/l	0.0015	2.53	0	0.93395
20 mg/l	0.0215	1.90	0	2.4646
30 mg/l	0.0010	2.46	0	2.2170
40 mg/l	0.0010	2.46	0	2.1141
50 mg/l	0.0015	2.40	0	1.6509

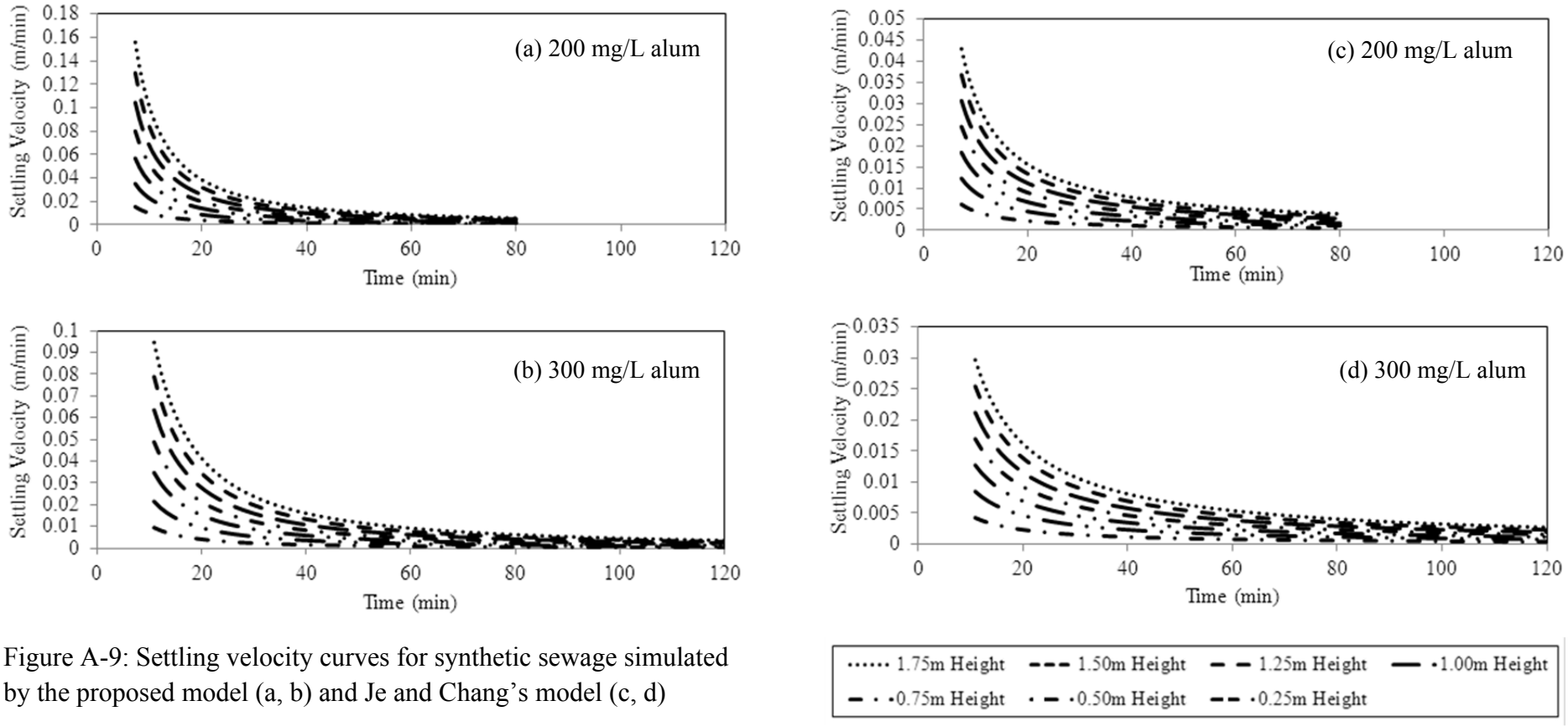

Figure A-9: Settling velocity curves for synthetic sewage simulated by the proposed model (a, b) and Je and Chang's model (c, d)

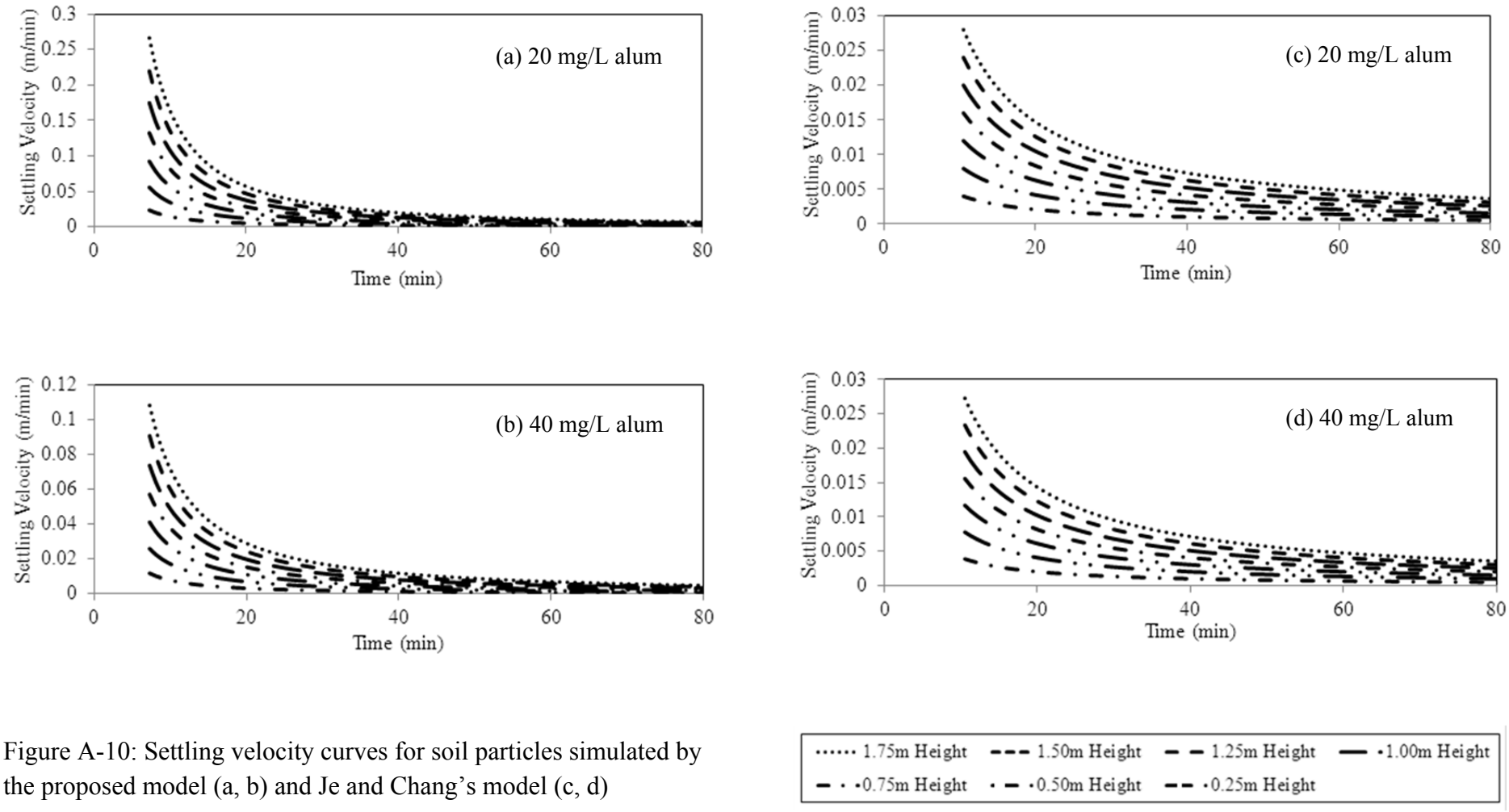

Figure A-10: Settling velocity curves for soil particles simulated by the proposed model (a, b) and Je and Chang's model (c, d)

APPENDIX B

INTERPOLATION SCRIPT: OCTAVE VERSION 3.2.4

```
close

clear all

sample = [58.08   48.05   46.02   40.72   43.82   32.72   38.55;
          68.66   57.85   58.08   51.67   45.81   40.91   34.60;
          78.43   66.19   70.69   62.62   50.44   50.17   45.24;
          83.16   79.65   70.82   67.94   71.64   67.69   60.28;
          92.17   87.74   83.73   76.75   73.04   69.56   66.70;
          92.61   90.29   88.53   82.19   78.75   73.76   71.71];

Hmax = 2;

Exptime = [20 40 60 80 100 120];

H = [1.75 1.5 1.25 1 0.75 0.5 0.25];


K = 1;

% plots sample data

[rr c] = size(sample);

for cp =1:c

 for rp =1:rr

   if sample(rp, cp)> 0

    text(exptime(rp),H(cp),num2str(sample(rp,cp)),'Fontsize',16);

          hold on

   end

 end

end
```

```
for percentage_removal = 60:10:90
P = percentage_removal;
% rp = 1;     % counter for interpolation checking rows
% cp = 1;    % counter for interpolation checking columns
n =1;          % check between exp height and time
TT = [ ];
HH = [ ];
cc = 1;
for cp = 1:c
  interp_time(n) = interp1(sample(:,cp),exptime,percentage_removal);
  if interp_time(n)>0
  TT = [TT interp_time(n)];
  HH = [HH H(n)];
  % plot(interp_time(n),H(n),'o')
  n = n+1;
  end
end
hold on

for rp = 1:rr
  interp_H(n) = interp1(sample(rp,:),H,percentage_removal);
  if interp_H(n)>0
  TT = [TT exptime(rp)];
  HH = [HH interp_H(n)];
  % plot(exptime(rp),interp_H(n),'*')
  n = n+1;
  end
```

```
end
% sorting the values so that it plots logically
   for j = 1:length(HH)-1
     for i = 1:length(HH)-1
      if HH(i)<HH(i+1);
       hh = HH(i);
       tt = TT(i);
       HH(i) = HH(i+1);
       TT(i) = TT(i+1);
       HH(i+1) = hh;
       TT(i+1) = tt;
      end
     end
   end
TT = [0 TT];
HH = [Hmax HH];
 plot(TT,HH,'r')

% model plot
if P == 60
P = 90/100;
end
if P == 70
P = 80/100;
end
if P == 80
P = 70/100;
```

```
end
if P == 90
P = 60/100;
end
t = linspace(0,exptime(end));
% model parameters
b = 2;
c = 5.2;
m =54.1667;
a = 2.6;
w = 6000;

% model plot
d = -(1./w).*log(a/m).*(P^c).*(t.^b);
h = 2 - d;
plot(t,h,'k')

% error calculation (SSE)
        sum_sq = 0;
        for i = 1:length(TT)
                err_sq = (interp1(t,h,TT(i)) - HH(i)).^2;
                sum_sq = err_sq + sum_sq;
        end
        % SSE is the sum of square error for each iso-percentile line.
                SSE(K) = sum_sq
        K = K+1;
```

```
end
 x_axis = exptime(end) +20;
  % legend('Interpolation','Model')
  set(gca,'FontSize',16)
  xlabel('Time min')
  ylabel('Height m')
  axis([0 x_axis 0 Hmax])
 SSE = sum(SSE(:))
```